A Study of the crystallisation kinetics in PEEK and PEEK composites

By

Luke Harris

A thesis submitted to

The University of Birmingham

for the degree of

MASTER OF RESEARCH

Department of Metallurgy and Materials
College of Engineering
The University of Birmingham
September 2011

Synopsis

The two main objectives of the current work were: 1) Isothermally crystallise samples of Carbon-Filled PEEK and Unfilled PEEK at a range of temperatures above the T_g and analyse them using the Conventional Avrami method and the Differential Avrami method. The results were then compared and conclusions drawn. 2) Characterise the crystallisation process by the use of two methods of determining polymer crystallinity. ATR-FTIR and Hyper-DSC were both used to determine sample crystallinity and correlations were drawn between the two methods to provide non-destructive crystallinity data of the samples.

The isothermal crystallisation behaviour of the filled samples showed that at lower isothermal crystallisation temperatures, carbon inclusions hindered the nucleation process compared to that of neat PEEK. However, at higher crystallisation temperatures the carbon inclusions could be said to act as stress initiators that increase polymer nucleation and subsequent growth. It could also be seen that the use of the Differential Avrami approach to analyse the Isothermal crystallisation process gave a more accurate determination of the Avrami exponent n. It was found that the Differential approach gave a higher value of n, closer to the integer 4. This therefore shows a shift in crystallisation growth mechanism and is conclusive with other literature findings.

FTIR and Hyper-DSC techniques can conclusively characterise crystalline presence within semi-crystalline PEEK. The crystalline fingerprint bands found within the FTIR spectra conclusively determined crystalline changes within pre-conditioned samples of PEEK, strongly correlating to other literature findings. Hyper-DSC results also showed that higher heating rates for determining crystallinity should be used in order to produce more accurate results and prevent any molecular melt and recrystallisation within the polymer samples.

Acknowledgements

I would like to thank all of my friends and family for their encouragement and support throughout my study. I could not have completed my project without their support. I would also like to thank Dr. Mike Jenkins for his constant mentorship, time and patience in supporting me throughout the whole project. His help has been crucial to the completion of the work.

Finally I would like to thank Frank Biddlestone for his relentless work in supporting this project and maintaining the polymer department and its instruments, as I am sure he will continue to do so for many years to come.

Contents **Pg.**

1.0 Introduction

1.1 Polymer Background

1.1.1 Long chain molecules

The advances of science within the early 20th century allowed polymer chemistry and engineering to flourish, providing the world with new polymers and engineering materials. The increase in knowledge and understanding of polymer chemistry gave rise to new polymers with increased molecular weights, and more complex structures[1].

A polymer is a long, sometimes branched, chain molecule constructed of smaller structural units known as *monomers*, covalently bonded together. The monomer or structural repeat unit is unique to each polymer, with each having two or more available bonding sites to allow for these units to bond to form molecular chains. The number of available bonding sites of a monomer unit is known as the *functionality*.

Techniques developed in the 1950's now allow for the synthesis of molecules with weights in excess of a million, with uHMWPE (Ultra high molecular weight polyethylene) having molecular weights between 2 and 6 million on average[2].

1.1.2 Molecular Weight distribution

Molecular weight is described in terms of two parameters:

$\bar{M}_N$ = number average molecular weight,

$\bar{M}_W$ = weight average molecular weight.

The number average defines the total molecular mass divided by the number of molecules present. These molecules vary in length, with half of them being in excess of the number average and the other half being smaller. The weight average describes the molecular size, where the total mass typically consists of half of the molecules being large chains and the other half consisting of considerably smaller ones[1].

During polymer synthesis it is hard to assign an exact molar mass to a polymer, as during polymerisation reactions, chain formation is a consequence of random events. These random events can be a consequence of many things, for example, in condensation reactions; it depends on the availability of suitable reactive groups. Therefore, molecules of varying length are produced during synthesis due to the random nature of polymerisation.

Molecular mass information can be used to provide a molecular distribution curve as seen in fig. 1.0, as an example for PEEK[3].

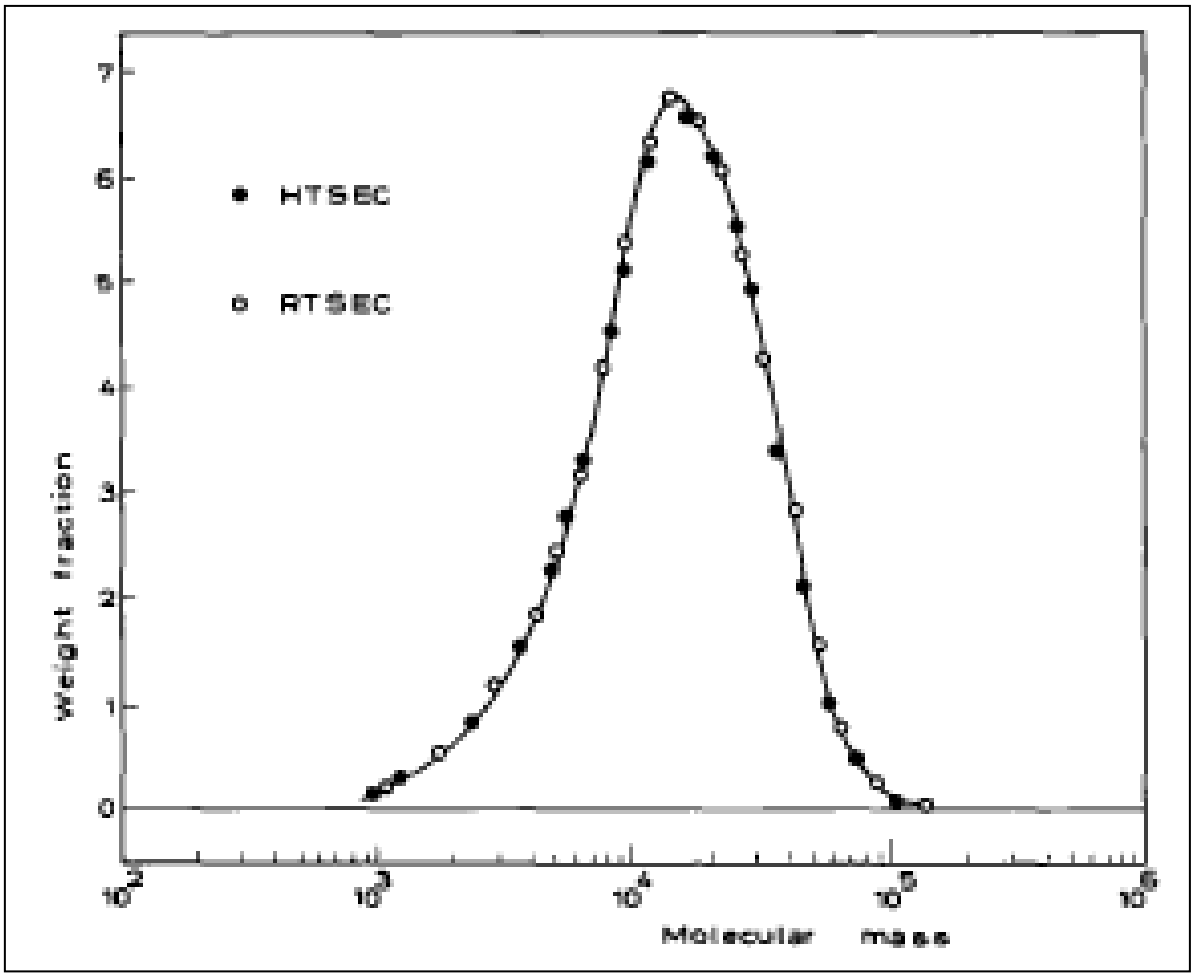

Fig 1.0 Molecular distribution curve for PEEK[3].

If the molecular weight is too low in a polymer, chain entanglement becomes insufficiently low, therefore providing a low level of toughness which is often lower than required[1, 2]. Short chains must also be longer than a critical length to ensure enough entanglements are created to provide a higher level of toughness. $\bar{M}_N$ is therefore the critical factor for toughness within a polymer. Longer chains however provide the bulk of the matrix when in a molten state. It is the energy of releasing the long chain entanglements that needs to be overcome to ensure flow within the molten state. The critical factor here is therefore$\bar{M}_W$. It is therefore ideal to have a narrow molecular weight distribution. To ensure a sufficient level of toughness but still be able to use the polymer for producing parts etc.

1.2 Morphology

1.2.1 Amorphous State

Long chain molecules such as polymers can exist in two states of matter, the liquid (amorphous) and solid state. In the liquid phase, although very confined by their neighbouring molecular chains, polymers exist in a random orientation within three dimensional space. This random orientation of these molecular chains is characteristic of amorphous polymers, a contrast to the ordered regions of the solid crystalline phase. These chains act as kinetic units, interconnected, yet independent of each other. Chain movement is limited to rotation about the single bonds connecting atoms in the chain, and a single polymer can possess many conformational states. All of this depends on the energy barrier within the polymer system and the ease at which the polymer chains can overcome this. As chains overcome the energy barrier, the ease at which conformational changes can take place increases and with more energy applied to the system, the polymer starts to act like a viscous liquid.

1.2.2 Semi-Crystalline

Semi-crystalline polymers consist of a two phase morphology, an amorphous region and a crystalline region. See Fig.1.1. The majority of polymers consist of this two phase morphology and always possess an amorphous phase, as complete crystallinity is rarely (if ever) reached. Many material properties in a polymer change when a significant amount of crystallinity is present in the polymer. Some of these properties are increased chemical resistance, increased service temperatures, increased modulus and increased impact strength. The polymer then, no longer behaves in a visco-elastic fashion as with amorphous polymers and properties such as strength and modulus are improved[2].

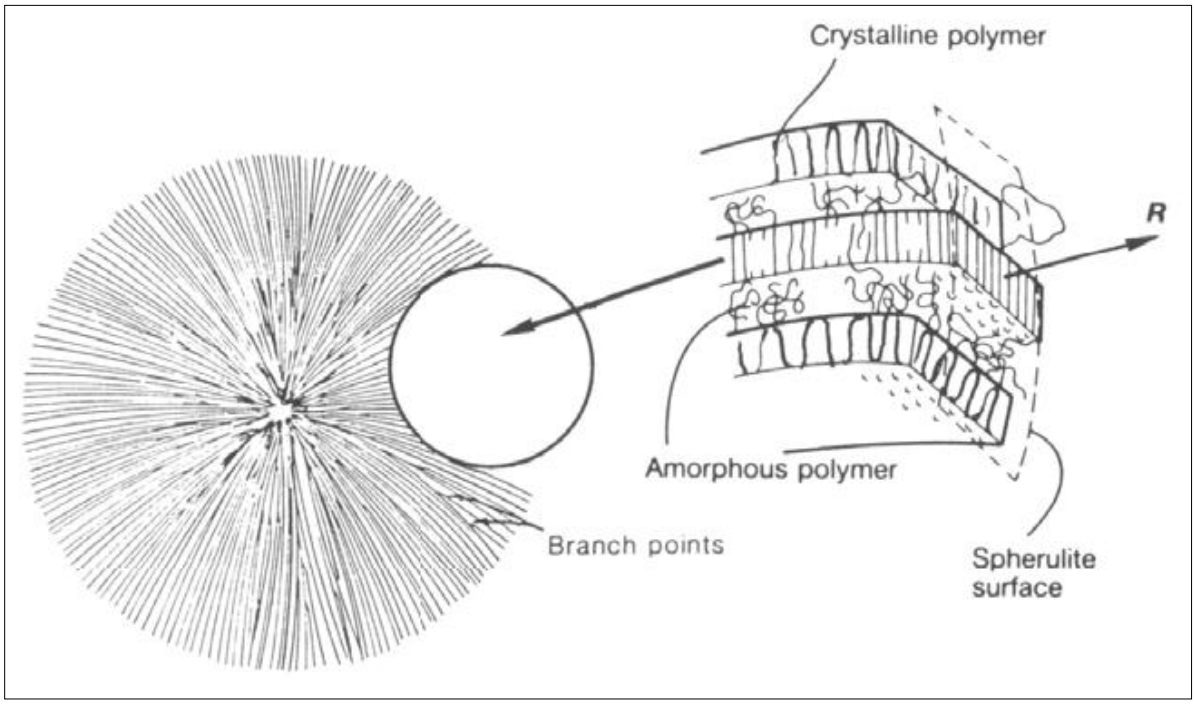

Figure 1.1 A Polymer Crystalline Spherulite[2]

1.3 Crystallisation

The crystalline phase is obtained through solidification of the under-cooled isotropic melt within the amorphous polymer. Nuclei form within small regions of the tangled and randomly orientated molecules to produce the ordered chain folded layers we associate with crystallites[2]. This nucleation occurs either homogeneously, whereby Nuclei develop by a random orientation of the parent polymer chains, or alternatively, heterogeneously, which occurs due to the inclusion of dust particles or nucleating agents within the polymer melt.

The lamellae are in turn arranged in spherulites (several tens of micrometres in diameter growing radially by small-angle non-crystallographic branching in all directions)[4]. Changes in dimension at a given temperature of crystallisation are normally linear and the spherulite radius, r, will be related to time by a constant factor[5]. These two morphological

regions exist dependently upon each other as the extended polymer chains fold to form crystallites within the amorphous mass. The formation of these polymer crystallites involves a two stage process of nucleation and growth. Nucleation occurs through the creation of a stable nucleus brought about by the ordering of chains in a parallel array. This is stabilised by secondary valence forces within the melt, which aid in packing of molecules in a three-dimensional order. The second stage of crystallite creation is growth. This is where temperature plays a key role in slowing the disordering process and allows the addition of chains to the stable nucleus to form three dimensional crystallites[2].

Crystallisation occurs in two stages, primary crystallisation and secondary crystallisation. Primary crystallisation is the process of heterogeneous nucleation of three dimensional spherical growth, as mentioned previously. The secondary process is the one dimensional fibrillar growth that occurs between the spherical primary crystallites filling the amorphous regions of the inter-crystallite voids.

1.4 PEEK – Polyetheretherketone

1.4.1 Background

In the early 20th Century new polymer molecules were being discovered and the development of Poly(etherether)ketone or PEEK, was underway at ICI. Staniland[6] among others reviewed this newly available polymer discovering that the properties were to become part of a new age for the polymer world, bringing advancing technologies, especially within the composites industries. It is now widely known that PEEK is a high temperature engineering thermoplastic with excellent chemical, mechanical and thermal stabilities.

PEEK is a high profile engineering material and its properties allow it to be used for highly prized engineering applications. With a modulus of around 3.2GPa, and service temperatures of up to 260°C, PEEK is now common place within the aerospace and automotive industries[7]. Alongside this, is it's high resistance to chemical and biochemical degradation, with the only known common solvent of PEEK being highly concentrated sulphuric acid[1], making PEEK an ideal candidate for application within areas where fuel lines are located and other chemical degradation may take place.

The necessity and importance of heat resistant materials in the aerospace, automotive and electronic industries has become driving force for researchers on high performance for target applications[8]. PEEK has therefore become one of the most researched and documented engineering thermoplastics over the past few decades and continues to be with present research continually taking place.

In the 1980's many studies were carried out to determine the structure of the repeat unit of PEEK and its crystallographic nature. Dawson and Blundell, 1980[9] carried out many x-ray experiments to determine the repeat unit of PEEK, which would later lead to investigations into the crystalline packing of the molecule as crystallisation occurs. We can therefore determine the repeat unit of PEEK, as seen in fig 1.2.

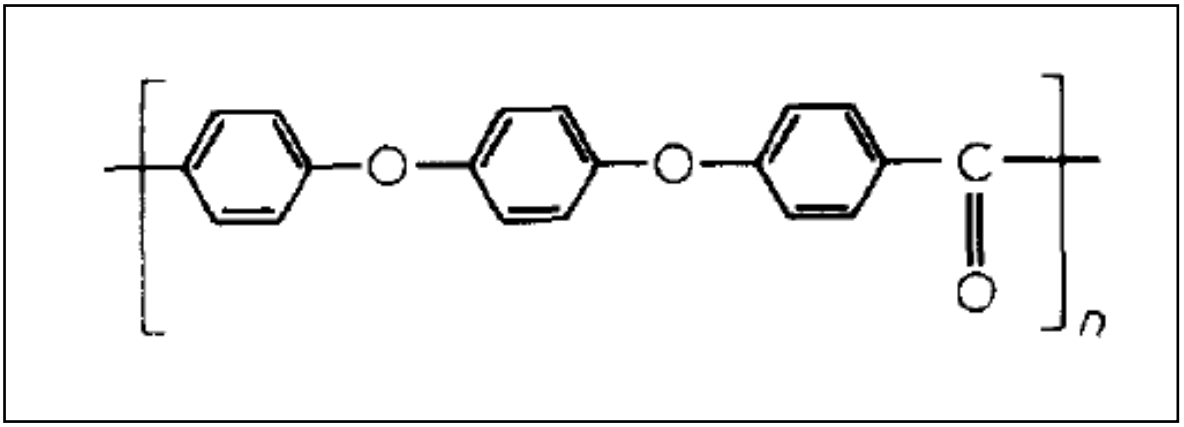

Figure 1.2 Repeat Monomer unit of PEEK[10].

Following the determination of the monomer repeat unit of PEEK, investigations by Blundell and Osborn, 1983[10] determined that the melt behaviour of PEEK was similar to that of PET from previous studies[11]. The resulting morphology of this semi-crystalline polymer is of a spherulitic nature, with packing of the large aromatic phenyl rings able to produce this repeat stacking as the polymer crystallises[2, 10, 12, and 13].

1.4.2 Synthesis

Poly-aryl-ether-ketones are generally synthesized by an aromatic nucleophilic substitution reaction of activated aryl dihalides with aromatic diphenolates in a dipolar aprotic solvent, or by electrophilic (Friedel-Crafts) acylation of aryl ethers[14].

The nucleophilic aromatic substitution reaction involves use of activated aromatic dihalides and aromatic diphenolates. The general reaction is shown in fig 1.3.

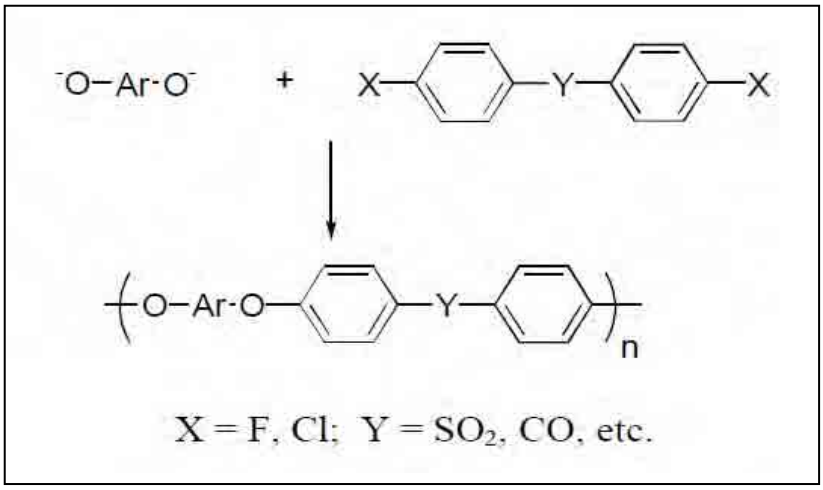

Fig 1.3 Nucleophilic aromatic substitution reaction[15].

In general, a strong electron withdrawing group such as carbonyl, sulfone or phosphine oxide is necessary to activate the aromatic dihalides. The reactivity of the halogens are in the order of F>>Cl>Br. Typically potassium carbonate is used as base to avoid the side reaction of alkali metal hydroxides and dipolar aprotic solvents such as DMSO, DMAc and NMP are utilized.

Johnson *et al*.[15] reported the first attempt to synthesize PEEK by polycondensation of bisphenolate with activated dihalides using DMSO as a solvent and NaOH as a base. High molecular weight polymers were difficult to obtain due to the crystallinity and the resulting insolubility of polymers in DMSO. To circumvent the solubility problem, Attwood[16] and Rose[17] used diphenyl sulfone as a solvent to obtain high molecular PEEK (Scheme 1.6). The polymerization was carried out near the melting point of the polymer to maintain solubility. Victrex PEEK was commercialized by ICI in 1982 using this method. At high temperatures, side reactions such as ether exchange and cleavage became important. Under careful optimization, high molecular weight poly(ether ketone)s can be obtained[18].

1.4.3 Crystallisation Kinetics

PEEK's notably high nucleation density allows the polymer to crystallise readily during cold and melt crystallisation. As noted by Hay and Mehmet-Alkan in 1992 the use of DSC allows for accurate calculation of the crystallinity X_c, of PEEK by analysing the melting endothermic trace to gain the Heat of fusion, ΔH_f. The use of a literature value for the ΔH_f of a completely crystalline sample of PEEK, $130 Jg^{-1}$, then allows for the degree of crystallinity of PEEK to be calculated.

Through the work of authors such as Avrami, extensive work on crystallisation behaviours reached a conclusion of a model describing the development of crystallinity[19-21]. Shown below is X_t described as a function of time:

$$X_t = \left[1 - \exp\left(-Zt^n\right)\right] \qquad \text{(Eq. 1)}$$

where Z is a rate constant incorporating the growth rate and characteristics of crystallite growth. X_t is the volume fraction of crystallised material at time t. n is the Avrami exponent of the equation which adopts different values depending on the crystallisation mechanism involved[22].

The Avrami exponent, n, adopts different values for different crystallisation mechanisms. The type of crystallisation and nucleation processes, which occur within a polymer can be obtained from the n and Z values. A table of various n values are listed below[2].

Table 1.0 Avrami exponents and morphological units

Crystallisation Mechanism	n	Geometry
Spheres	4.0	3-D
Sporadic discs	3.0	2-D
Fibril	2.0	1-D
Predetermined rods	1.0	1-D

The Avrami equation (Eq. 1) can then be expressed as the equation of a straight line,

$$\log\left[-\ln\left(1-\frac{X_t}{X_\infty}\right)\right] = n\log t + \log Z \qquad \text{(Eq. 2)}$$

From equation 2, the differentiation between primary and secondary processes can be determined as the Avrami analysis is only valid for primary crystallisation processes. Determination of Z values can then be determined using the following equation,

$$Z = \frac{\ln 2}{\left(t_{1/2}\right)^n} \qquad \text{(Eq. 3)}$$

For the present work, focus will be on the isothermal crystallisation kinetics and analysis of PEEK and the relevant PEEK composites.

2.0 Literature Review

2.1 Crystallisation behaviour of PEEK and PEEK composites

Polymer crystallisation kinetics gives an insight into the mechanisms occurring when crystallisation occurs. From early studies it is now known that differing the crystallisation temperature during isothermal crystallisation will alter the intrinsic crystallinity of the polymer[23]. Cebe and Hong in 1986[24], agreed that as T_c increases the level of crystallinity present also increases. The increase in temperature gives rise to a longer crystallisation time for spherulitic growth. It could therefore be said that increasing the isothermal crystallisation temperature of PEEK will therefore give rise to higher levels of crystallinity, which are needed to acquire the desired chemical resistance levels and strength properties. Cebe's work further reinforces the previous work done by Blundell and Osborn in 1983, in that the Avrami kinetic analysis provided an n value of around 3, which is indicative of a spherulitic morphology. The confirmed spherulitic morphology within PEEK[10] forms in two distinctive populations. The first population is formed first, and makes up the bulk of the spherulites early on in the crystallisation process. The second population forms later in the process, and is indicative of the crystallisation of amorphous material trapped between the spherulite chain folding and the boundaries between neighbouring spherulites[25].

Introduction of a fibre into polymers to create composites therefore adds an extra parameter to focus on when studying these mechanisms. The integrity of thermoplastic composites relies on the thermal history and processing of the parts, and its subsequent morphology[26]. It is therefore imperative to have a full understanding of the implications of fibre additions on the morphology of the polymer matrix. An early study in 1988, by Mingbi

et al.[27], showed some of the first evidence of the effect of carbon fibre addition. Samples of APC-2, a continuous fibre composite, were subjected to a variety of isothermal crystallisation temperatures, and the results of crystallinity and crystallisation time were recorded. The findings were suggestive that the fibre inclusions acted as stress inhibitors within the matrix causing increased nucleation of the PEEK matrix. This thereby increased the rate of crystallisation and also increased the resulting crystallinity.

In contrast to this Hay and Mehmet-Alkan in 1993 suggested that the inclusion of carbon fibre within PEEK resin does not significantly affect the crystallinity of the sample. They did however suggest that the fibres could act as a nucleating agent to increase the rate of crystallisation for a given T_c, thereby reinforcing some of the earlier findings. In 1991 Jar et al. investigated the implications of different melt temperatures before isothermal crystallisation on long fibre (APC-2) PEEK composites. This study provides an interesting addition to Hay's work, suggesting that the presence of carbon fibre does not affect the crystallinity of the sample if the conditions of processing are identical. If however, the samples are heated beyond the optimum T_m, variations in the matrix morphology could arise.

There have been many studies on the interaction of fibre additions to the polymer matrix of PEEK. Majority of the works completed are on the well-known grade APC-2 which is a long continuous fibre reinforced laminate. Early work by Blundell et al., 1989, indicates that the crystal growth habits within the laminates are identical to that seen within the pure polymer. Under certain conditions, nucleation of crystal growth can occur either in the matrix itself or from the carbon fibre inclusions. The amount and resultant crystallinity would depend on processing conditions applied to the samples. From Blundell's works (1989), it was found

that at lower temperatures, nucleation was most favour able within the matrix itself, and at elevated temperatures fibre nucleation was favoured. This may be due to the high mobility of molecular chains at elevated temperatures, therefore reducing the ability of chains to fold and form a crystal structure by themselves without having some form of nucleation site. It was also noted that nucleation from fibres, happened more readily at fibre-fibre contact points within the matrix and not from the more obvious fibre-matrix interfaces. However, APC-2 is a long continuous fibre laminate which does constrain the matrix to the channels between the fibres.

Interaction between fibre and matrix is an important aspect of crystallinity within the polymer composite and therefore becomes a very expansive topic. The current work will not investigate further into the specific interactions between fibre and matrix, but will focus on the effect of the fibres present on the overall crystallinity of the matrix.

With the present work being related to short fibre reinforced composites it is imperative to understand the influence of short fibre additions on the crystallisation behaviour of the matrix. Studying the influence of mould temperature on the crystallinity of short fibre reinforced PEEK, Sarasua et al.[28] drew some interesting conclusions. Extending investigation to previous works[29] Sarasua and his colleagues saw no significant increase in overall crystallinity with addition of short glass fibres to the PEEK matrix as crystallisation temperature increased. However, there was a noticeable change of increased crystallinity with increasing crystallisation temperature when there were carbon fibre additions. This is similar to that of the work by Hay and Mehmat-Alkan in 1993 whereby the addition of glass fibre gave poor crystallinity values. The PEEK component here has been shown to act like a poorly

crystalline PEEK sample such as a rapidly quenched sample. However, carbon fibre reinforced samples gave rise to crystallinity values similar to that of neat PEEK resin. This shows that the carbon fibres could potentially act as nucleation sites for crystallisation, and trans-crystallisation could also occur during the cooling of PEEK samples from the melt[28-30]. The current work, will therefore investigate the influence of short carbon fibre additions to new grades of PEEK matrix, supplied by Victrex Plc.[31].

2.2 Measurement of Crystallinity using FTIR

As DSC techniques developed other techniques for measuring the crystallinity of polymers were used to provide a comparative source for crystallinity values. FTIR techniques allow for polymers to be analysed non-destructively within the mid-infrared spectrum.

Early reports by Blundell and Osborn, 1983, show that PEEK's crystallisation behaviour is exactly analogous to that of PET, with a two-phase morphology. This simple amorphous and crystalline phase morphology makes PEEK an ideal polymer for studying with infrared spectroscopy techniques. The typical spectra for PEEK are well documented[32-34] through use of FTIR (Fourier Transform Infrared Spectroscopy) techniques and many studies are still being undertaken within this field.

Due to the majority of the highly appealing properties within PEEK being associated with crystallinity, studies of the crystallisation behaviour have been the focus for many academics (as noted in section 2.1). This principle was extended to the techniques of infrared spectroscopy to give further insight to the molecular behaviours within PEEK and its composites. In general, the mid-infrared (MIR) spectrum of a semi-crystalline polymer is

affected by morphological changes, and more precisely, crystallinity[33]. Aromatic polymers such as PEEK provide a good medium for infrared investigation due to the higher absorption within the MIR spectrum. One of the first studies investigating the crystallisation of PEEK with infrared techniques was by Chalmers et al., 1984, whereby he set out to determine a relationship between absorption bands within the spectra and crystallinity of the sample (as previously measured by WAXS studies)[10]. By locating certain absorption peaks within the spectra, determinations could be made as to the absorption change in these fingerprint regions as a function of degree of crystallinity. A ratio of peak absorbance was used for 1305/1280cm^{-1} and 970/952cm^{-1} which was then plotted against the predetermined WAXS crystallinity measurements, giving a linear relationship between absorbance and crystallinity. These aforementioned absorption bands have were used as they have been found to be fingerprint absorption bands directly affected by the samples crystalline content.

Following the work of Chalmers in 1984, Nguyen and Ishida, 1986, set about documenting the melt behaviour of PEEK using FTIR techniques. It was noted that the spectra of quenched, amorphous, PEEK was significantly different to that of the spectra of an annealed sample, showing spectral shifts and differing band intensities. A main part of the work carried out by Nguyen was to look at the disordered phase, or amorphous phase by comparing the spectra of the two different sample types. It was shown that intensities of amorphous bands decreased as crystallinity within the sample increased. It was also noticeable that the crystalline absorption bands would increase in intensity or cause spectral shifts, which in turn blurs the boundaries to be able to distinguish the resulting effects on the amorphous intensity bands. The investigation gave some very clear indications that crystallinity, or more specifically, ordered chain stacking, gives rise to the largest change in

spectral data. This was shown by Nguyen in his study by using two samples, identical, except for the melt temperature used to pre-melt the samples. It was found that nucleation sites were still present within the sample when melted out at 380°C, giving rise to a bigger spectral difference. This was compared to a sample melted out at 400°C, whereby more nucleation sites were destroyed as a result of higher initial temperatures, giving rise to better clarity and more intense spectral peaks rather than broader, less accurate intensity bands.

Jonas et al, 1991, also looked at assessing the level of crystallinity within PEEK through FTIR based on previous works[33, 35]. This study took a different approach, by using different absorption bands to the ones discussed within Chalmers' work. The study condemns the use of the crystalline band at 965cm^{-1} due to its apparent independence from sample crystallinity above 15%. Turning from this, the method of approach was to use deconvolution of the peak areas of 952±.5cm^{-1} and 947cm^{-1}, using 965cm^{-1} as reference, to give an area ratio relationship. The study found that the peak in the spectra at 952cm^{-1} changed with increasing crystallinity, giving a shoulder at 947cm^{-1}. It was therefore stated that this shoulder was indicative of crystalline regions within PEEK and its repeat stacking units within crystallisation. However, the study does mention the use of a deconvolution process in order to make sense of the peak obtained from the shoulder of the existing 952cm^{-1} band. This process therefore leads to inaccuracies due to the nature of the deconvolution process to estimate the area of the new shoulder in the spectra. Through preliminary work carried out prior to completing the current study, discrepancies and difficulties were found when trying to use deconvolution methods to distinguish the newly forming shoulder in the PEEK spectra as suggested by Jonas et al. At lower crystallinities, the 947cm^{-1} shoulder appears as little more than an irregular distortion of the host peak at 952cm^{-1}, this therefore poses a clear

discrepancy with trying to estimate its clear significance at lower crystallinities. Errors in calculating the new peak's area would therefore give rise to further implications when calculating area ratios.

Later studies from 1993 onwards [36-38] all investigated various rationales involving PEEK and it's morphological structure. Although these studies used slightly different techniques, they all agreed with earlier studies such as the one by Nguyen in 1986 about the significance of FTIR data for investigating PEEK and it's composites. Chalmers et al., 1998, extended their work from their first study by investigating more recent FTIR techniques to that used previously[33]. It was found that reproducible sampling became difficult when using certain FTIR techniques, in particular ATR. Contact sampling of the ATR reflection element and the surface of the PEEK samples proved to be impractical to achieve in repetition and it was also suggested that the existence of high local pressures could increase the possibility of pressure induced crystallisation occurring. These investigations lead to a change in approach, using specular reflectance as part of an experimental on-going investigation. Although the study highlights the negative aspects of ATR techniques the current study will progress to use them for the illustrated reasons discussed later.

2.2.1 ATR-FTIR techniques.

Within industrial manufacturing methods, thermoplastic parts are made from injection moulding or other moulding processes. Due to time constraints and manufacturing cost in creating the parts, serviceable parts are manufactured with relatively quick turnarounds in order to maximise production and increase sales. Due to these constraints, moulded parts need to leave the production line as quickly as possible; therefore knowledge of the part's integrity

would be a useful tool. However, this would preferably be a non-destructive method for quality control, and in the case of PEEK, ensure the right levels of crystallinity are met in order to meet tight specifications for high-end engineering use. A method that would enable a non-destructive measure would be the use of ATR (Attenuated Total Reflection)-FTIR techniques. Here, an ATR element (usually diamond) has to be in contact with the sample surface that is to be interrogated. The evanescent wave produced in the ATR approach may only reach a depth of a few microns or more and is a function of wavelength, refractive index of the ATR element and the angle of incident of the laser source. The depth of penetration can be calculated more precisely with the following equation:

$$d_p = \frac{\lambda}{2\pi n_1 \sqrt{sin^2\,\theta - n_{21}^2}} \qquad \text{(Eq. 4)}$$

where λ is the wavelength of the radiation; θ is the angle of incidence of the beam; n_{21} is the ratio of the refractive indices of the sample n_1 and the ATR crystal n_2[39]. So for studies where retention of the sample, and it's physical properties are important, external reflection spectroscopy, such as ATR is a useful non-destructive means of sample analysis[32].

However, the drawback is the fact that this method only analyses the sample surface and isn't an indication of the bulk of the material. Alongside this, it has been reported that in some cases ATR produces "shifted" peaks in the recorded spectra within strongly absorbing bands. As an absorption within the material occurs, the refractive index of the sample material changes instantaneously, giving a distortion in the peak intensity or location along the

spectra[39]. In comparison, other infrared techniques also incur spectra shifts and irregularities, and therefore relative comparisons have to be made with “like for like” data.

Other infrared techniques have been noted for investigating the crystallinity of PEEK[40] yet a lot of these techniques still use the spectral peak ratios highlighted by Chalmers et al in 1984. The present work will focus on using an ATR-FTIR technique alongside other techniques to expand the basic work as completed by Chalmers et al, 1984.

2.3 Hyper-DSC thermal analysis techniques

Jonas and colleagues[41] recognised the need for another way of characterising the crystallinity of PEEK highlighting the possibility of melt and re-crystallisation of polymers during heating runs to determine the sample crystallinity. The study comments on the possibility of growth of the lamellae structure as the temperature increases when determining the sample crystallinity through DSC techniques. It therefore raises a question as to whether DSC alone is sufficient enough to determine sample crystallinity, and whether new techniques can provide more accurate measures.

The recent introduction of Hyper-DSC techniques, or fast scanning DSC techniques is becoming popular with the pharmaceutical world for investigation into polymorphs and amorphous contents within semi-crystalline substances[42-44]. The technique allows better accuracy and increased resolution of the output heating scans that the calorimeter produces. This in turn allows for better distinction of glass transitions and melting peaks within the DSC trace.

In 2004 a study by McGregor and colleagues used new Hyper-DSC techniques to overcome the outlined problems that can occur with testing samples using conventional DSC techniques. The study was concerned with pharmaceutical polymorphs, which are organic compounds that can occur in multiple crystalline forms, and the determination of the heat of fusion of such crystalline forms. This is imperative within pharmaceuticals as the amount of each crystalline form present within the compound can have detrimental effect on the dosage needed for use. Conventional DSC techniques measuring the heat of fusion are usually done by heating samples at rates that are usually quite slow and well recorded and trialled within the literature. However, McGregor realised that these rates gave rise to several problems in calculating the data needed. The rates allowed concurrent heating and re-crystallisation of crystalline phases, giving rise to multiple thermal events being witnessed as the samples are analysed. The use of higher heating rates (250+°Cmin^{-1}), only accurately achievable with the use of Hyper-DSC allowed for the enthalpy of fusion determination of the crystalline form being examined without recrystallisation occurring upon heating.

Following the earlier study in 2004, McGregor and co-worker, 2008, continued to build on their work by investigating the use of Hyper-DSC techniques in the use of enthalpy of fusion determinations of pharmaceutical compounds. The study is based around the earlier study and investigates the use of the fast heating rates to inhibit any recurrent melting and re-crystallisation of crystalline phases when determining enthalpies of fusion. Although both of these studies are investigating pharmaceutical polymorphs, there are definite links with semi-crystalline polymers. Within conventional DSC techniques the same aforementioned irregularities can occur when heating samples to determine the enthalpy of fusion of semi-crystalline thermoplastics[41].

3.0 Project Aims and Objectives

1. *Isothermal Crystallisation of PEEK*

The first objective is isothermally crystallise both 450PF and 450CA30 (carbon filled) grades of Victrex® PEEK, using conventional DSC techniques. The isothermal crystallisation will take place over a range of temperatures laid out within the methodology, and analysed using both the Avrami method, and the Differential Avrami approach. A comparison between these methods can then be made

2. *Characterisation of Crystallisation*

The second objective is to characterise the crystallisation process by using two different techniques. FTIR and Hyper-DSC will be the techniques used for investigating crystallinity within 450PF PEEK. The objective of this is to determine if a correlation between the FTIR spectroscopy results and Hyper DSC data can be made, thus producing a confident method of non-destructively characterising polymer crystallinity.

4.0 Materials and Methodology

4.1 Sample preparation

The samples of PEEK adopted for this study were supplied by Victrex® Plc.[31]. Two grades of unfilled PEEK were supplied, 150PF, and 450PF, whereby the numerical value relates to molecular weight, with the higher number referring to a high molecular weight grade of PEEK (molecular weight unknown). The PF suffix indicates a fine powder grade. The filled grade of PEEK material received was 450CA30, whereby the 450 indicates a high molecular weight and the CA30 represents 30% additional (chopped) carbon fibre by volume. This was supplied as a fibre filled pellets. All samples were dried at 120°C for 5 hours to remove any moisture within the polymer and then stored in large airtight universal containers until required.

Table 4.0 Victrex PEEK material data (as supplied by Victrex® plc.)

Grade	T_m (°C)	T_g (°C)	M_w	M_n
150PF	343	143	68560	23630
450PF	343	143	99400	31740
450CA30	343	143	99400	31740

Samples were then weighed out to 12mg in DSC Aluminium pans and heated using the DSC to 380°C and held for 2 minutes. Samples were then removed from the DSC and placed immediately into liquid Nitrogen to quench the samples. This process is undertaken to ensure no thermal or processing history remains within the sample prior to experimentation.

4.2 Differential Scanning Calorimetry (DSC)

A Perkin Elmer DSC 7 interfaced to a PC was used to measure variation in relative heat flow with temperature. The DSC unit consisted of a sample and reference cells both of which had separate heaters and platinum resistance temperature sensors. The heaters are coupled such that the differential power required to maintain the two cells at the same temperature could be measured. The DSC was calibrated using the melting points of high purity metals: Zinc (T_m = 419.53ºC) and Indium (T_m = 156.63 ºC). The melting point of each of these materials was found by heating in the DSC at a heating rate of 5°Cmin^{-1} and corrections for thermal lag were made by extrapolating to zero heating rate.

The samples were held in Aluminium pans without lids and an empty pan was used as a reference. Nitrogen gas was used to purge the sample and minimise any degradation and a liquid cooling system was used to aid in the rapid cooling needed to control temperatures and cooling rates. This resulted in a block temperature of 3°C. The thermal history of each sample was erased by heating to 380°C and holding for 2mins. The samples were then quench cooled to below the glass transition of PEEK. Therefore, the samples were amorphous.

4.2.1 Isothermal crystallisation

A sample was heated at a constant rate of 10°Cmin^{-1} to give a melting curve for the material up to 380°C. The sample was then cooled at a rate of 5°C to give the melt-crystallisation curve. The purpose of recording the cooling curve was simply to identify the crystallisation temperature range for further study.

Isothermal melt-crystallisation experiments were run, where the sample was held at a temperature above the melting point (380°C) for two minutes to ensure a full amorphous state was reached. The samples were then rapidly cooled to the relevant crystallisation temperature at which point the DSC was set to record the relative heat flow until the trace had returned fully to the calorimeter baseline. The crystallisation exotherm for a crystallisation temperature of 311°C is shown in fig. 4.1.

The crystallisation data obtained from DSC was used to calculate the relative crystallinity, this assumed that the heat evolution detected by the DSC was solely the result of crystallisation such that the extent of crystallinity at time t could be determined by integration of the exotherms [45] according to equation 5.

$$\frac{X_t}{X_\infty} = \frac{\int_0^t \left(dH_t / dt \right) dt}{\int_0^\infty \left(dH_t / dt \right) dt} \qquad \text{(Eq. 5)}$$

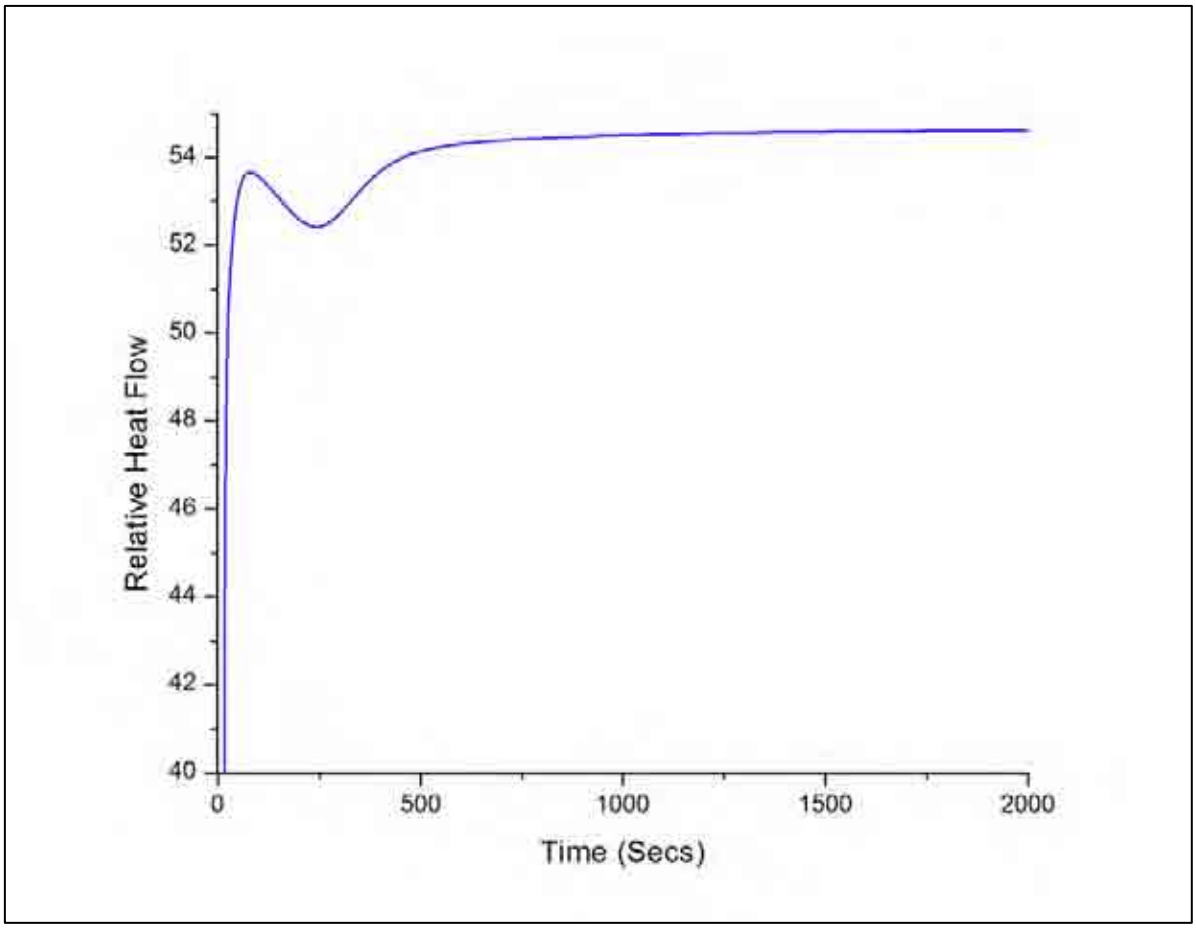

Figure 4.1 Relative heat flow with time for 450PF at 311°C. Depicting crystallisation over time.

4.2.1.1 Avrami Analysis

$$X_t = \left[1 - \exp\left(-Zt^n\right)\right]$$ (Eq. 1) – See Page 10

This equation can then be expressed as the equation of a straight line,

$$\log\left[-\ln\left(1 - \frac{X_t}{X_\infty}\right)\right] = n\log t + \log Z$$ (Eq. 2) – See Page 11

where the components are representative of y = mx + c, respectively.

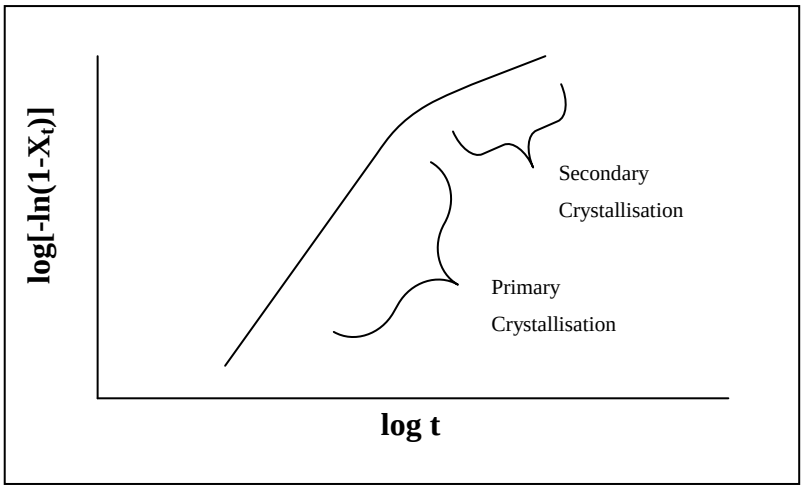

Figure 4.2 Schematic diagram of Primary and Secondary crystallisation

The end of the primary process is then found by inspection.

Using the rate constant Z, and the n value, the half-life, $t_{1/2}$, could then be calculated for the primary process, by re-arranging the equation,

$$Z = \frac{\ln 2}{(t_{1/2})^n} \qquad \text{(Eq. 3)}$$

4.2.1.2 Differential Avrami Analysis

The Avrami equation is used to determine the extent of crystallisation for isothermal melt-crystallisation related to time, t.

$$1 - \frac{X_t}{X_\infty} = \exp(-Zt^n) \qquad \text{(Eq. 6)}$$

This can then be re-arranged to give

$$n = t\left(\frac{dX_t}{dt}\right)\left[\left(1 - \frac{X_t}{X_\infty}\right)\ln\left(1 - \frac{X_t}{X_\infty}\right)\right] \qquad \text{(Eq. 7)}$$

The n value here is diagnostic of the transition between primary and secondary crystallisation of the polymer.

An average of the rate constant Z was calculated from the half-life, $t_{1/2}$, and the Avrami exponent n at $t_{1/2}$ using

$$Z = \frac{\ln 2}{(t_{1/2})^n} \qquad \text{(Eq. 3)}$$

4.2.2 Non-Isothermal crystallisation

A Perkin Elmer DSC 7 interfaced to a PC was also used to measure variation in relative heat flow with temperature. The DSC was again calibrated using the melting points of high purity metals: Zinc (T_m = ºC) and Indium (T_m = 156.63 ºC). Similar to the Isothermal experiments, samples were heated to 380°C, and held for two minutes to ensure a full amorphous state was reached. The samples were then cooled from 380°C at a range of cooling rates from 10°Cmin^{-1} to 100°Cmin^{-1}, to below T_g, approximately 140°C.

4.3 FTIR – Fourier Transform Infra-Red Spectroscopy

Infra-red (IR) spectra were obtained using an attenuated total reflectance (ATR) cell with a Nicolet MAGNA 860 FTIR spectrometer (spectral range 4000–700 cm^{-1} and resolution 2 cm^{-1}). The ATR accessory (ATR single reflection Golden Gate) uses a diamond crystal, and has a spectral range of 4000–650 cm^{-1}.

Slight variation in recorded spectra may occur when using ATR techniques, especially with regions of high absorption bands. The refractive index of a material can change rapidly in the region of absorption, with a derivative-shaped appearance centred around the centre of the absorption wavelength. The sharp rise in refractive index may cause the criterion of internal reflection to be lost. This is due to the nature of the penetration depth being directly proportional to the wavelength. The net result is a slight distortion of the peak shape and a shift to lower frequency[39]. The spectral software, OMNIC, used to record the spectra uses an internal algorithm to account for any of the previously mentioned problems, and corrects for them.

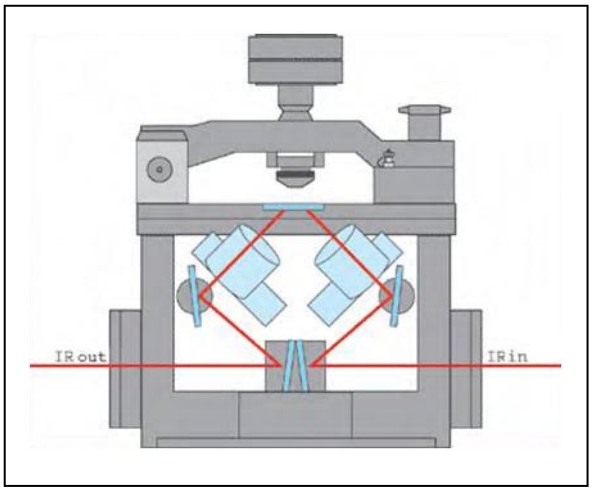

Figure 4.3 Schematic of the ATR accessory used in conjunction with the FTIR.

A PC interface then allows for the spectra to be recorded and analysed. Using the OMNIC software available, spectra was taken at 1cm^{-1} resolution over 600 scans. This allowed the data to be as accurate as possible, and with 600 scans per sample, noise reduction could be optimised. An example of the recorded spectra can be seen in fig. 4.4.

It is clear that the absorbance bands are overlapped and further analysis of the peak areas required deconvolution of the peaks. This was achieved using the Nicolet OMNIC software. The data was first subjected to a baseline correction through the spectral range of interest (1400-1000cm^{-1}) to remove the slope in the spectra. The deconvolution fitting was then achieved through a fitting algorithm similar to that of the Pearson VII function[46].

When dealing with spectra that have different degrees of overlap, a sum of several Pearson VII lines can be used. The Pearson VII function provides variety of peak shapes from Gaussian to Lorentzian and others. Examples of the Pearson VII lines are shown below in equation 8.

$$A(\nu) = \sum_{i=0}^{n} \frac{A_{i,o}}{\left[1+4Z_i^2\left(2^{\frac{1}{m_i}}-1\right)\right]^{m_i}} + \text{noise} \qquad \text{(Eq. 8)}$$

where $A_{i,0}$ is the absorbance in the centre of the peak i, $Z_i = (\nu - \nu_{i,0})/H_i$, where $\nu_{i,0}$ is the peak position of peak i, H_i the half width of peak i, m_i the tailing factor of peak i, and n is the number of peaks[46]. This is assuming that the peaks are all of Lorentzian shape[41].

The algorithm that the OMNIC software uses is the Fletcher-Powell-McCormick algorithm (information held by Thermo Fisher Scientific)[47] and the only other parameters used within the OMNIC software when producing the deconvolutions, was the target noise, which was set to 10.0 by default. An example of the deconvoluted peaks can been seen in fig. 4.5.

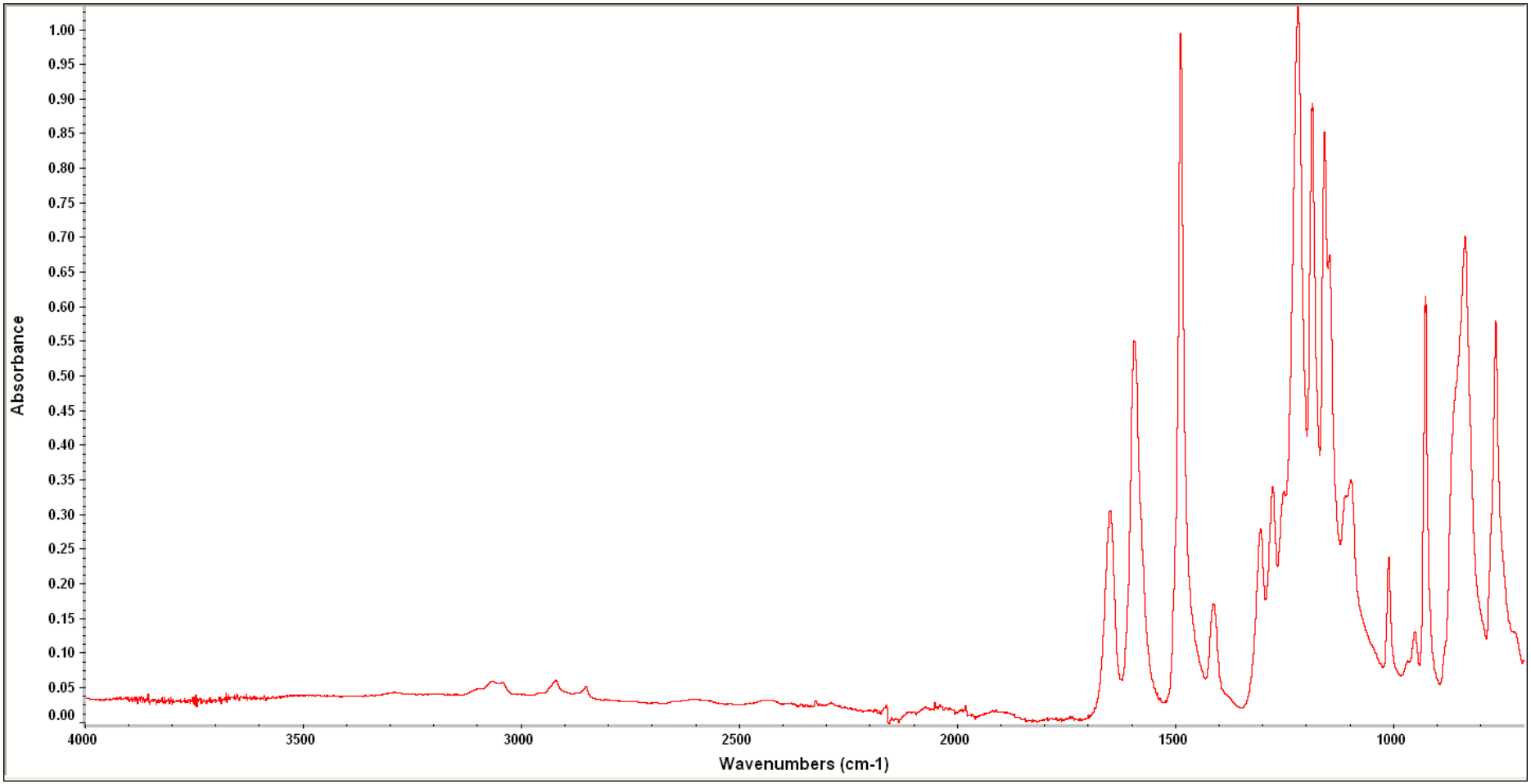

Figure 4.4 FTIR spectra of amorphous 450PF PEEK.

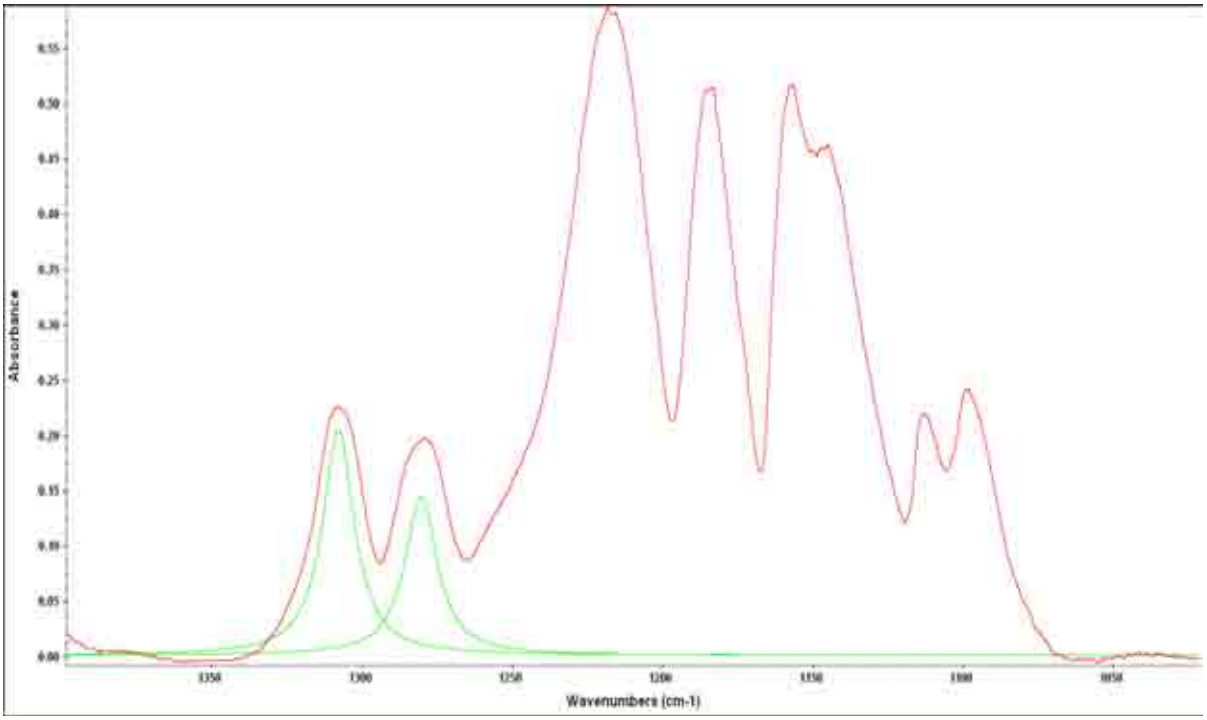

Fig 4.5 An example of the deconvoluted peaks within the 'Chalmers region' for 450PF cooled at 10°Cmin^{-1}

4.4 Measurement of the degree of crystallinity

Samples were conditioned using conventional DSC as mentioned previously, and 10 identical samples cooled at 100°Cmin^{-1} were produced. Testing of these samples was performed by Perkin Elmer[48] at their laboratories and a range of heating rates were applied to these samples, ranging from conventional heating rates to Hyper-DSC cooling rates in excess of 700°Cmin^{-1}. All of the measurements of degree of crystallinity were performed in line with ISO 11357-3[49].

5.0 Results and Discussion

5.1 Characterisation of Crystallisation using DSC

5.1.1 450PF – Isothermal Crystallisation and Avrami analysis

Figure 5.0 shows the crystallisation traces obtained from the isothermal experiments completed using DSC.

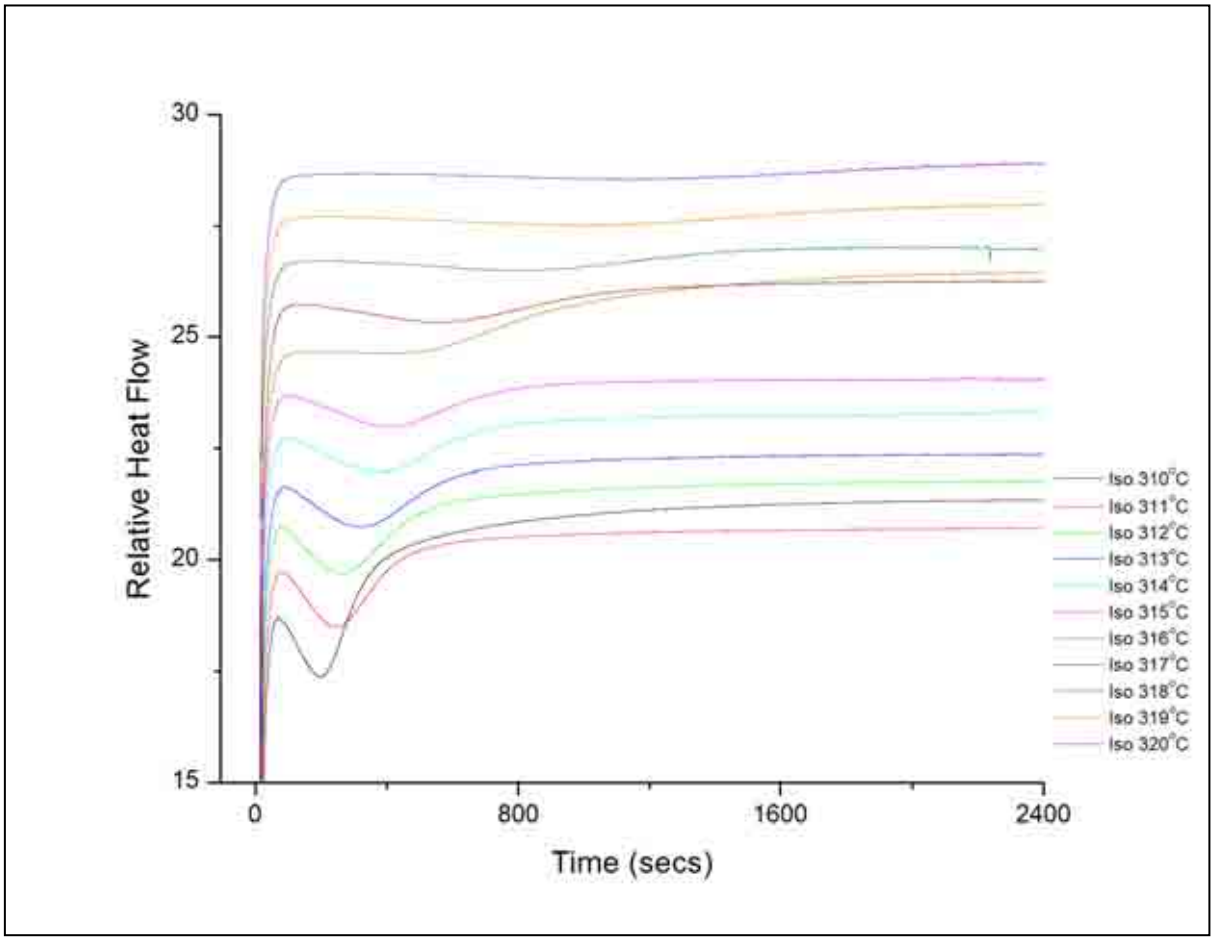

Figure 5.0 Relative heat flow with time for isothermal crystallisation of 450PF. Traces are staggered for clarity.

From figure 5.0, it is clear to see the exothermic process which is characteristic of an isothermal crystallisation. The minima of the trace shows that heat is being dissipated from the polymer as crystallisation occurs. This exothermic response is a result of the chain behaviour of polymer molecules with other neighbouring chains within close proximity. If the factors effecting the relative position to one another are favourable, then chain mobility and ordering can take place. This ordering of chains into firstly, a parallel array to form a nucleus, is aided by secondary valence forces keeping molecular packing stabilised as the nucleus forms[2]. This is then preceded by the growth of the available nuclei to form the three-dimensional crystalline phase.

The time corresponding to the minima of the trace, is the Half-time, $t_{1/2}$, assuming there is little secondary crystallisation, it is related to the time in which it takes 50% of the crystallisation process to take place. It is clear from fig 5.1, that $t_{1/2}$ varies with crystallisation temperature (T_c), in that T_c increases, so does the half-life. It is also apparent that with increased crystallisation temperature, it is easier to observe the start of the crystallisation process. This originates from the development of an induction time for the crystallisation process at the elevated region of the temperature range, which is evidence of the effect of decreased nucleation density at these elevated temperatures.

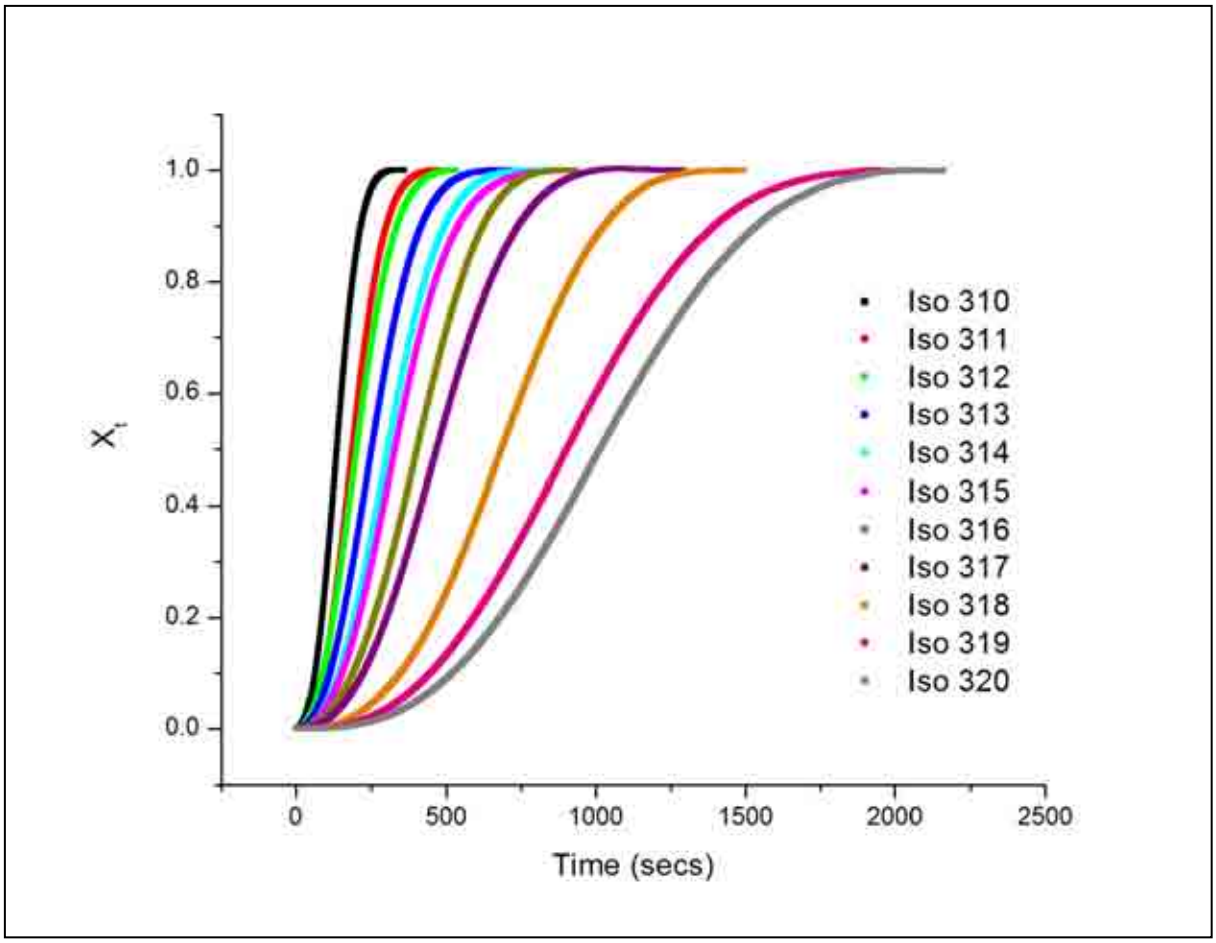

Figure 5.1 development of relative crystallinity, X_t, with time t, for 450PF isothermal crystallisation.

The relative crystallinity was calculated by evaluating the cumulative area and the total area contained within the exotherms shown in figure 5.0 according to equation 5. The variation of relative crystallinity with time for each crystallisation temperature is shown in fig 5.1. As noted previously, the effect of crystallisation temperature on the half-life and induction time are again apparent.

$$\frac{X_t}{X_x} = \frac{\int_0^t \left(dH_t / dt \right) dt}{\int_0^\infty \left(dH_t / dt \right) dt} \qquad \text{(Eq. 5)}$$

The variation of X_c with time can be analysed using the Avrami equation, seen in Eq. 1. This approach yields kinetic data for the process which comprises of the rate constant (Z), the half-life ($t_{1/2}$) and the mechanistic constant (n). A typical plot of $\ln(-\ln(1-X_t)$ against ln t is shown in fig 5.2a. Two linear sections can be observed, the first linear section corresponds to the primary process (over which the Avrami equation applies) and a second linear section of reduced slope, which corresponds to the secondary processes (over which the Avrami equation does not apply). The transition from primary to secondary crystallisation processes is not well defined and corresponds to the section of the plot in which the slope is changing.

In this approach, the end of the primary process is found by inspection and then the linear regression analysis is limited to the first linear section of the plot. A representation of a theoretical, ideal double-log plot can be seen in fig. 5.2b. Of course, given the logarithmic nature of the time axis, this approach can lead to significant errors in the determination of the rate constant and as a consequence, the half-life. Nevertheless, the Avrami equation is commonly used in the characterisation of crystallisation.

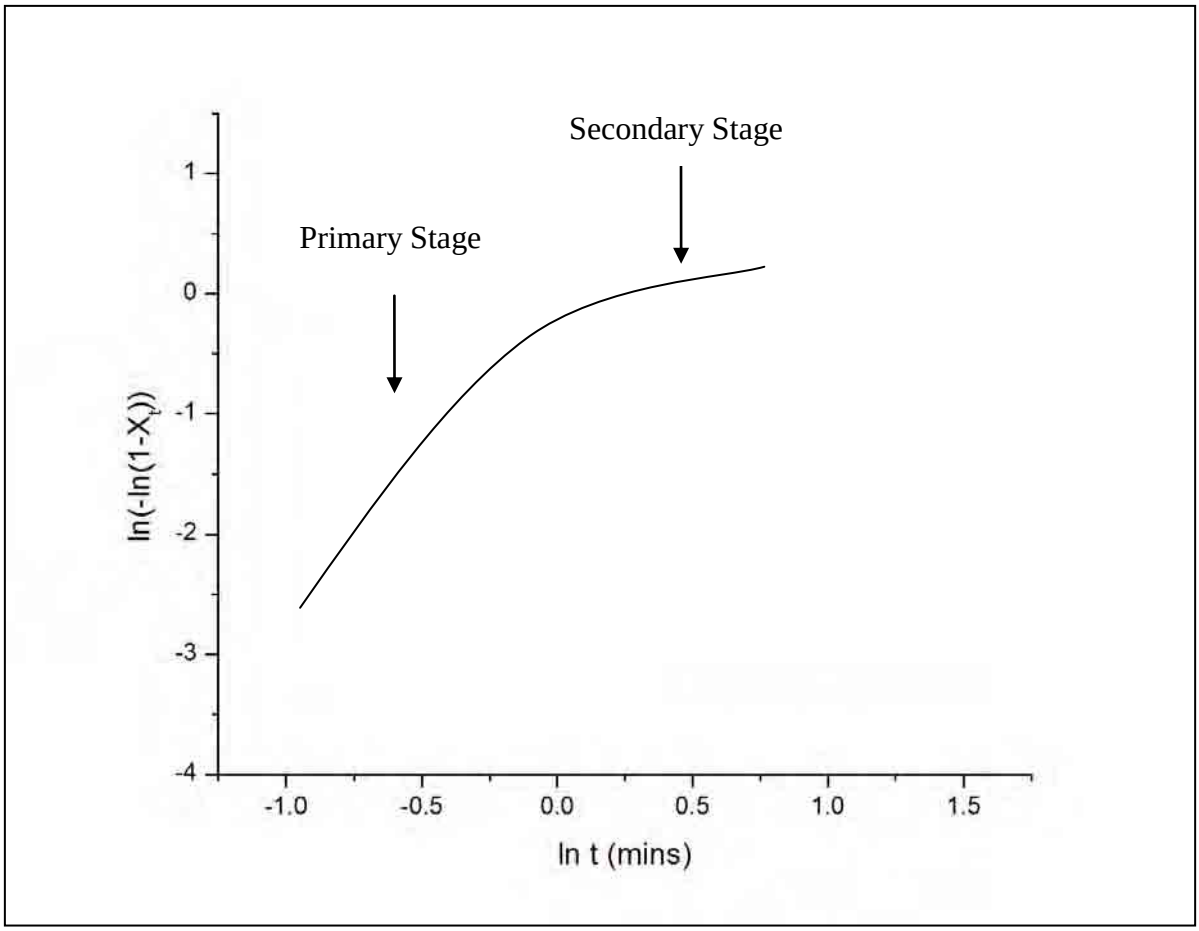

Figure 5.2a Typical double log plot used to determine both n and Z values.

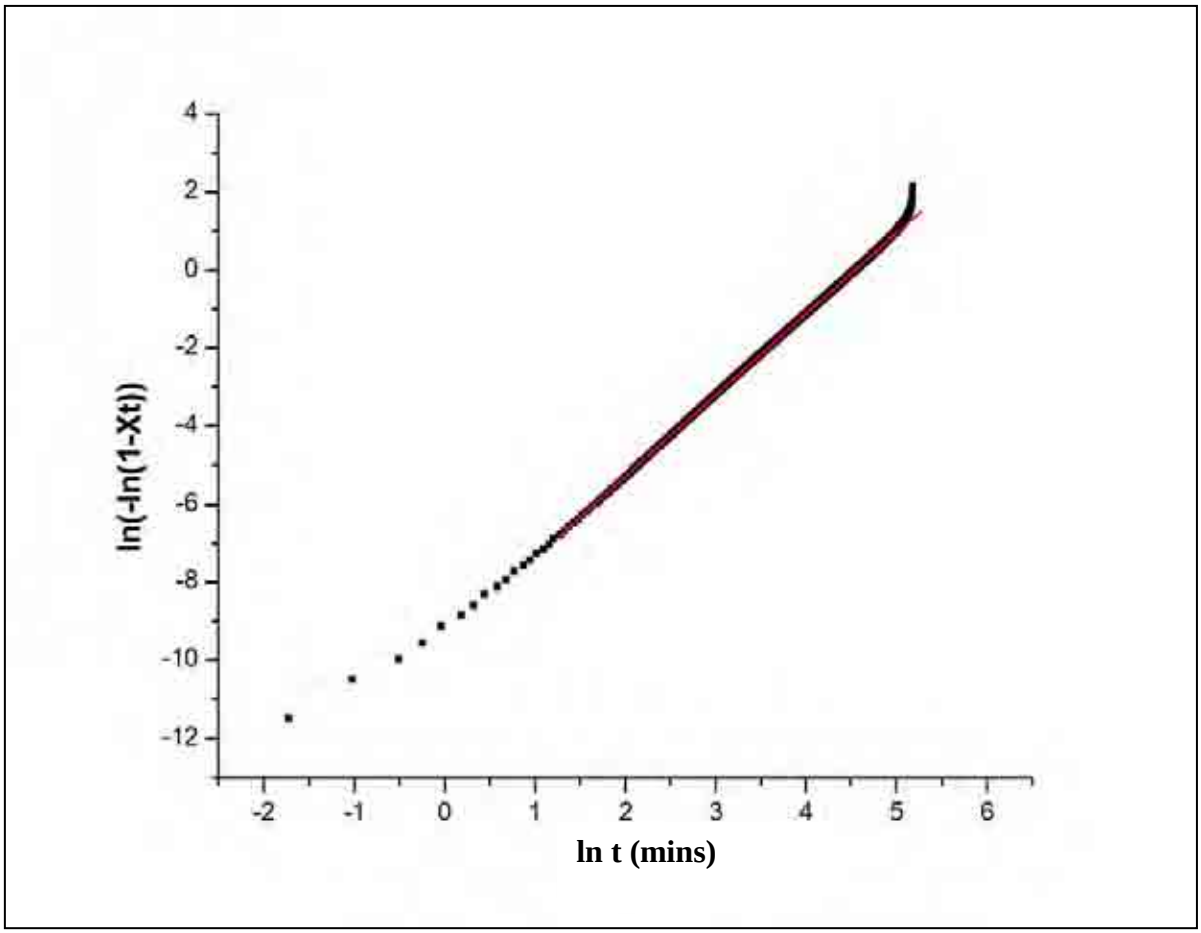

Figure 5.2b Typical linear fit of a double log plot to determine both n and Z values (Experimental data).

Figure 5.2b shows a typical double-log plot produced from experimental data. As you can see, the data does not conform to the ideal depiction seen in fig. 5.2a. Although the appearance of the plot does not conform to that of the ideal, the graph is still significant as it clearly depicts the point of deflection from primary process to secondary. The red linear fit line was plotted on the first linear section of the double-log plot. This linear fit was produced on the most linear section of the plot before the data deflects in the vertical direction, thus indicating the change from primary to secondary crystallisation processes.

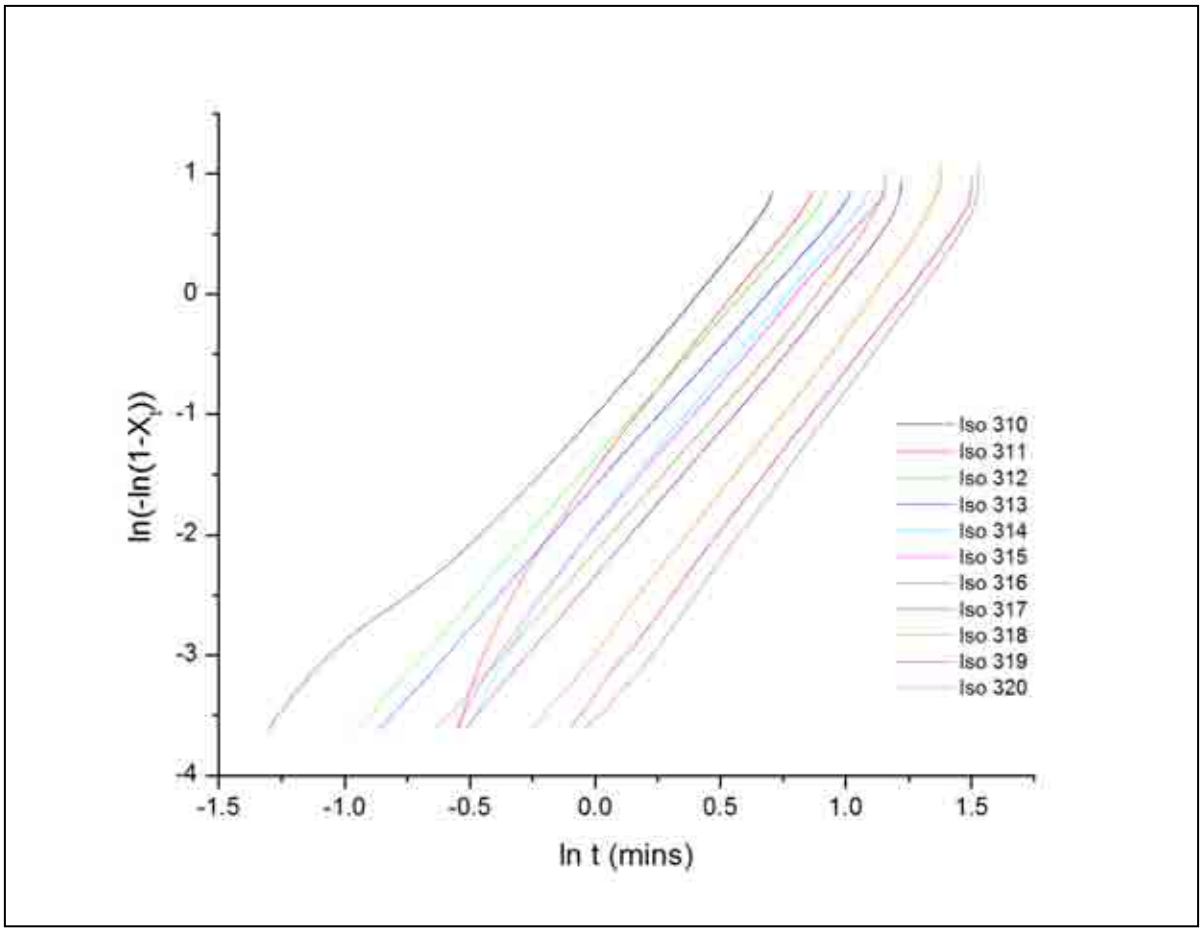

Figure 5.3 Double log plot for Isothermal Crystallisation of 450PF.

From the double-log plot, the Z value and n value could then be calculated for the isothermal crystallisation. The relevant n and Z values for the isothermal crystallisation temperatures are presented in table 5.0. From the calculated n values, there is no strong trend across the differing isothermal crystallisation temperatures, however, at the higher temperatures between 318-320°C, n tends to be closer to 3. This shows that there may be a change in dimensions of the crystallites formed during crystallisation closer to the melt. As mentioned by Cowie, 1991[2], the numerical value of n refers to the dimensional mechanism that is at work within the polymer. The change of value from 2 to 3 at higher crystallisation temperatures would suggest a change from disc-like crystallites to spherulites[12]. Although the n values are

calculated from experimental data, it cannot always be a true prediction of the unit shape, and non-integer values show that morphological units cannot always be of discrete dimensions[2].

Table 5.0 Kinetic values for isothermally crystallised 450PF

Temperature (°C)	n Value	Z Value (±0.01)	$t_{1/2}$ 1° (secs)
310	2.51	0.36	77.7
311	2.59	0.24	90.9
312	2.34	0.25	92.4
313	2.35	0.2	101.6
314	2.49	0.15	111.5
315	2.4	0.14	115.6
316	2.52	0.11	123.6
317	2.52	0.09	133.5
318	2.78	0.05	157.6
319	2.72	0.04	179.3
320	2.86	0.03	189.1

Values for the rate constant, Z, were calculated from the y-intercept of the double-log linear fit, and are tabulated as mentioned previously. If we plot the Z value against the isothermal crystallisation temperature we can see the trend that occurs as T_c is increased (see fig 5.4).

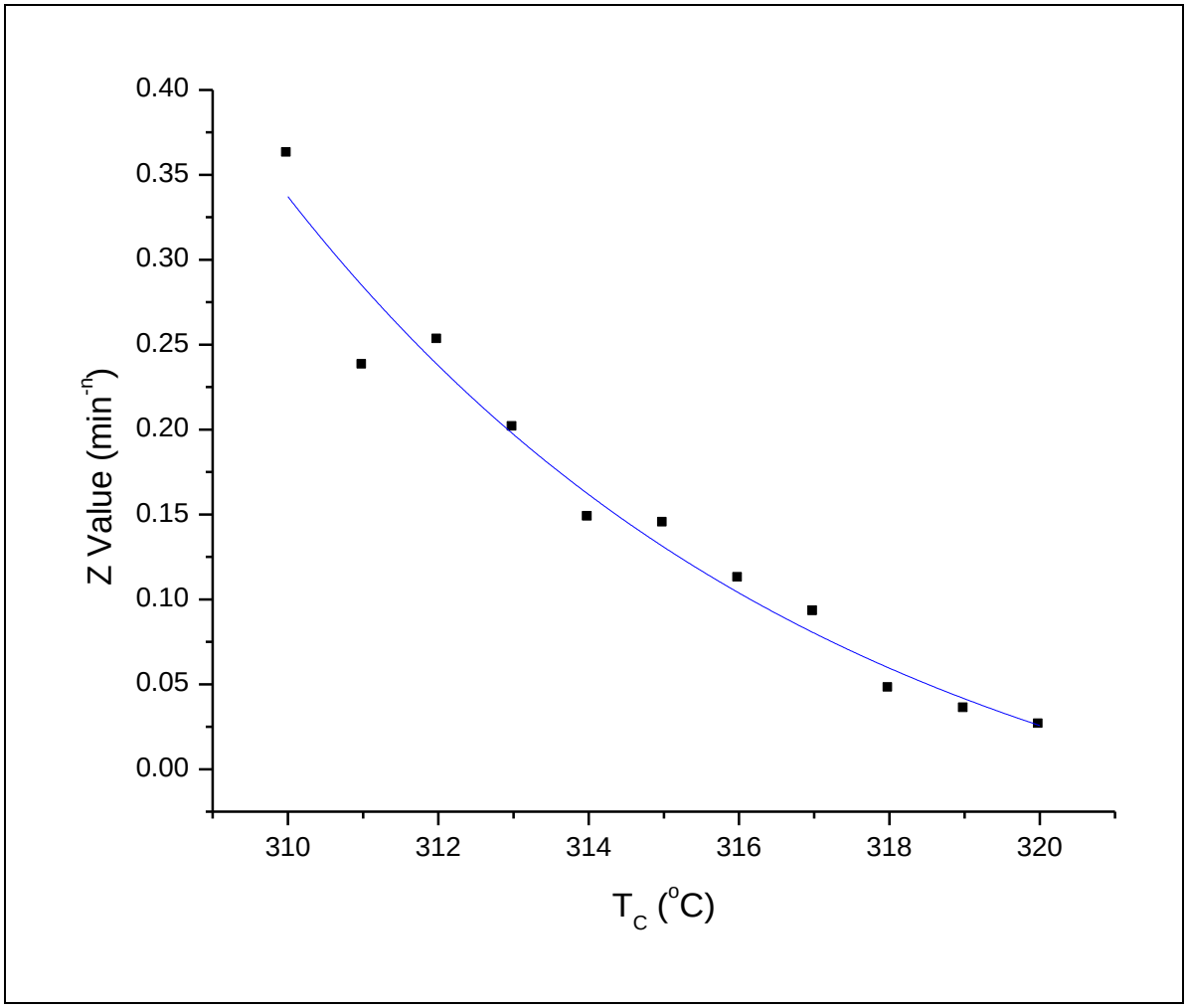

Figure 5.4 Rate constant, Z, against crystallisation temperature for 450PF.

As seen in fig 5.4 the rate of crystallisation is significantly faster at temperatures closer to the T_g, and in comparison, the rate of crystallisation is notably slower as temperatures tend towards the melt.

From the Z value and n value, the half-time, $t_{1/2}$, can be calculated by re-arranging eq. 3. These values are also tabulated in table 5.0. Plotting the values of the half-time, reinforces the trends seen with the rate values. In figure 5.5 it is clear to see the increase in time for half of the crystallisation to be complete, as the crystallisation temperature nears T_m. This increase in $t_{1/2}$ for increased T_c has been widely researched and many models offer explanation to the increase in $t_{1/2}$.

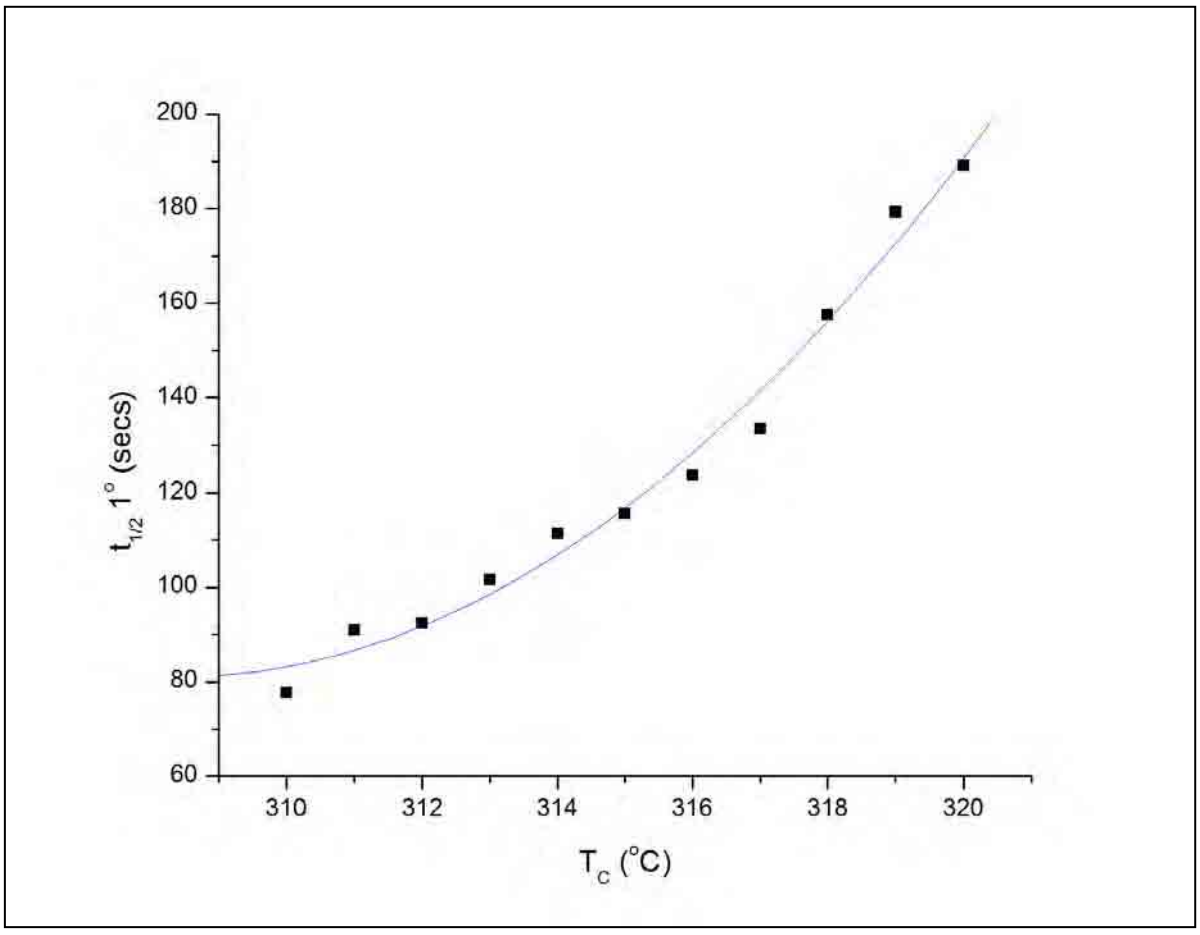

Figure 5.5 Half-life of the primary process against crystallisation temperature in 450PF.

The relationship of increased $t_{1/2}$ with increasing T_c can be described using one of two theories. The growth theory as described by the Turnbull-Fisher model[50], uses a dual

exponential model to outline how growth changes towards temperatures near the T_m. The basic principle of the Turnbull-Fisher model (see fig 5.6) is that at crystallisation temperatures above but close to the glass transition, T_g, the molecular chains cannot reptate and align themselves rapidly due to the high viscosity of the liquid phase. This therefore increases the time in which nucleation embryos take to grow and form spherulites. As seen in fig 5.6 the radial growth rate increases with temperature until a maximum somewhere between the T_g and T_m. It also shows the opposite is therefore true as temperatures climb towards the melt, T_m. Here the chain mobility is increased significantly with the amount of energy within the system. This therefore allows chain realignment to occur easier and faster, which in turn increases the growth rate.

Secondly the Hoffman-Lauritzen model[51] describes the nucleation event and is still in widespread use today. As temperature increases towards the melt, T_m, the ability of chain re-alignment is easier due to reduced viscosity of the melt and the increase of free energy within the system, so much so that any potential nuclei is disrupted before growth can take place. This therefore increases the time taken for the polymer to nucleate and form spherulitic crystallites. However, as temperatures reach close to the T_g, the opposite effect takes place, causing the chains to decrease their mobility and the viscosity of the liquid phase increases. This decreases the possibility of potential nuclei embryos being disrupted and therefore being able to form nucleation sites for spherulitic growth. These embryos either shrink and dissolve back into the liquid phase or become large enough to reach a critical size. Once this critical size has been reached, there is a higher probability that the nucleus will become stable enough to grow rather than dissolve into the liquid parent phase. The then stable nuclei will be able to grow within the bulk non transformed volume at a rate which is temperature dependant. The

nucleation of the polymer can either be homogeneous or heterogeneous. Homogeneous nucleation is temperature dependant, taking place across the bulk of the parent material and occurs due to self-initiated chain folding and reaching the free-energy threshold. Heterogeneous nucleation occurs through pre-existing nucleation sites within the bulk polymer. These can be either catalytic agents within the material (added by manufacturers), or grain boundaries, impurities, or surface faults of the sample giving rise to nuclei formation. Although the nucleation rate within Heterogeneous nucleation should be constant, temperature variations within the system allow for fluctuations within the rates[52].

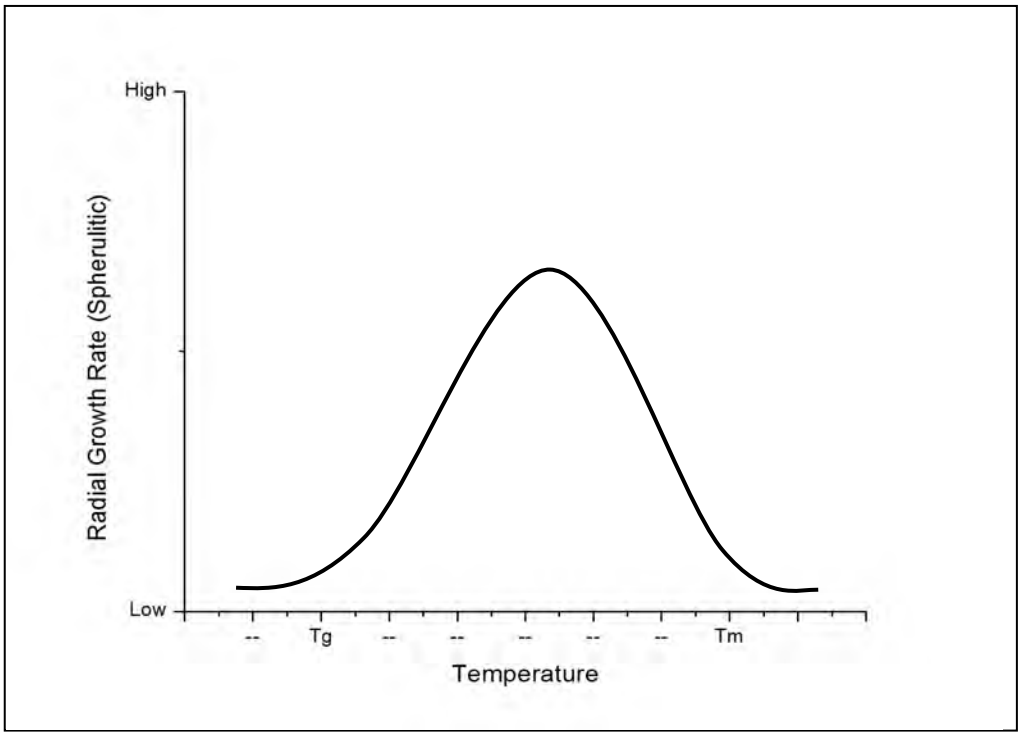

Figure 5.6 Radial growth rate of spherulitic crystallites as a function of temperature (Based on the Turnbull-Fisher model)[50].

These trends become more apparent when plotting both $t_{1/2}$ values and Z values against the crystallisation temperature (see fig 5.7). This clearer figure shows how the

increase in crystallisation temperature leads to a slower rate of crystallisation and an increase in time for half of the primary process to come to completion.

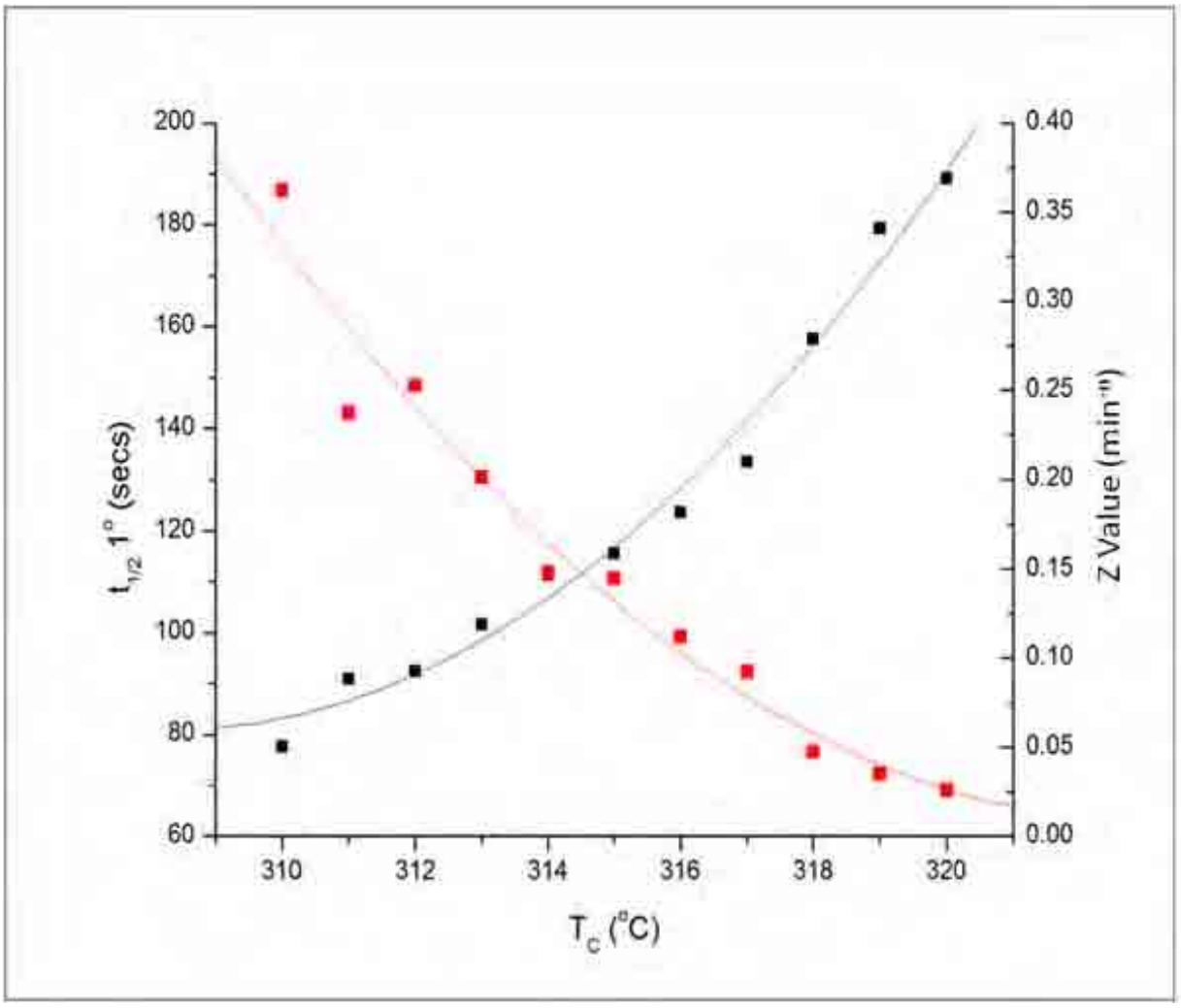

Figure 5.7 Combined figure showing both half-time. $t_{1/2}$, and rate constant, Z, against T_c for 450PF.

5.1.2 450PF – Differential Avrami Analysis

Using the differential form of the Avrami equation, the change in primary and secondary processes is marked by the observed change in value of the Avrami exponent, n.

$$n = t\left(\frac{dX_t}{dt}\right)\left[\left(1-\frac{X_t}{X_\infty}\right)\ln\left(1-\frac{X_t}{X_\infty}\right)\right] \qquad \text{(Eq. 7)}$$

Within the primary crystallisation process, theoretically, the n value should be constant, and any significant change will show a transition from primary to secondary processes[45, 53].

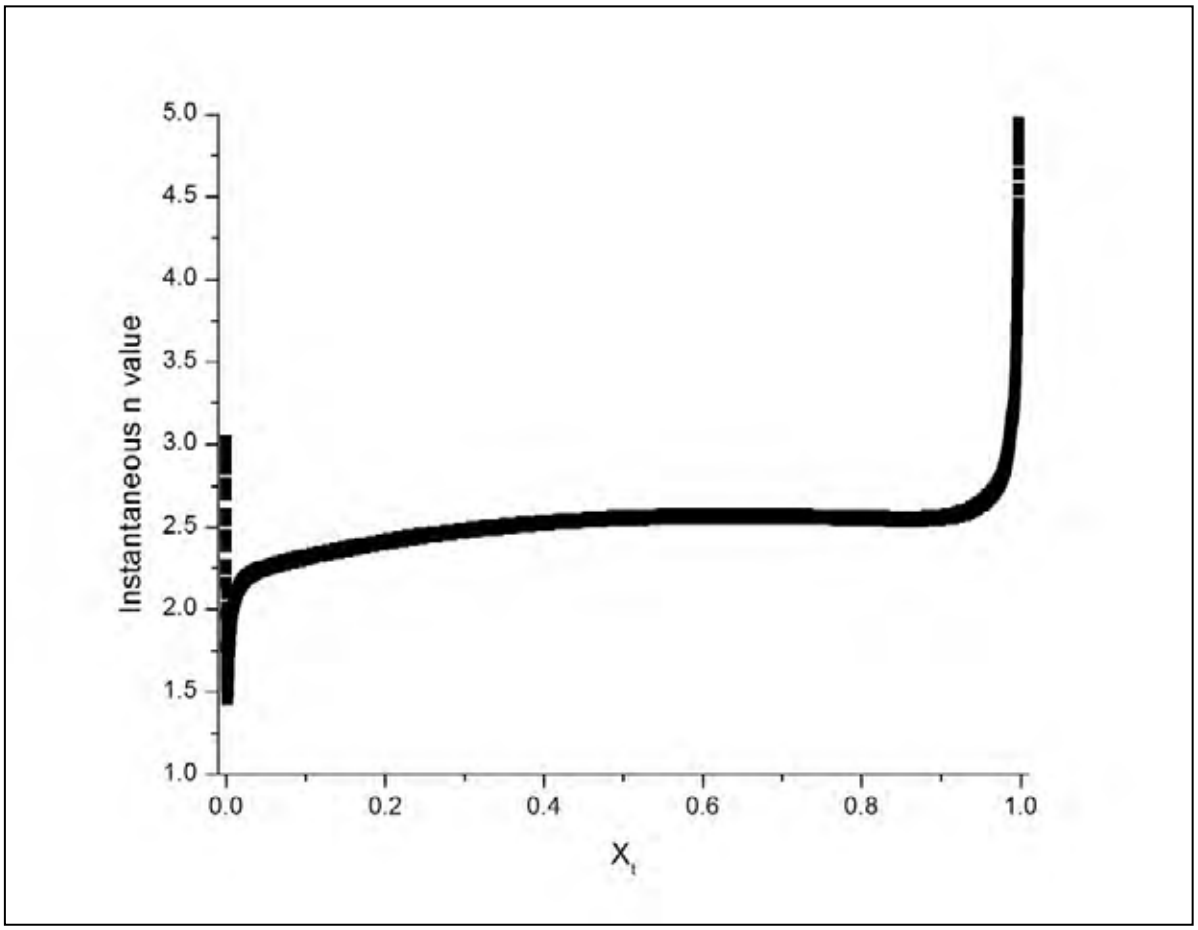

Figure 5.8 Instantaneous n values against relative crystallinity, X_t, for isothermal crystallinity at 310°C.

As seen in Fig 5.8 the Avrami component changes progressively from the erratic starting values until a plateau is reached, whereby the n value is steady and constant. As relative X_t increases towards 0.9 an increase in n value is clearly seen, thus marking the completion of the primary process and the change to secondary crystallisation[45].

The n values, z values and half time, $t_{1/2}$, for the differential method are calculated by the Avrami Software Program, which is a LabView based software that has been programmed to follow the differential Avrami equation and produce the parameters required. This differential approach of the Avrami analysis is a more analytical approach that distinguishes the primary process by the change in Avrami exponent, n. This technique is therefore more accurate when distinguishing the boundary between the primary and secondary processes than the conventional method, as it limits the effect of human error. Results of the output have been tabulated in 5.1.

Table 5.1 Differential Avrami output values for isothermally crystallised 450PF

Temperature (°C)	**310**	**311**	**312**	**313**	**314**	**315**	**316**	**317**	**318**	**319**	**320**
n Value (±0.01)	2.52	2.44	2.33	2.36	2.39	2.5	2.62	2.63	2.88	2.69	2.6
$t_{1/2}$ (secs)	2.4	3	3.6	4.2	4.8	5.4	6.6	7.8	11.4	15	16.8
Z value	2810.9	1120.6	579.9	378.7	280.3	284.1	217.9	140.8	82.78	28.6	24.7
$X_{p\infty}$	1	1	1	1	1	1	1	1	1	1	1

As seen with the conventional Avrami analysis technique, the $t_{1/2}$ values increase as crystallisation temperature increases (see fig 5.9 below). A decrease in crystallisation rate is also seen as crystallisation temperature increases towards the melt. Again, these observations are expected and correlate with the conventional Avrami analysis.

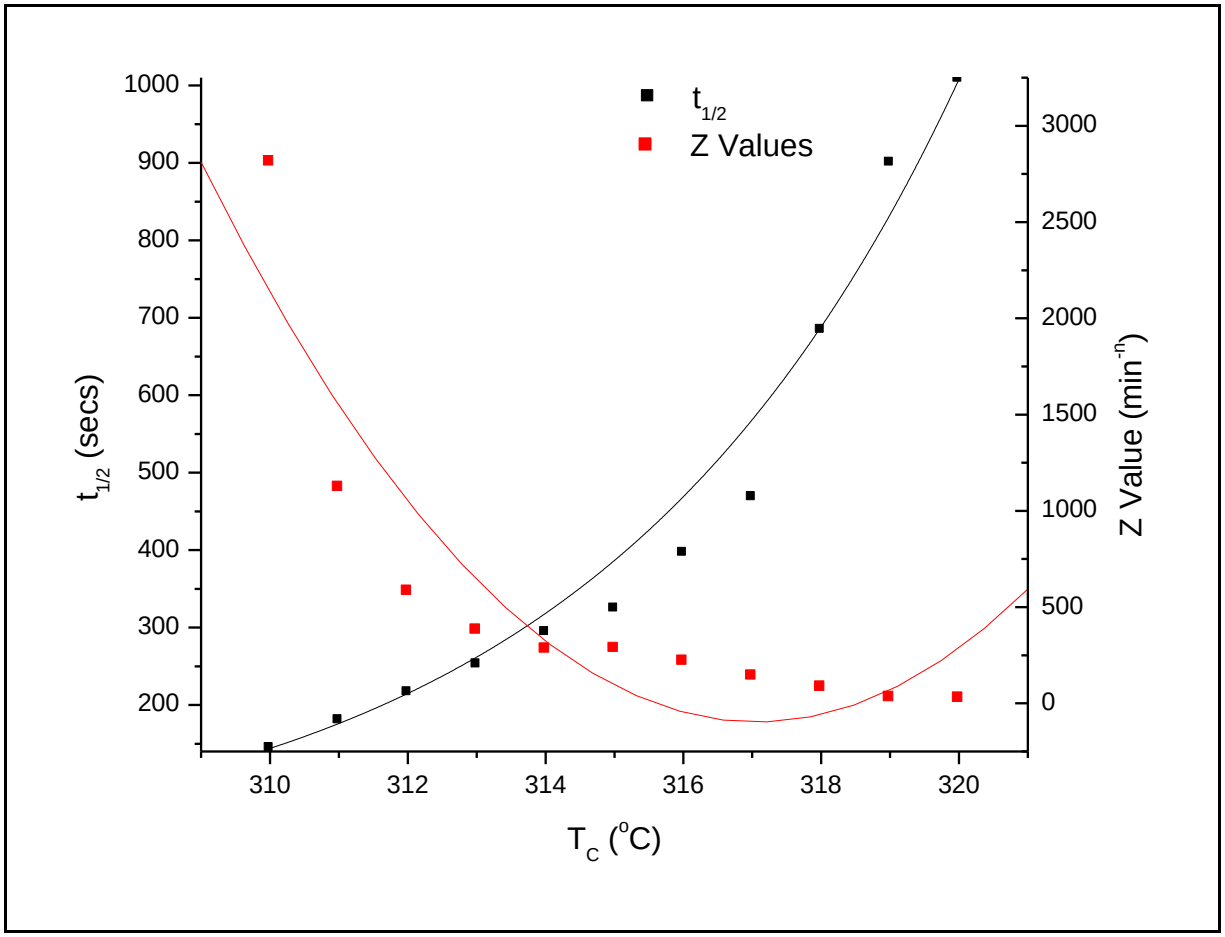

Figure 5.9 $t_{1/2}$ and Z values for isothermally crystallised 450PF, obtained through differential avrami analysis.

5.1.3 450CA30(Carbon Filled) – Isothermal crystallisation and Avrami analysis

Fig 5.10 below shows the isothermal DSC traces for the carbon filled PEEK grade 450CA30.

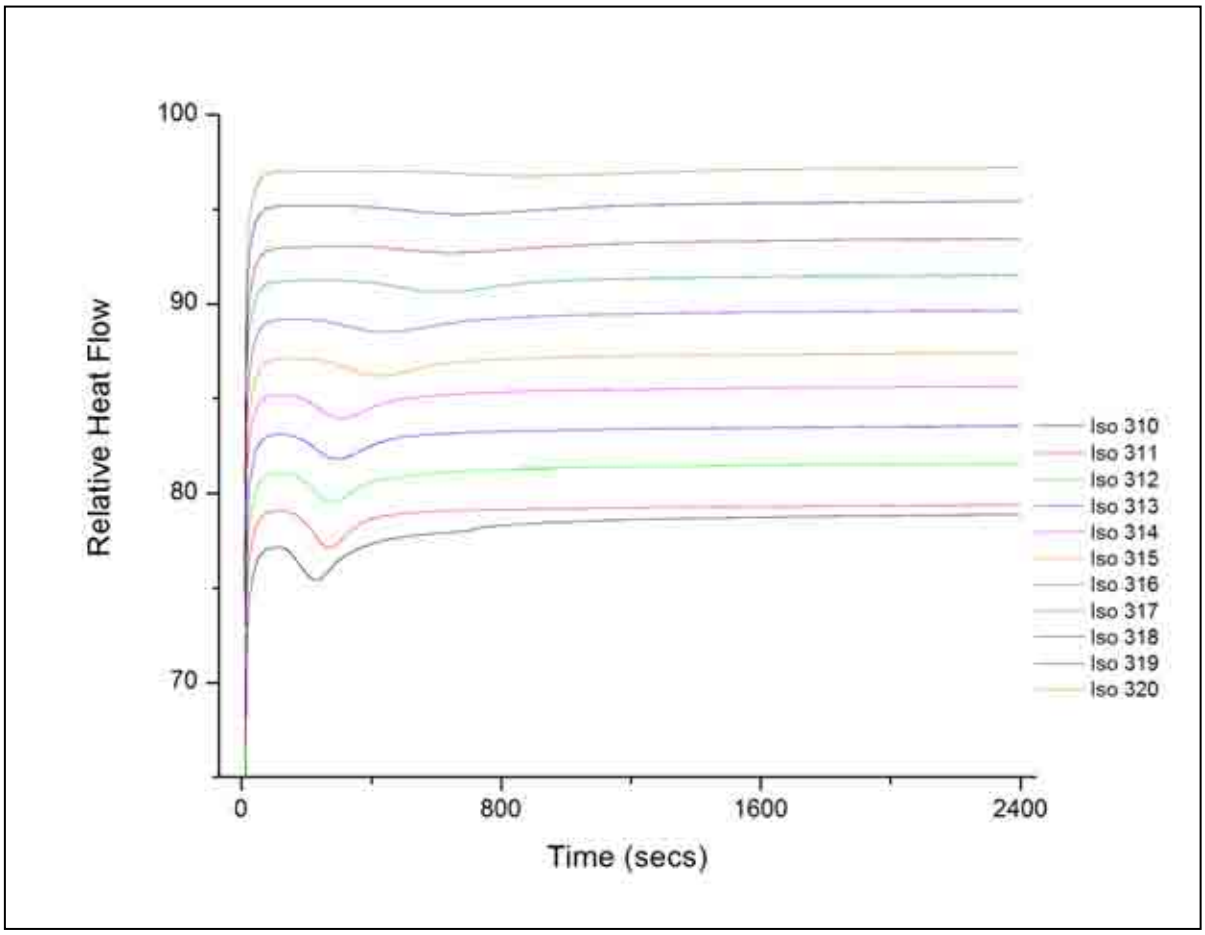

Figure 5.10 Relative heat flow against time for isothermal crystallisation of 450CA30. Traces are staggered for clarity.

As seen with the 450PF samples, the carbon filled samples also show a trend of shifting minima of the trace with increasing crystallisation temperature. It is also clear that the same exothermic process of crystallisation is occurring as within the pure PEEK sample.

Fig 5.11, shows the development of relative crystallinity with time, t, for the 450CA30 samples, which were also obtained by the integration of the relative heat flow curves using equation 5, mentioned previously. Again, both primary and secondary processes are present, limiting the data to the primary process will have to be addressed, as previously shown for the 450PF samples. It is clear to see that the same trends are apparent with increasing T_c and that the time for the crystallisation process to be completed increases with temperatures nearing the melting temperature.

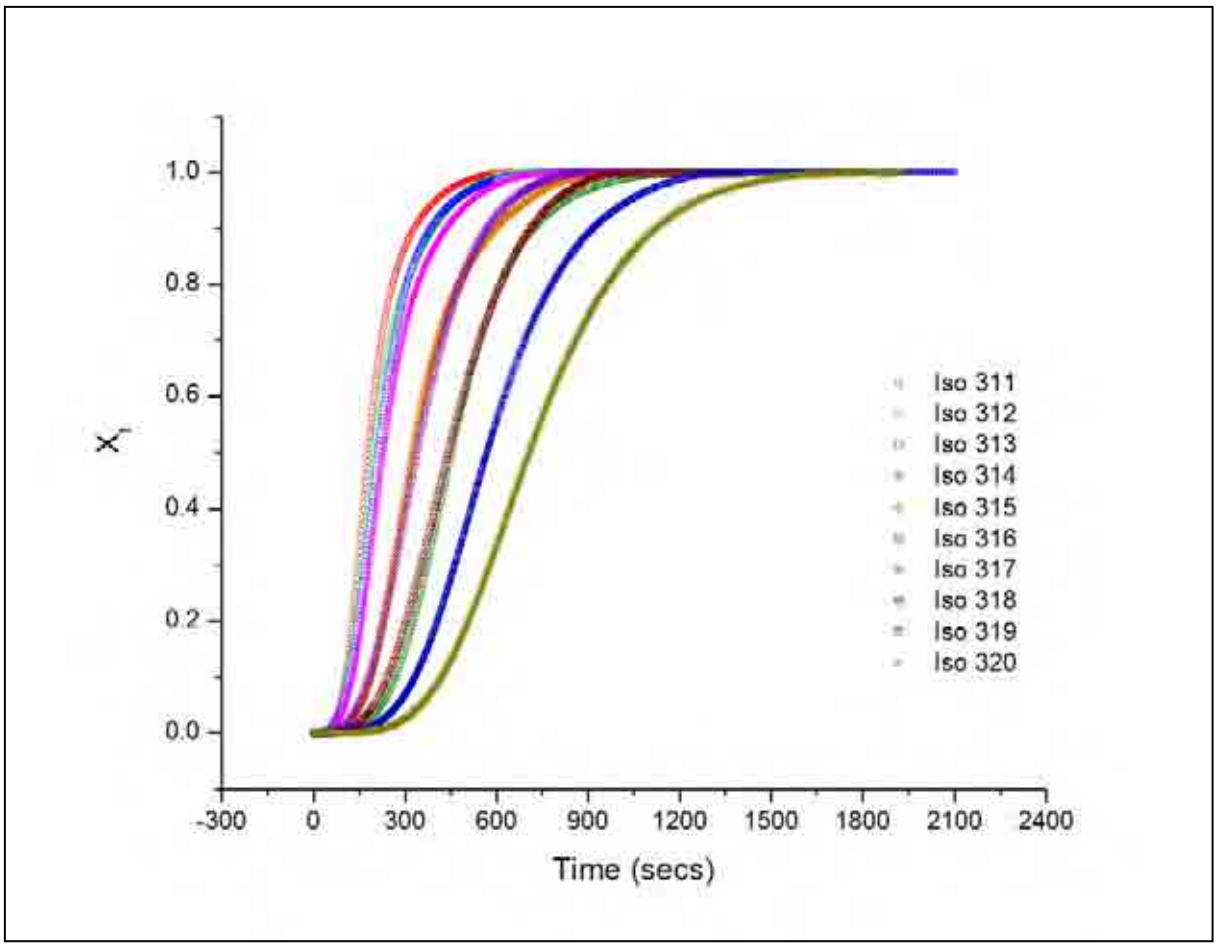

Figure 5.11 Development of relative crystallinity, X_t with time, t, for 450CA30 isothermal crystallisation.

Similar to that of the 450PF results, the relative crystallinity can be expressed as a line function in order to analyse, $X_c - t$, in terms of the Avrami equation. This is done by the creation of the double-log plot (see section 5.1.1).

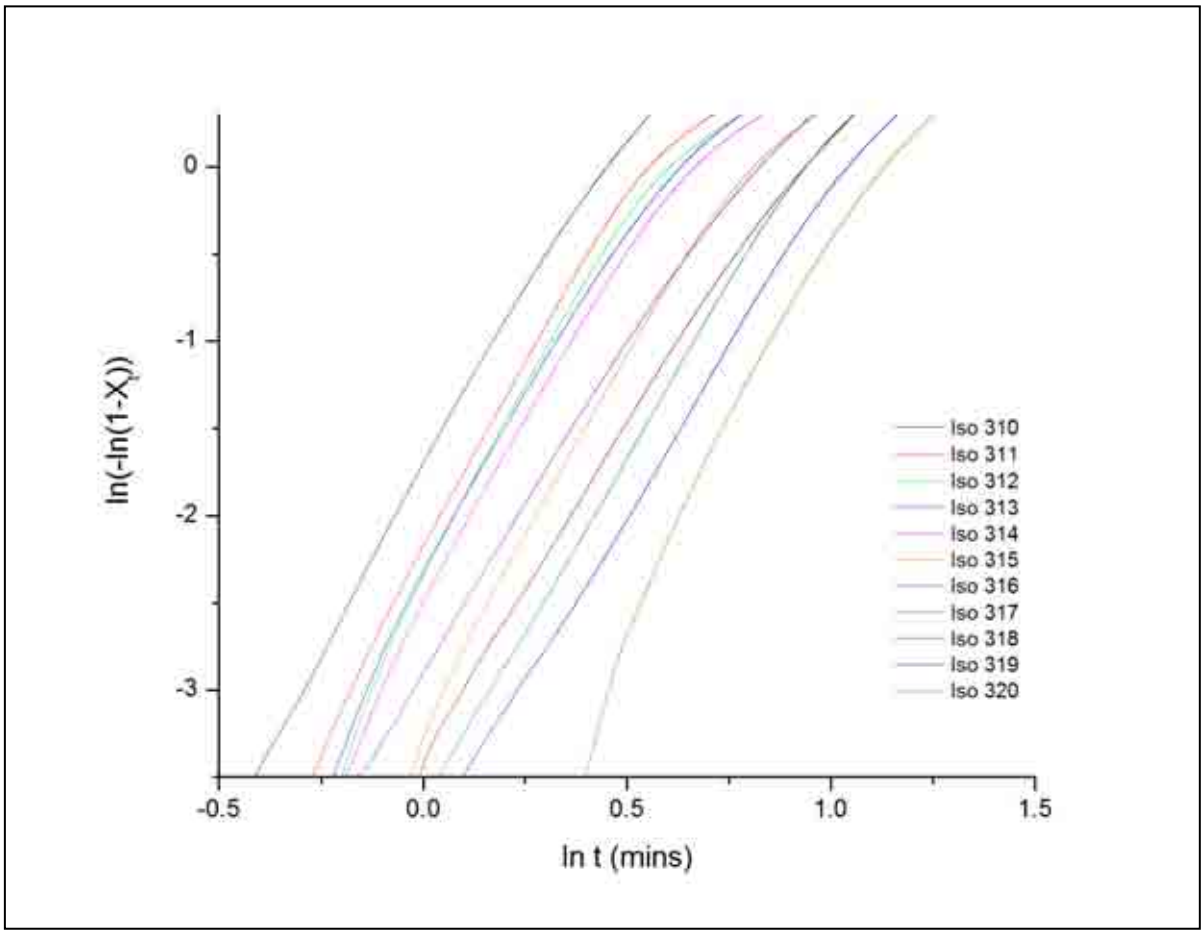

Figure 5.12 Double log plot for Isothermal Crystallisation of 450CA30.

It is clear to see the increase in gradient for the 450CA30 samples at both lower and higher temperatures. This may suggest that the fibre content in the filled grade is affecting the n value, and therefore the geometry of the morphological units within the polymer matrix. This can also be shown by calculating the n value from the gradient of the double-log plot. The results of the n value, Z value and $t_{1/2}$ can be seen tabulated in table 5.2.

Table 5.2 Kinetic values for isothermally crystallised 450CA30

Temperature (°C)	n Value	Z Value (±0.01)	$t_{1/2}$ 1° (secs)
310	4.35	0.18	81.7
311	4.19	0.11	92.4
312	3.86	0.11	97.4
313	3.63	0.1	99.9
314	3.68	0.09	103.3
315	3.81	0.05	119.9
316	3.83	0.07	120.6
317	3.91	0.03	137.8
318	3.5	0.04	135.4
319	3.8	0.02	151.9
320	3.98	0.01	166.3

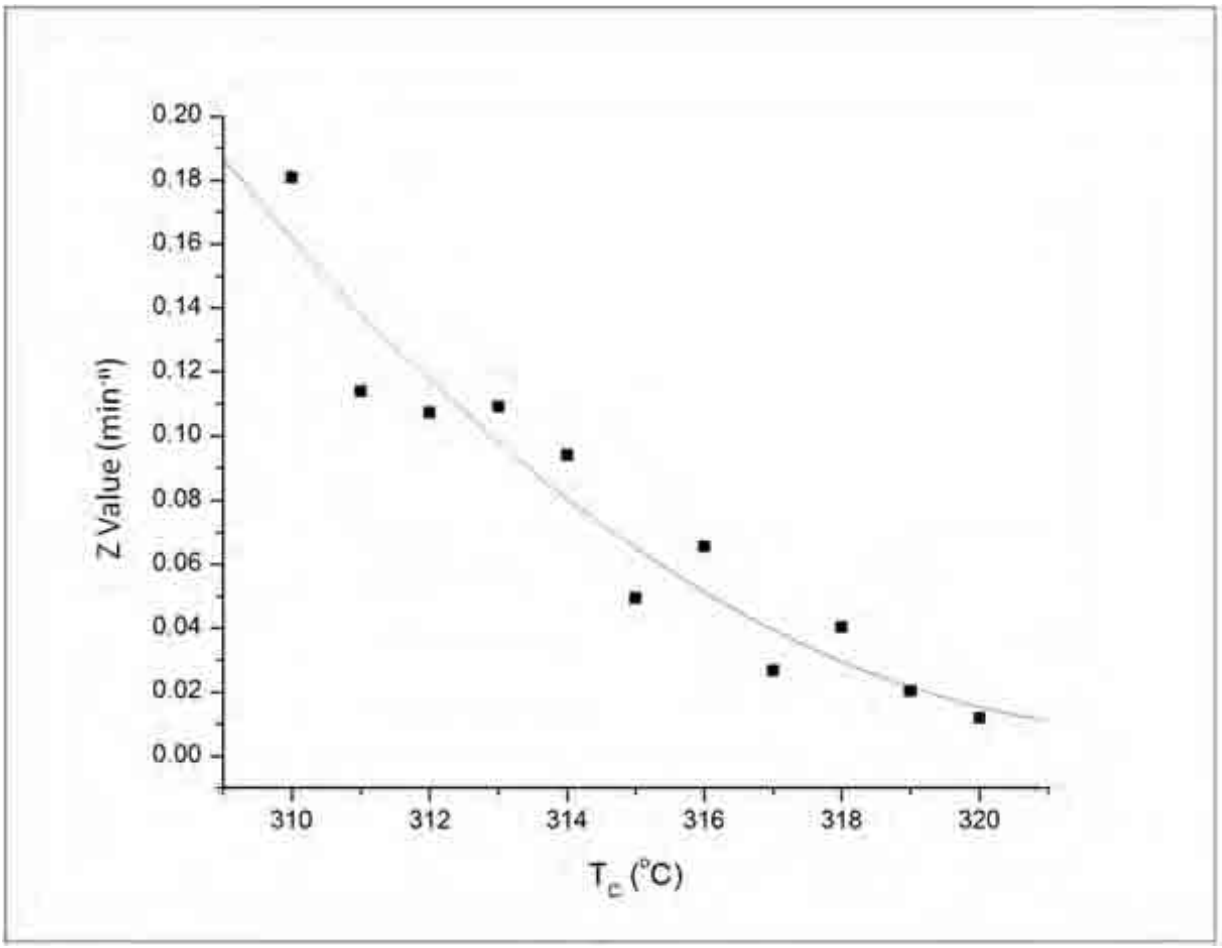

Figure 5.13 Rate constant, Z, against crystallisation temperature for 450CA30.

As seen in fig 5.13 for the Z value of 450CA30, it is clear that the same trends are apparent, that as crystallisation temperature increases the rate at which the polymer crystallises drops dramatically. Similar trends within the half-time values can be seen compared to the values of 450PF (see fig 5.14).

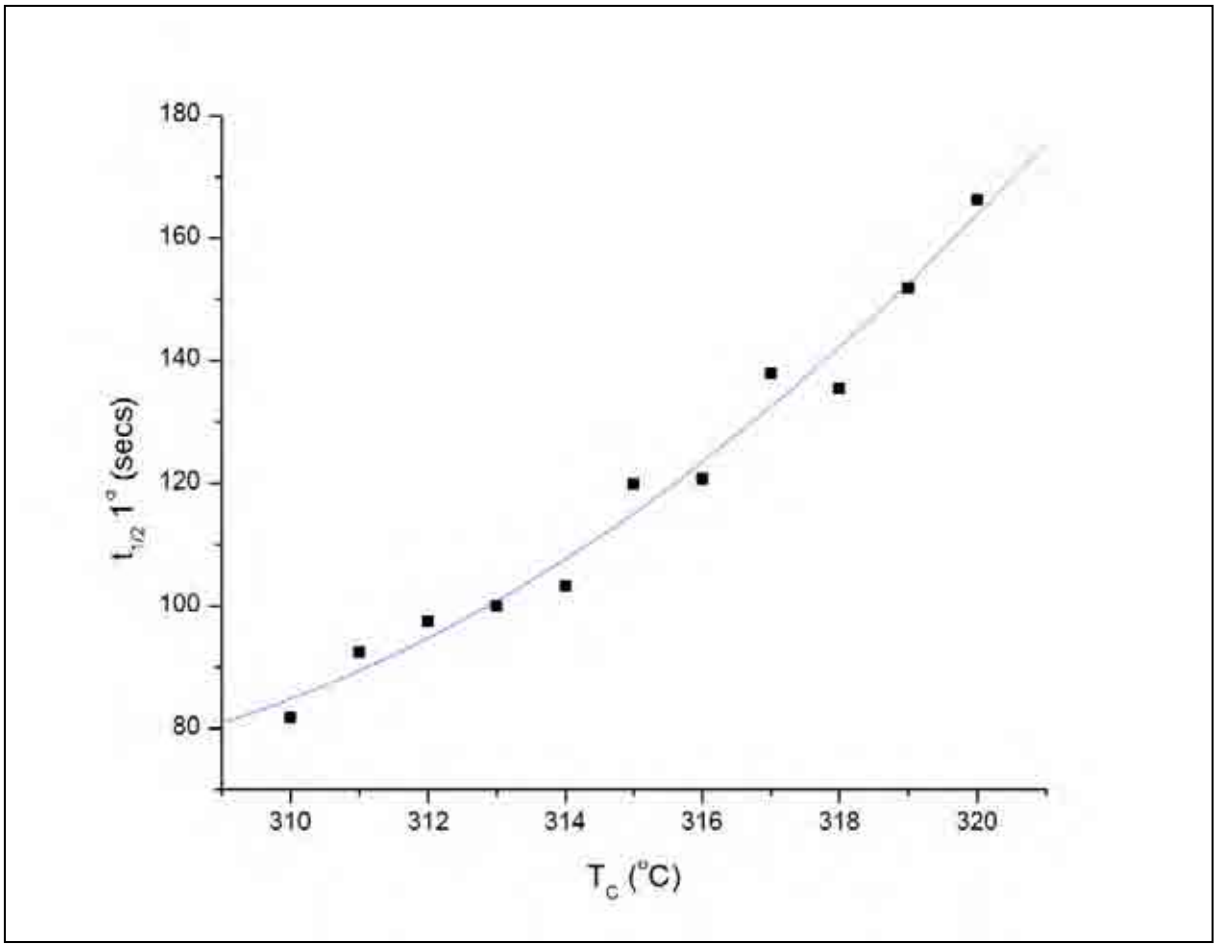

Figure 5.14 Half-time of the primary process against crystallisation temperature for 450CA30.

Combining the values for Z and $t_{1/2}$ in fig 5.15 gives a clear comparison of the increase in time, t, for the half-life of the primary process with increasing crystallisation temperature and decreasing crystallisation rate, Z.

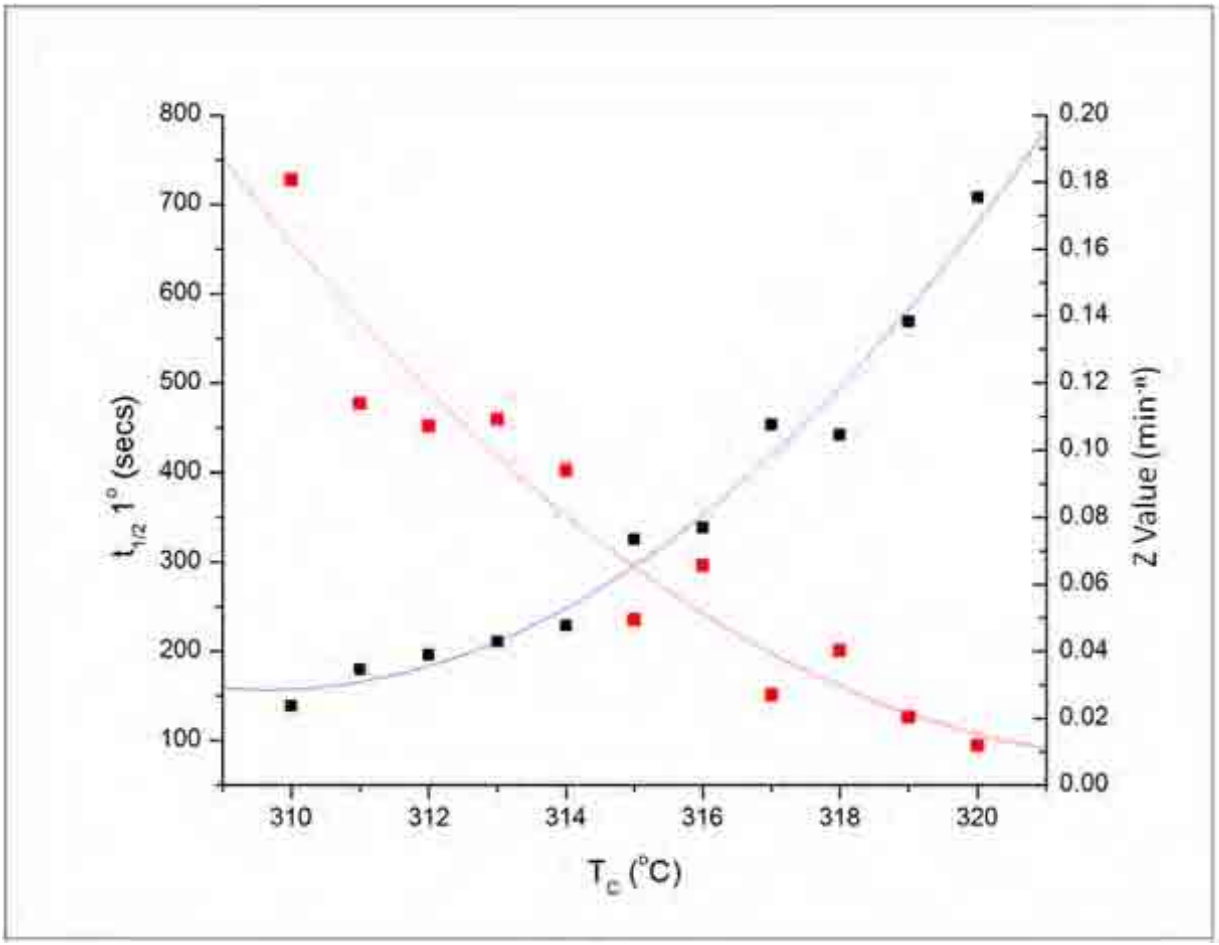

Figure 5.15 Combined figure showing both half-time. $t_{1/2}$, and rate constant, Z, against T_c for 450CA30.

5.1.4 450CA30 – Differential Avrami Analysis

As mentioned previously (section 5.1.3), the DSC results obtained from isothermal crystallisation of 450CA30 have been analysed with a differential form of the Avrami equation, and processed through the LabView software. All of the output values have been tabulated in table 5.3.

From the results, there do not seem to be any trends with the n values across the isothermal crystallisation temperatures. However, in correlation with the results from the conventional Avrami analysis, there seems to be an increase in n value between the 450PF samples and the carbon filled grade. Again, the average value of n for the carbon filled grade is markedly higher compared to its unfilled counterpart. This could mean a change in crystallisation mechanism, and morphological structural difference in crystallites. This change in unit shape of crystallites could then be held accountable to the inclusion of the carbon fibres.

Values for the half-time, $t_{1/2}$, are shown below in fig 5.16. It can be noted that as crystallisation temperature increases, the half-time also increases as chain mobility becomes increasingly easier; which coincides with decreasing Z values.

Table 5.3 Differential Avrami output values for isothermally crystallised 450CA30

Temperature (°C)	310	311	312	313	314	315	316	317	318	319	320
n Value (±0.01)	3.38	3.94	3.49	3.41	3.59	3.83	3.23	3.64	3.37	4.06	3.82
$t_{1/2}$ (secs)	2.4	2.4	2.4	3	3	4.8	4.8	6.6	6.6	8.4	10.2
Z value	56109.8	165436	41394	18427.6	25305.6	12701.2	2277.6	2226.4	1296.77	1890.5	612.2
$X_{p\infty}$	0.68	0.7	0.69	0.74	0.7	0.68	0.77	0.8	0.77	0.71	0.71

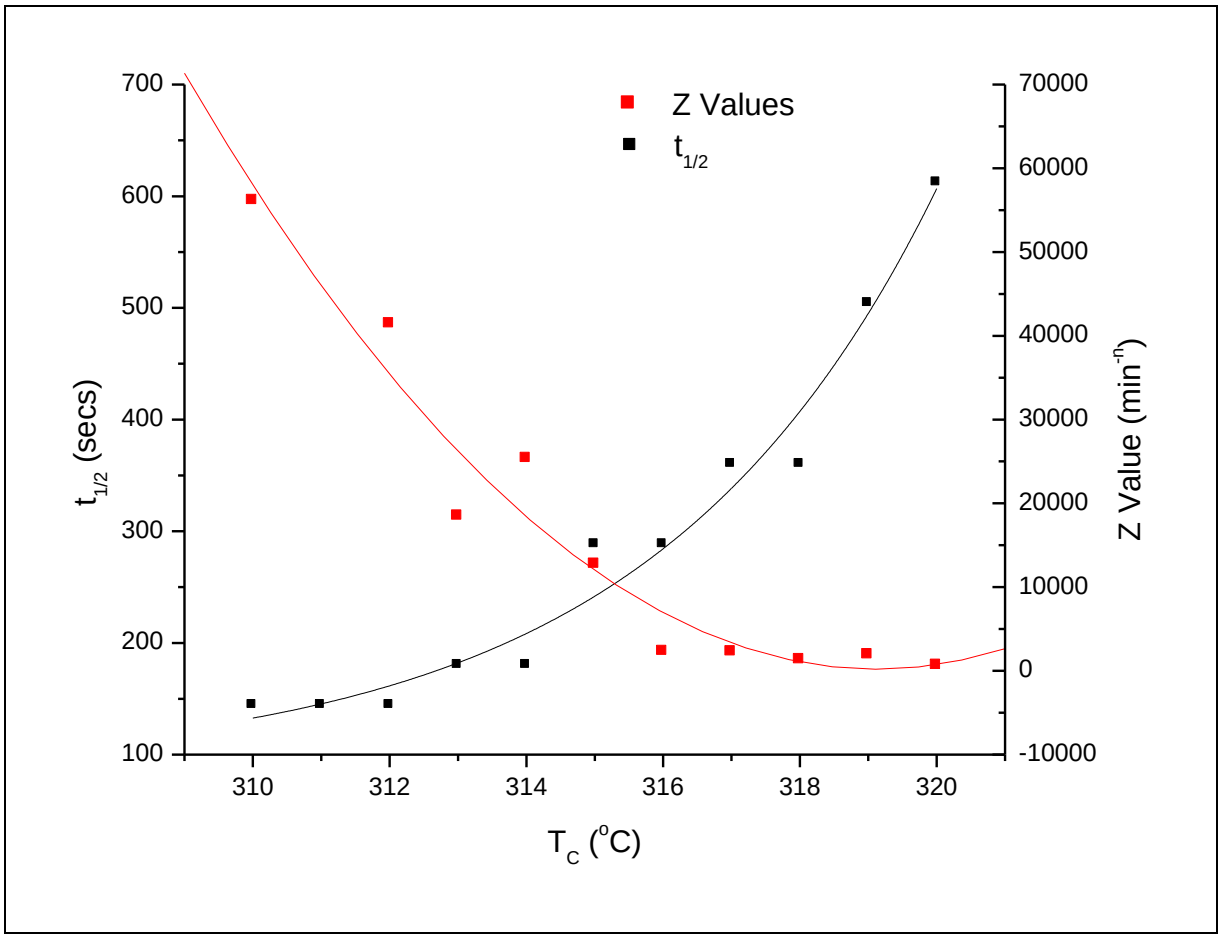

Figure 5.17 $t_{1/2}$ and Z values for isothermally crystallised 450CA30, obtained through differential Avrami analysis.

5.1.5 450PF and 450CA30 comparison

In this section a comparison between the two grades of PEEK can be made in order to distinguish any effects that the inclusion of carbon fibre may have on the crystallisation process. Comparison graphs have been compiled to be able to directly compare results from the differential Avrami approach.

Fig 5.18 shows the results for the development of X_t with time for both grades at the same temperature of 312°C. This comparison allows us to see if there are any differences in crystallisation initiation with the influence of the carbon fibre additions.

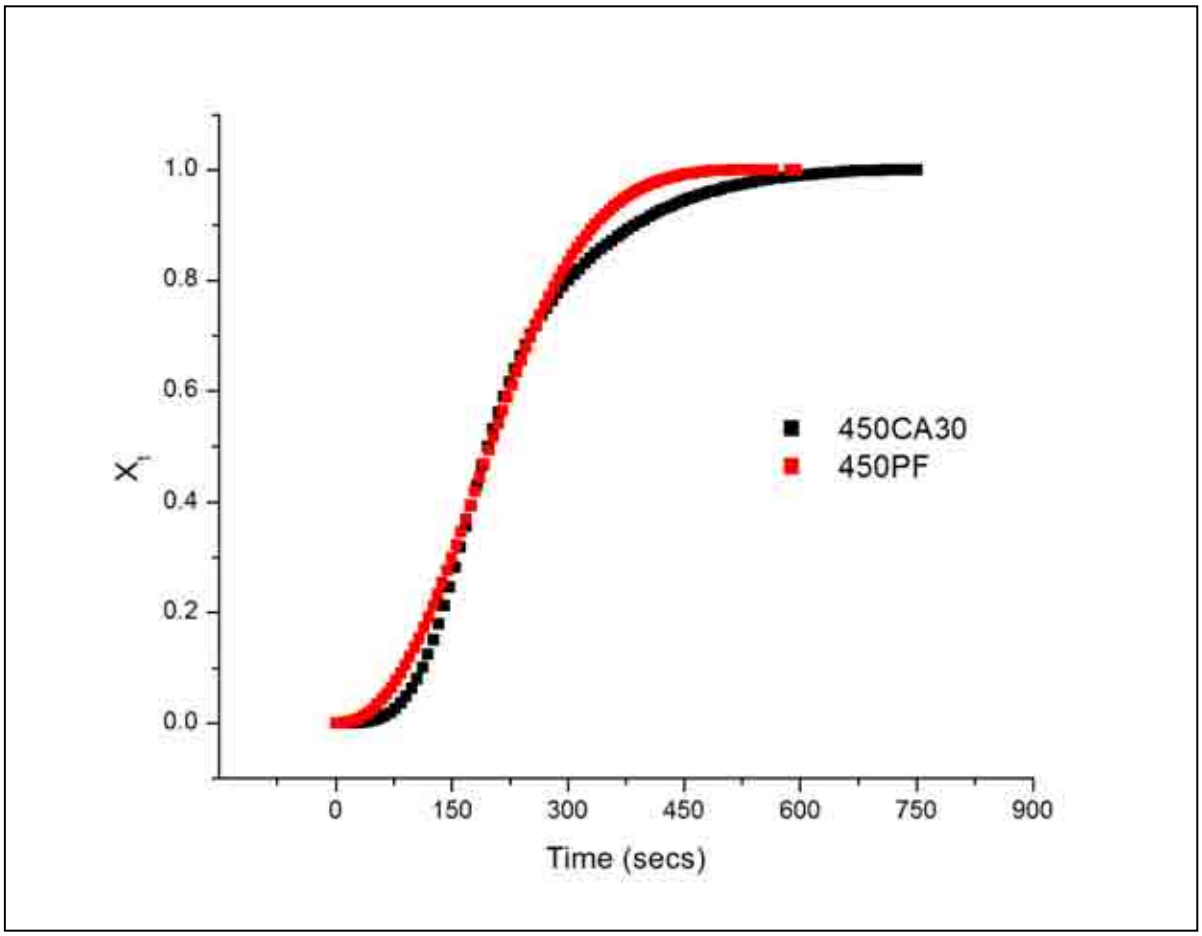

Figure 5.13 Comparison of development of X_t with time at 312°C for 450PF and 450CA30.

From the comparison figures, it can be seen that any potential influence of the carbon fibre filler is not present at the lower end of the isothermal crystallisation temperatures. At 312°C both the pure PEEK grade and the carbon filled grade, have relatively similar development of relative crystallinity. It could even be noted that the initial development of crystallisation occurs earlier for that of the 450PF, suggesting that at lower temperatures, the inclusion of carbon fibre hinders the nucleation of crystallites during isothermal crystallisation.

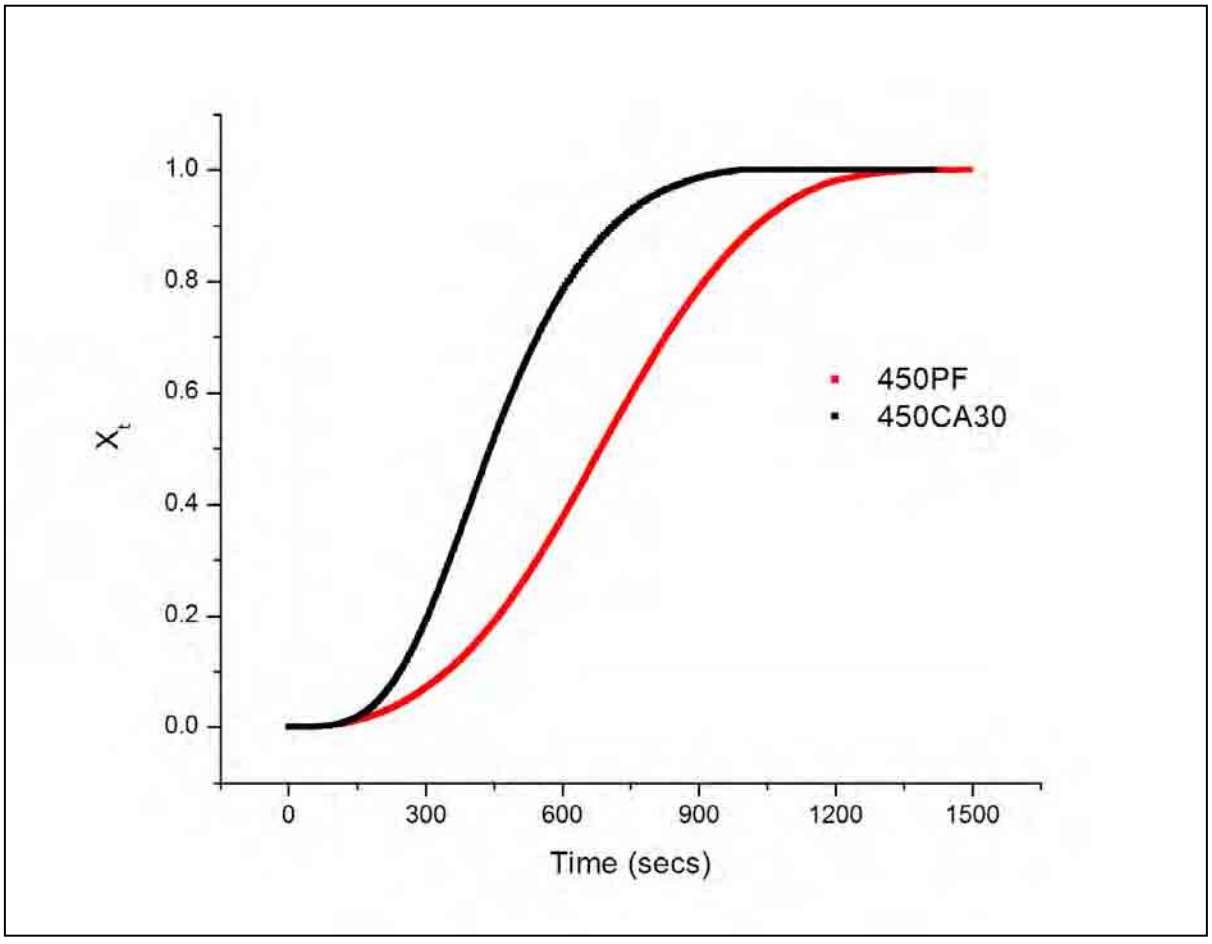

Figure 5.19 Comparison of development of X_t with time at 318°C for 450PF and 450CA30.

However, introduction of carbon fibres to a polymer matrix can influence the nucleation of crystallites[27] and therefore, as seen in fig 5.19, 450CA30 crystallised more rapidly at 318°C. This result therefore reinforces the work by Hay and Mehmet-Alkan in 1993, whereby it was

suggested that the inclusion of carbon fibre to the matrix increased the rate of crystallisation. It can be seen that as crystallisation temperature increases the influence of the carbon additions gives rise to a faster rate of crystallisation.

The differential Avrami analysis, allowed us to inspect the Avrami exponent, n, in better detail and with increased accuracy (see tables 5.1 and 5.3). The n value for 450CA30 shows no distinct trend or pattern from low crystallisation temperatures to high crystallisation temperatures. However, if an average value was taken across the sample set, the value of n would be 3.87, which is much closer to the integer 4. This shows a variation to that of the 450PF samples, which was closer to 3. Therefore there may be a change in mechanism of morphological units from the unfilled samples to the carbon filled samples thus supporting the theory outlined by Jar et al., 1991.

A comparison graph of the half-times for both sample grades (see fig 5.20) clearly shows the influence that the carbon filler has on the crystallisation of the polymer matrix. At higher crystallisation temperatures, it can be seen that the $t_{1/2}$ values for 450CA30 are suppressed and lower than that of the pure polymer grade meaning that the crystallisation proceeds more rapidly. However, for temperatures up to 317°C, the carbon filler does not seem to have an effect on the half-time of the crystallisation process. This shows that at temperatures closer to the melt, the fibre addition may act as a nucleating agent[30], thus increasing the spherulite growth rate and reducing the half-time of the process.

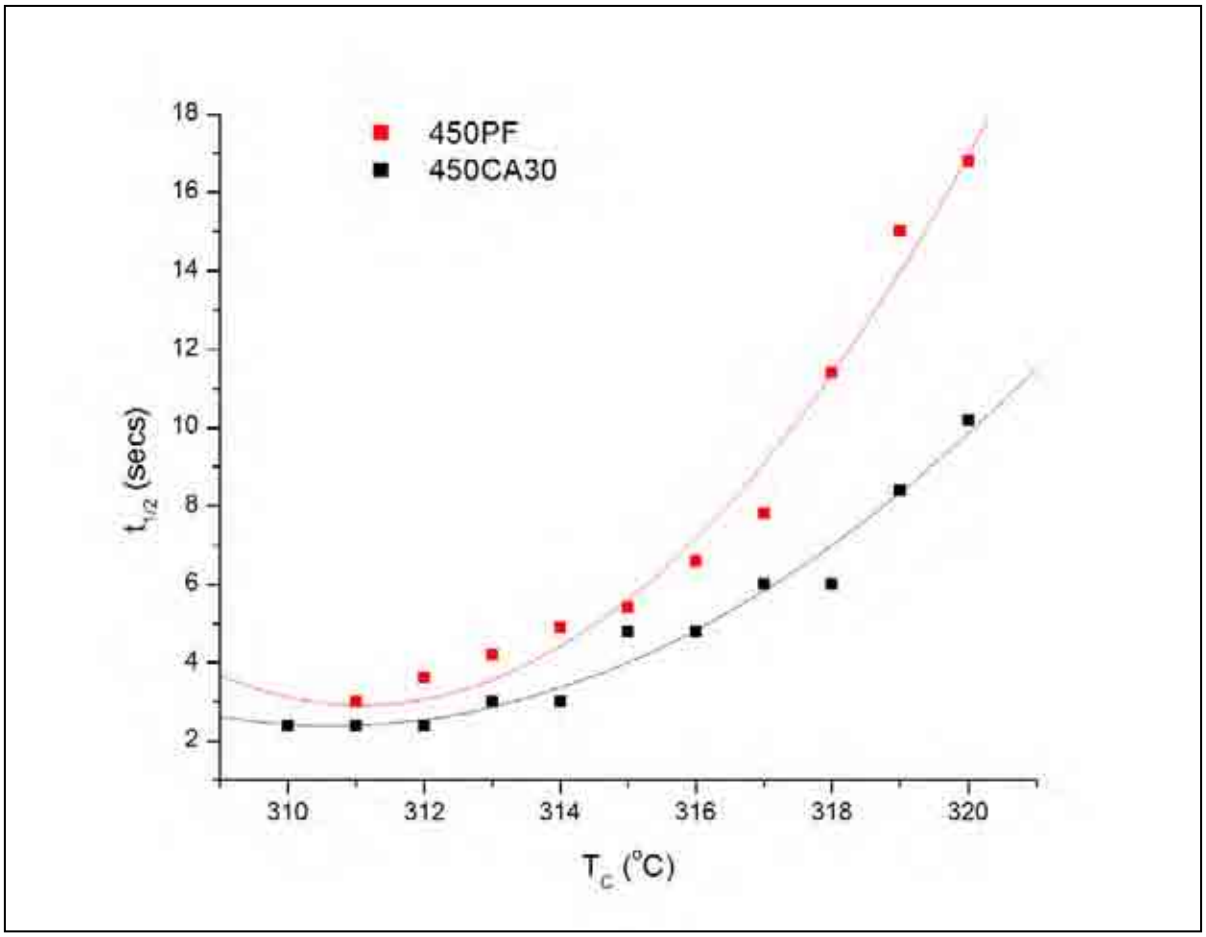

Figure 5.20 Comparison of $t_{1/2}$ values for 450PF and 450CA30 obtained from differential Avrami analysis.

5.2 FTIR Analysis

5.2.1 Initial FTIR Spectra

The conditioned samples of PEEK, cooled at various rates (previously mentioned in section 4.1), were analysed using the ATR IR technique. A typical spectrum of amorphous (liquid nitrogen quenched) PEEK can be seen in fig. 5.21. The spectrum is a typical trace distinctive of amorphous or heavily quenched PEEK[33, 34, and 36]. When compared to earlier IR studies undertaken by Chalmers et al. 1984[33], the similarities of the spectra are clearly evident. The Finger-print region of the spectrum ($1700cm^{-1}$ – $650cm^{-1}$) exhibits the distinctive spectral features typical to an IR recorded spectra of PEEK[33]. The spectrum has been split into sections (Fig 5.22 – 5.24) for further interpolation.

The key FTIR spectral peaks used to identify the samples have also been summarised in table 5.4 for ease of peak association. These peaks include the peaks that are used to identify the samples as thermoplastic PEEK, and peaks that can be utilised to calculate the crystallinity of the samples.

Table 5.4 Table of FTIR absorption bands associated with semi-crystalline PEEK.

Peak (cm^{-1})	Association	Comments
1653	Carbonyl Stretching Frequency	Common to PEEK
1648	Carbonyl Stretching Frequency	Common to PEEK
1490	Characteristic of ring absorption	Identifies the sample as an aromatic thermoplastic (common to all aromatic thermoplastics). Sometimes appears as a doublet.
1305	Intensity varies with sample Crystallinity	Used in calculations by Chalmers et al. to characterise sample crystallinity (exclusive to PEEK)
1280	Intensity varies with sample Crystallinity	Used in calculations by Chalmers et al. to characterise sample crystallinity (exclusive to PEEK)
1252	Carbonyl Stretching Frequency	Common to PEEK
1227	Carbon-Oxygen-Carbon Stretching Frequency	Common to PEEK
965	Intensity said to vary with sample Crystallinity	Used by Jonas et al. to calculate a factor of sample crystallinity
952	Intensity said to vary with sample Crystallinity	Used by Jonas et al. to calculate a factor of sample crystallinity
863	Ring Deformation Modes	Common to most aromatic thermoplastics
841	Ring Deformation Modes	Common to most aromatic thermoplastics
700	Ring Deformation Modes	Common to most aromatic thermoplastics

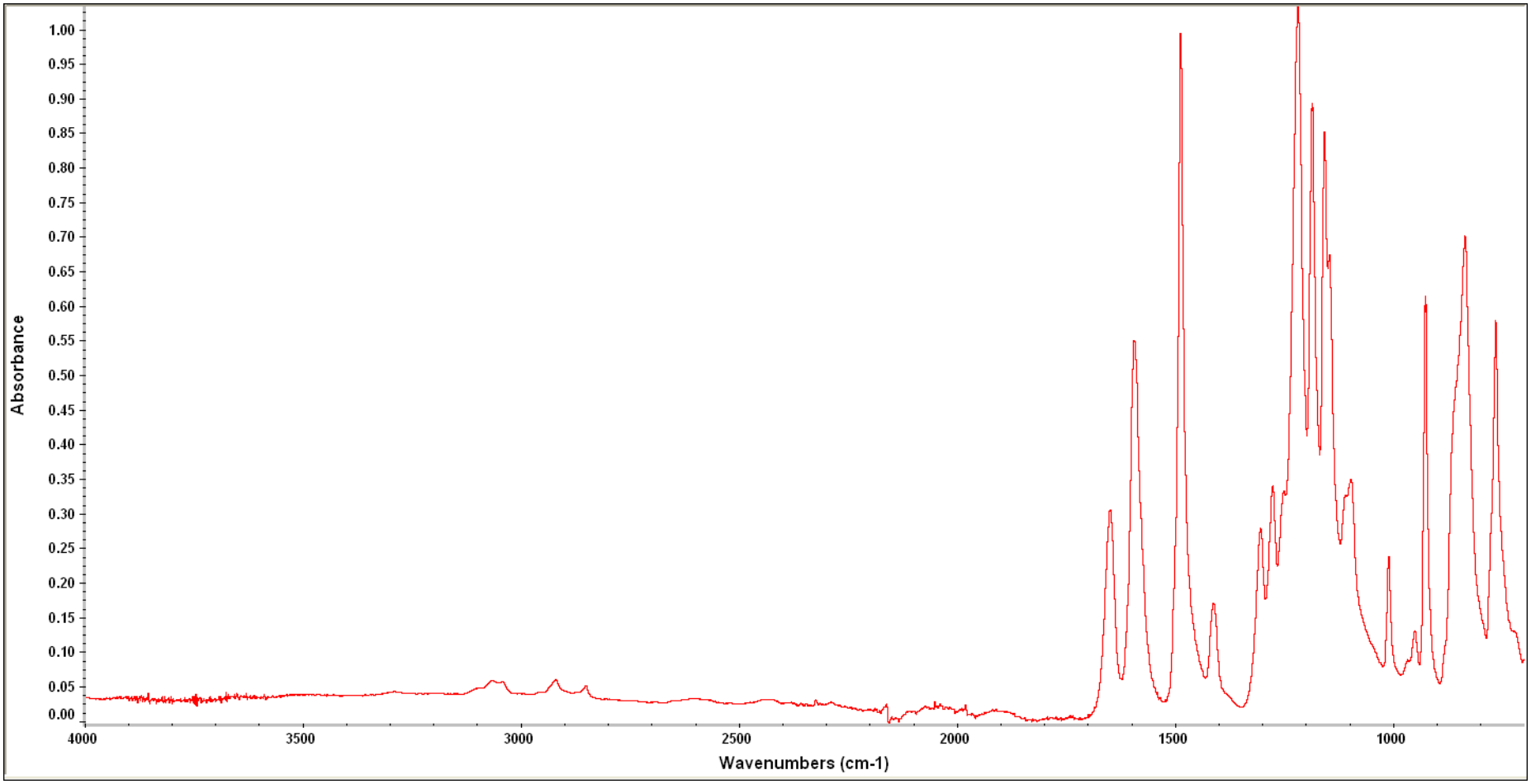

Figure 5.21 FTIR spectra of amorphous 450PF.

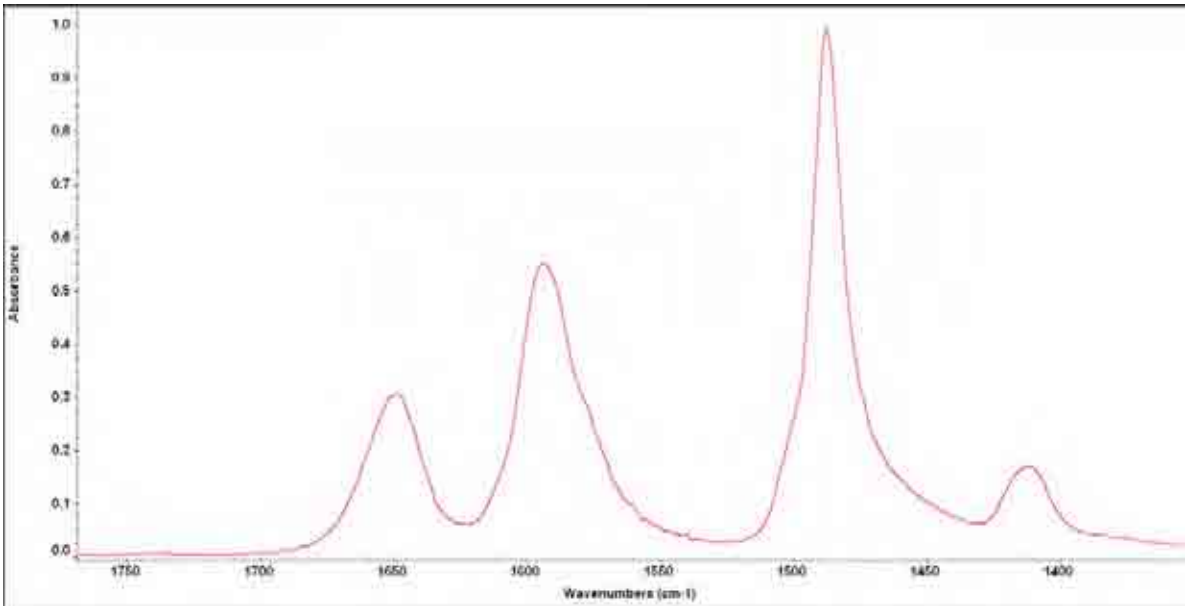

Figure 5.22 Section of spectra of amorphous 450PF: 1750cm^{-1} – 1350cm^{-1}.

Unconditioned amorphous PEEK shows a carbonyl stretching vibration at 1653cm^{-1} (Fig.5.22)[36] and an associated shoulder at 1252cm^{-1} and a distinctive intense band at 1227cm^{-1} (Fig 5.23)[34]. Also apparent is the intense sharp band noted at approximately 1490cm^{-1}, which is a distinctive characteristic of aromatic ring absorption, and identifies the sample as an aromatic thermoplastic. As discovered by Chalmers et al. in 1984, some absorption bands become both sharper and more intense with changing morphology, and in contrast to this, other bands decrease in intensity. Within fig. 5.23 the bands 1305cm^{-1} and 1280cm^{-1} are present, and clearly highlighted. These absorbance bands, similar to the work undertaken by Chalmers et al. 1984, are used to calculate an area ratio for investigation into the correlation between these ratios and polymer crystallinity.

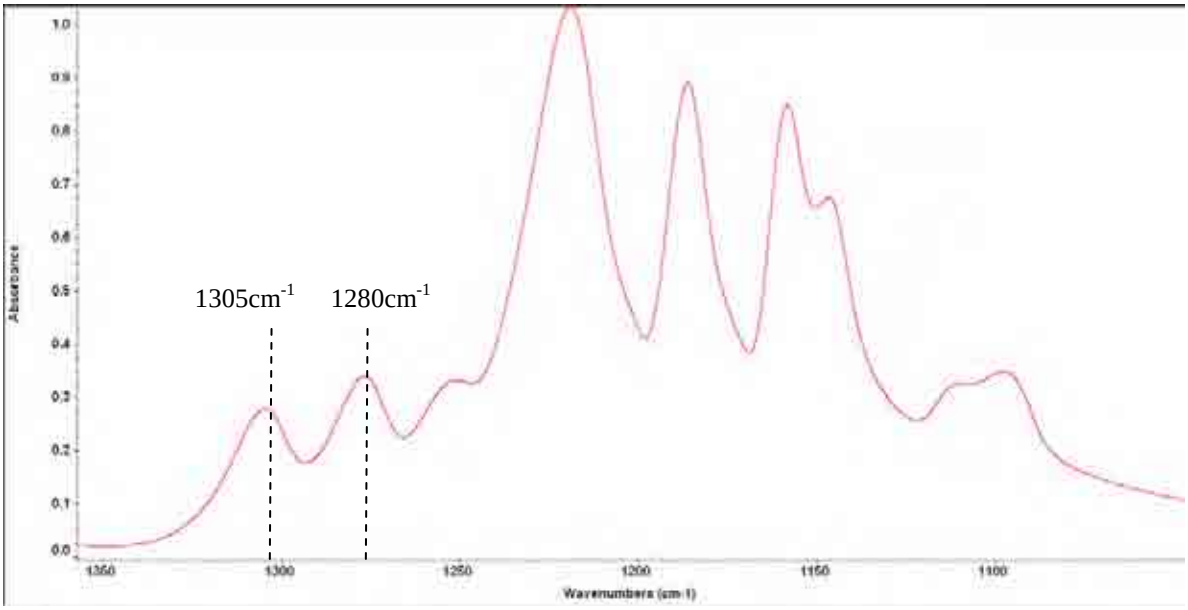

Figure 5.23 Section of spectra of amorphous 450PF: 1350cm^{-1} – 1050cm^{-1}.

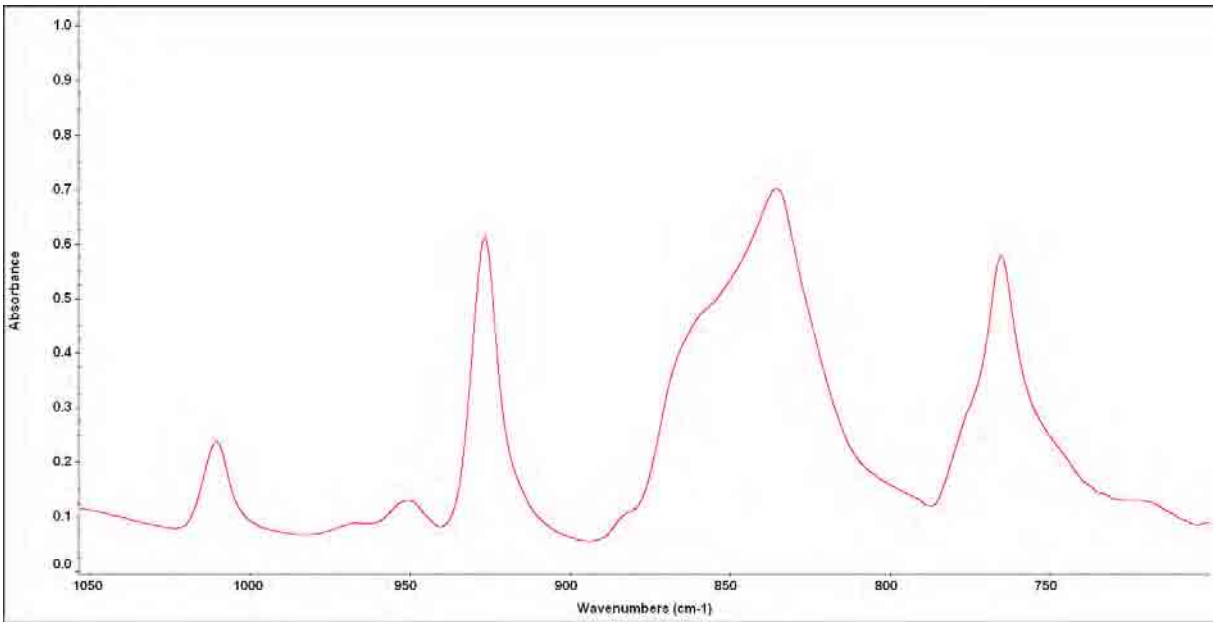

Figure 5.24 Section of spectra of amorphous 450PF: 1050cm^{-1} – 700cm^{-1}.

Other key features include two overlapping broad bands at approximately 863 and 841cm^{-1} as seen in fig. 5.24. Also present in fig. 5.24 are the bands 952cm^{-1} and 965cm^{-1}, which in 1991, Jonas et al.[41], investigated in depth, the use of these bands in correlating crystallinity to the area ratios of these absorption bands. Similar to that of Chalmers et al. the method of analysis is nearly identical, except that, an additional shoulder at 947cm^{-1} apparently becomes present

through the increase in polymer crystallinity. However, many follow the path of the current work and opt to use the ‘Chalmers’ method.

Within crystallised PEEK, a shift in the carbonyl stretching frequency from 1653 to 1648 cm^{-1} can be observed . This is probably due to the movement of the two phenyl rings of the benzophenone moiety to approach coplanarity upon crystallization, which result in an increase in conjugation[34].

5.2.2 Peak area ratio analysis

To facilitate analysis of the spectra, the peaks of interest need to be independently distinguishable. The use of a deconvolution algorithm, as part of the OMNIC spectral software, was used to estimate the exact location and independent dimensions of the peaks being analysed. As mentioned previously, the two absorption peaks of interest are located at approximately 1305cm^{-1} and 1280cm^{-1} (see figure 5.23). Chalmers et al. 1984, used these two peaks to correlate a relationship between changes in the mid-IR spectrum and crystallinity.

Comparing the spectra within the region of interest, clear transitions within absorption bands between the amorphous sample and slow cooled sample cooled at 10°Cmin^{-1} (semi-crystalline), can be observed. From fig. 5.25, the absorption band at 1280cm^{-1} is much more intense for that of the amorphous sample compared to that of the slow cooled sample. In contrast to this, the absorption band at 1305cm^{-1} shows the reverse effect, being much higher for that of the slow cooled sample than the amorphous one. This effect is indicative of changing morphology. This can also be seen through the different samples at different cooling rates as the ‘Chalmers’ peaks vary in intensity as the cooling rates increase up to amorphous

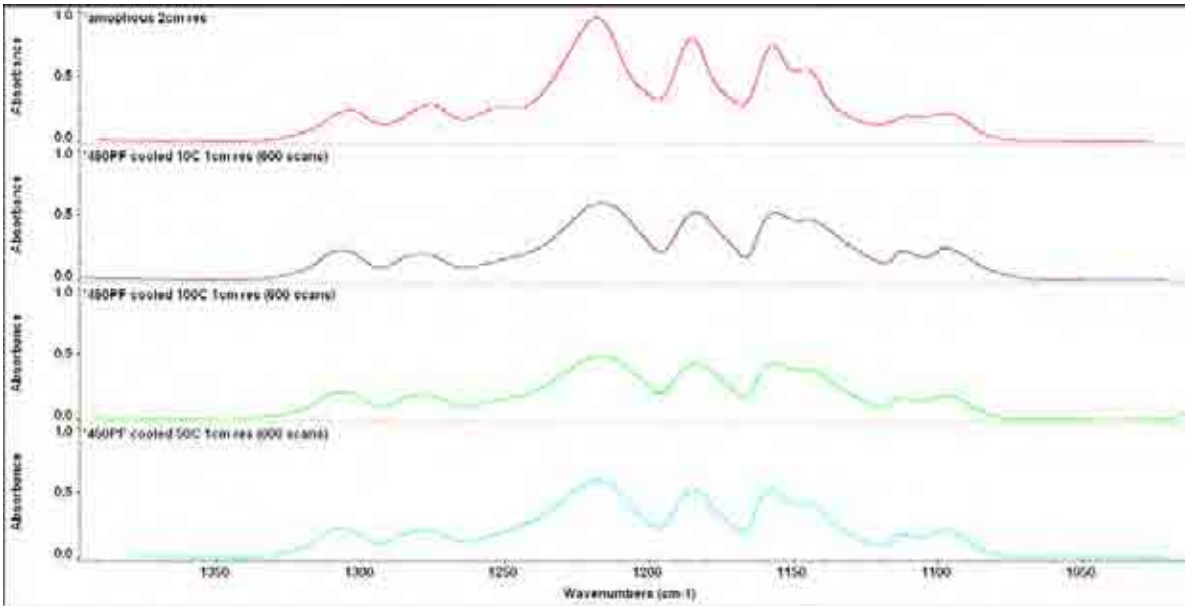

Figure 5.25 A comparison of the spectrum for 450PF cooled at varying rates, within the 'Chalmers' region.

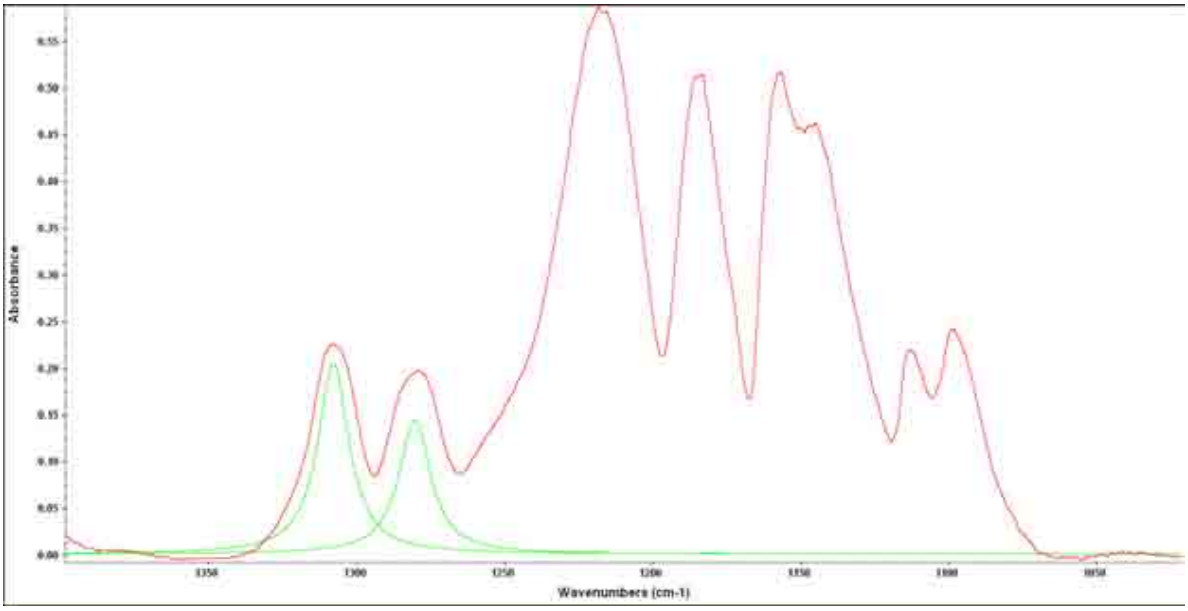

Fig 5.26 An example of a deconvoluted spectrum for 450PF cooled at 10°Cmin^{-1}.

Before the deconvolution algorithm was applied to the spectra, a baseline correction was made using the OMNIC software, between 1400cm^{-1} and 1000cm^{-1} to remove any slope within the spectra, and also give a common baseline reference for the peaks of interest. From fig. 5.26 an example of the deconvolution curve fitting can be seen. It is apparent, that there seems to be a dependence on neighbouring absorption bands in regards to intensity. This therefore makes deconvolution even more relevant, to isolate each peak, in order to analyse the peak heights and areas. Full data of the deconvolutions can be seen in Appendix I.

After completing the deconvolution of the 'Chalmers' peaks the peak area could be calculated. The peak area ratio could then be plotted against cooling rate. As seen in fig. 5.30, the peak area ratio decreases with increasing cooling rate. This correlation appears linear for the rates that were investigated. This shows a strong trend towards the theory that as cooling rate increases, the morphological structure also shows a change.

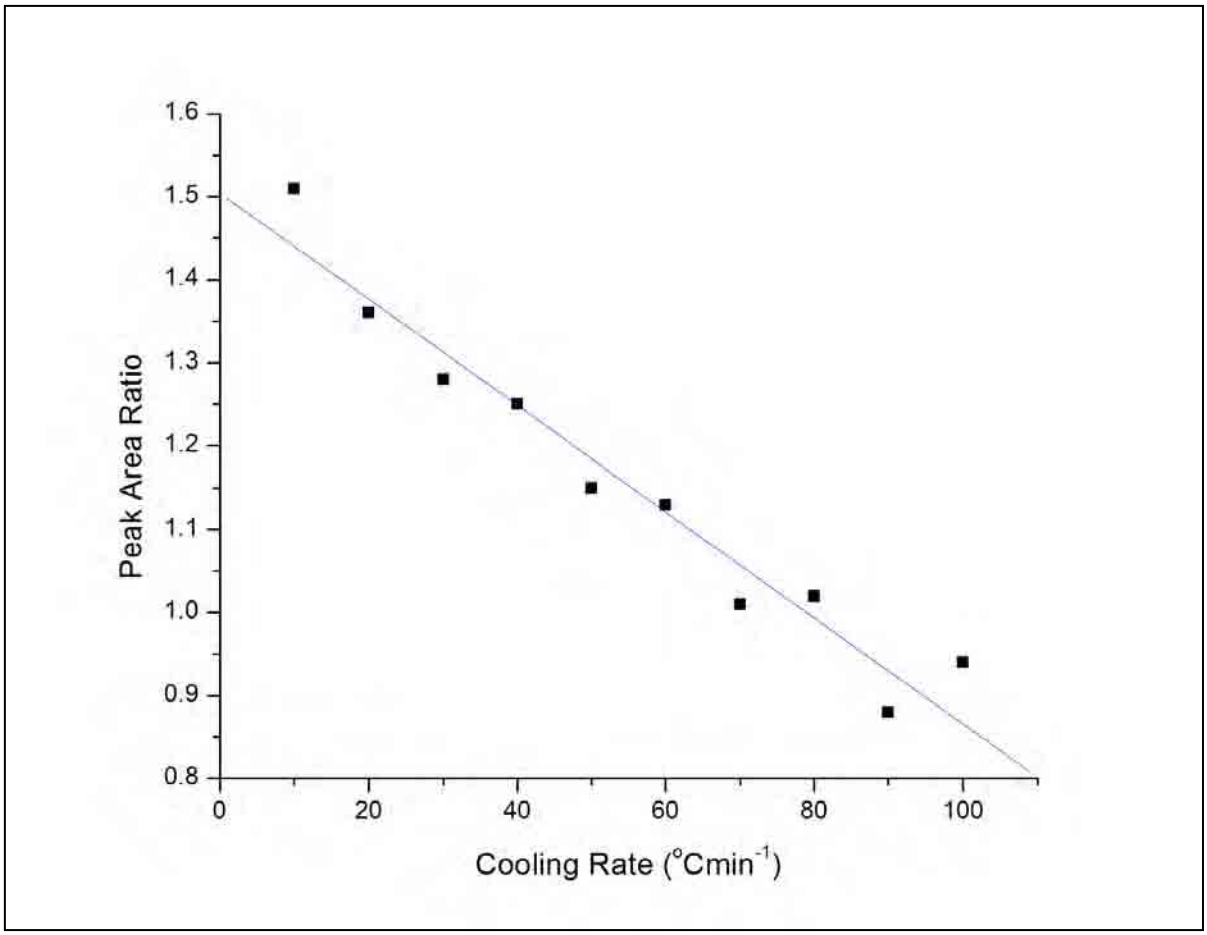

Figure 5.27 Peak area ratio against cooling rate for 450PF (1305/1280).

The trend seen from the results revealed in fig. 5.27 also show a good relationship with the results discovered by Chalmers et al. 1984. In fig 5.28 a relatively strong linear relationship can be seen between degree of crystallinity, X_c, and cooling rate, which again reinforces the relationship that as cooling rate changes, the degree of crystallinity also changes. With the two figures 5.27, and 5.28, a final comparison to the previous work by Chalmers et al. can be made.

Plotting peak area ratio against X_c gives a direct comparison to the aforementioned previous work. A linear relationship can be seen in fig 5.29, which yet again reinforces the relationship discovered by the early works of Chalmers et al. 1984 (fig 5.30), in that as crystallinity within the polymer increases, a higher ratio between the measured IR peaks can be seen. This therefore shows that IR techniques can pick up changes within morphology of polymers with a good degree of accuracy.

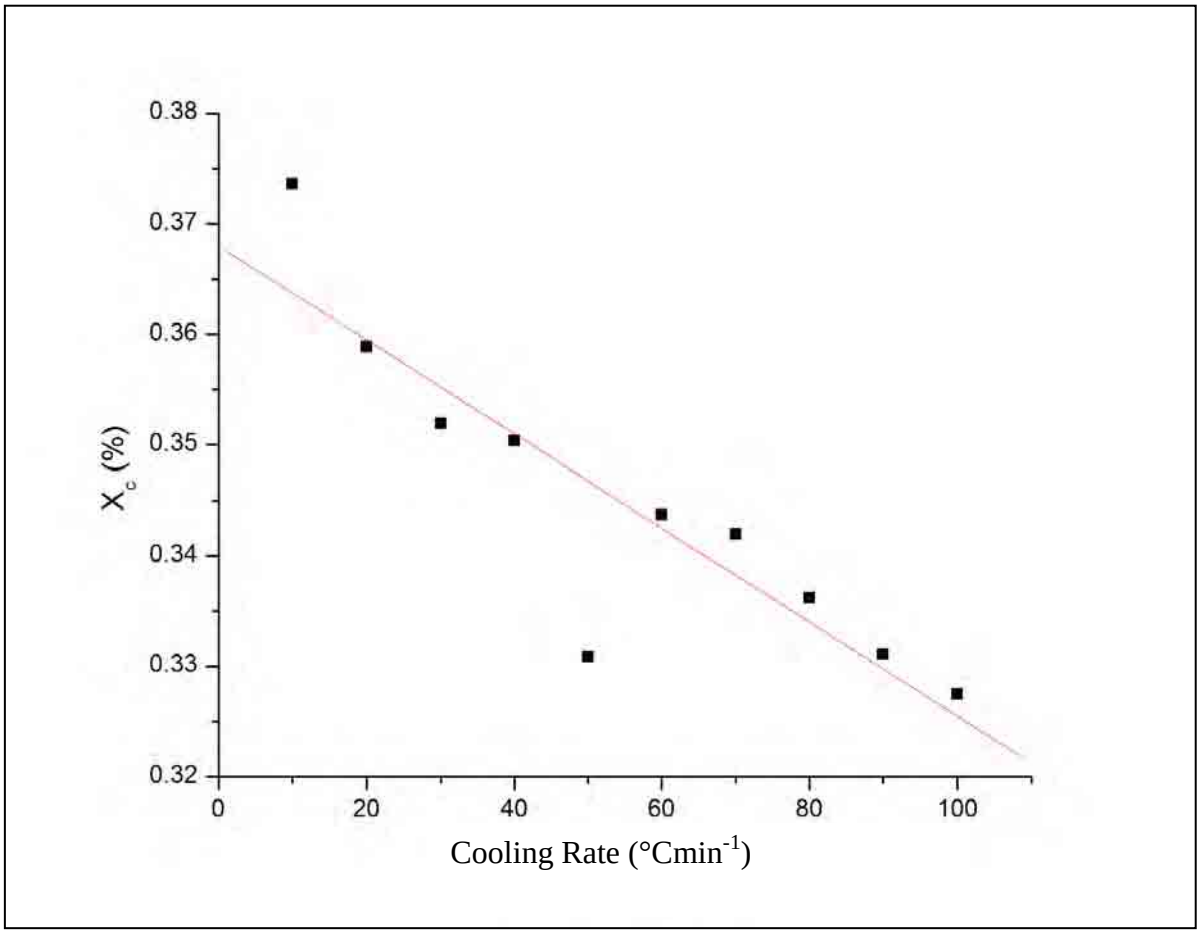

Figure 5.28 X_c against cooling rate for 450PF.

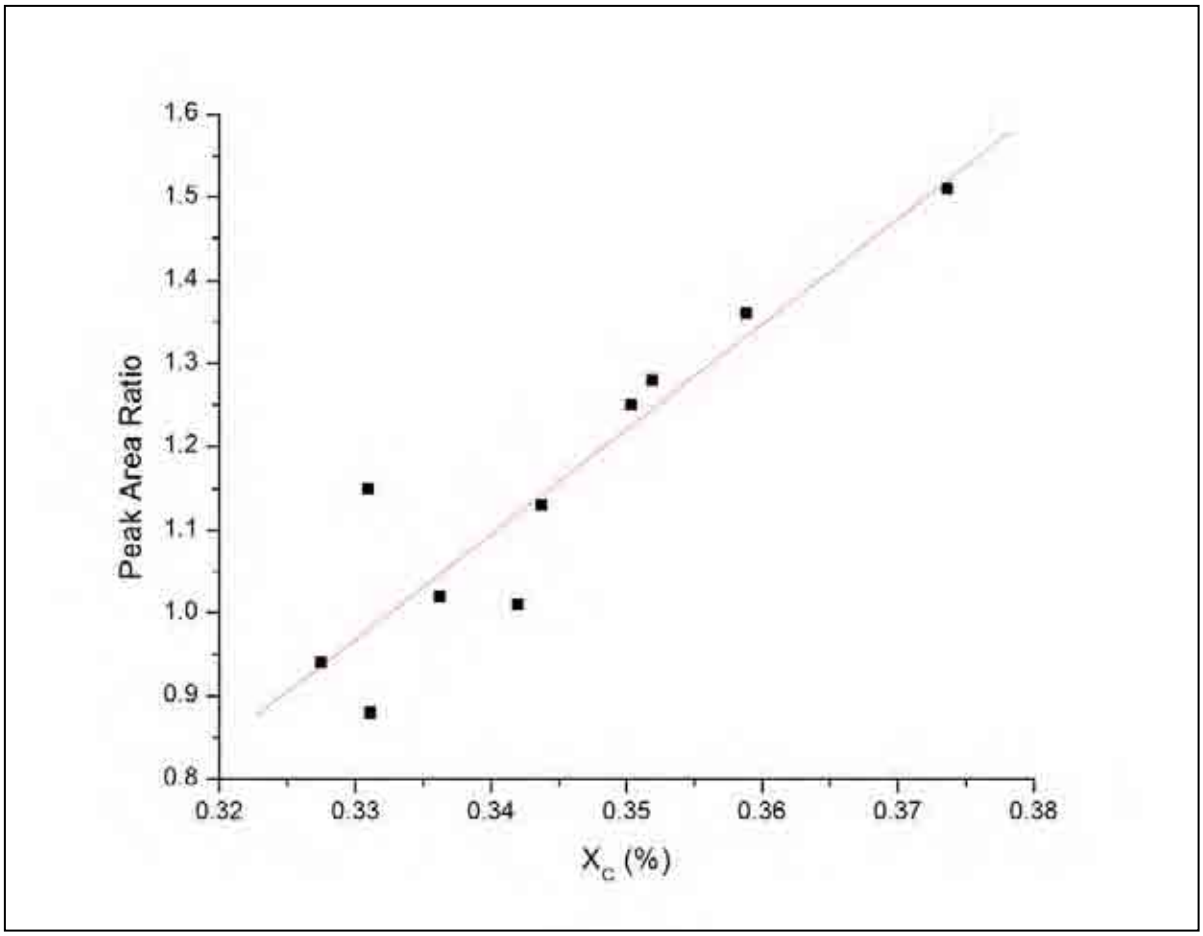

Figure 5.29 Peak area ratio against X_c for 450PF (1305/1280).

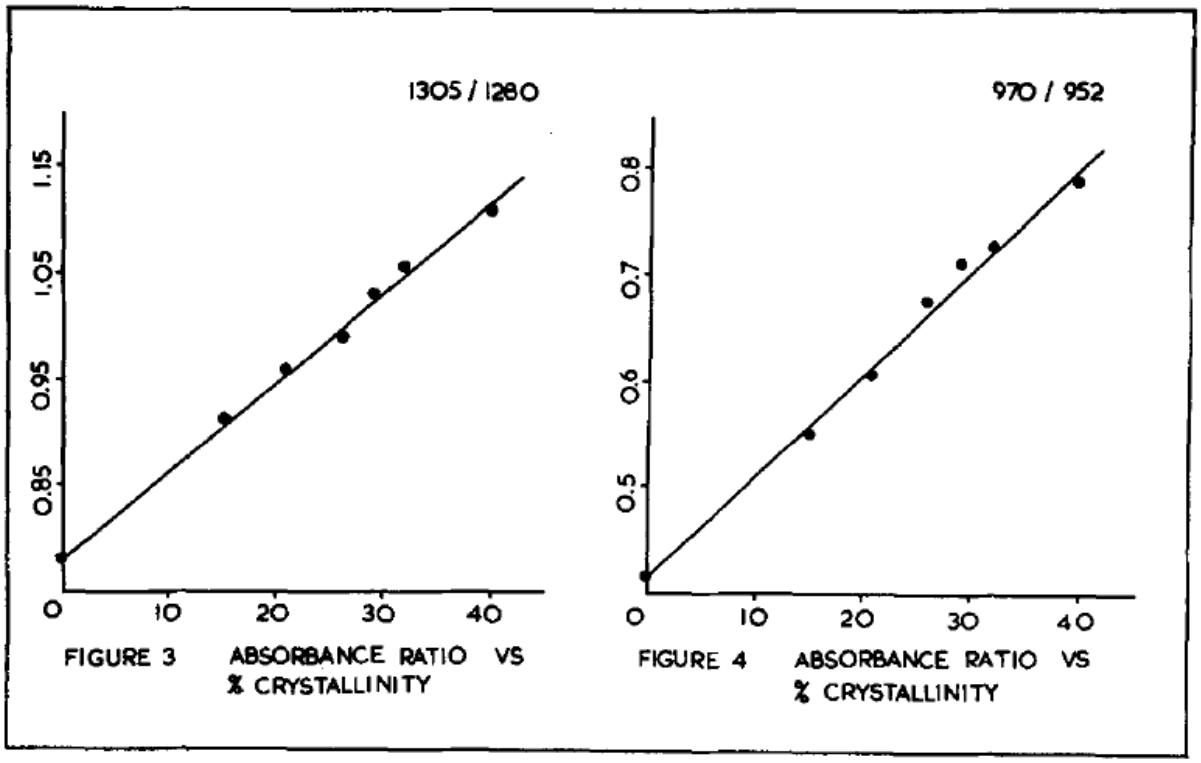

Figure 5.30 Absorbance peak area ratio vs. % crystallinity for PEEK samples. Taken from Chalmers et al. 1984[33].

The current work, when compared to the aforementioned previous works, shows a relatively consistent linear relationship between absorbance ratio and cooling rate/crystallinity. This may, however, not be the case, as there are unlimited cooling rates between the amorphous sample and those that were tested within the current work i.e. the variation of peak ratio with cooling rate may be non-linear above 100°Cmin^{-1}. If the results for the cooling rates that were tested were extrapolated past the ratio of that of an amorphous sample (0.61), other results become evident. From fig. 5.31, it could be said that as the cooling rate increases over 130°Cmin^{-1} this would always result in an amorphous sample, however as explained previously, this may not be the case.

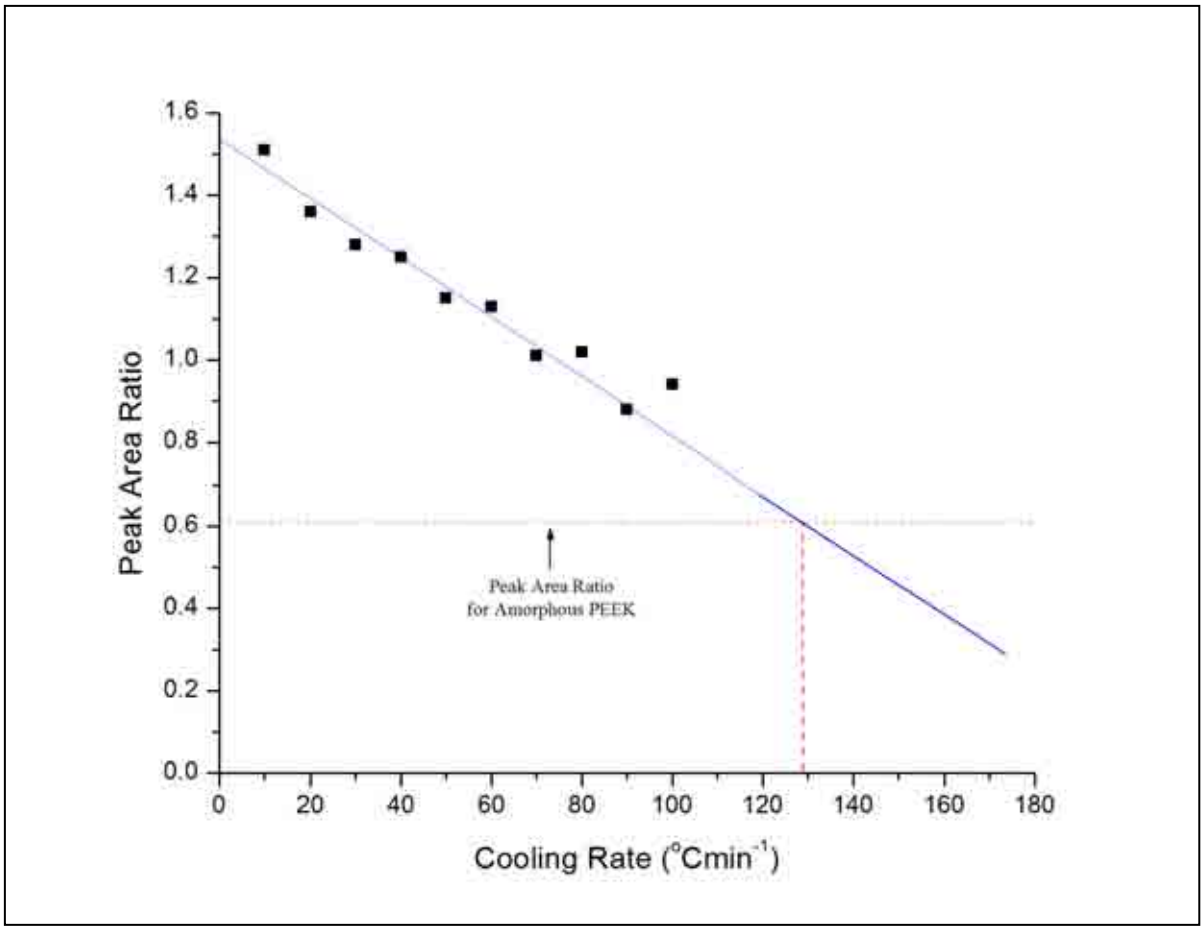

Figure 5.31 Theoretical extrapolation of peak area ratios for 450PF.

5.3 Rapid Scan (Hyper) DSC measurement of the degree of crystallinity

Pre-conditioned samples were sent to Perkin Elmer for Hyper-DSC analysis[48] 7 identical samples were conditioned according to the previously mentioned sample preparation (see section 4.2.1) and the cooled at 100°Cmin^{-1} from the melt. These samples were then re-heated from room temperature at varying heating rates up to the limit of the Hyper-DSC.

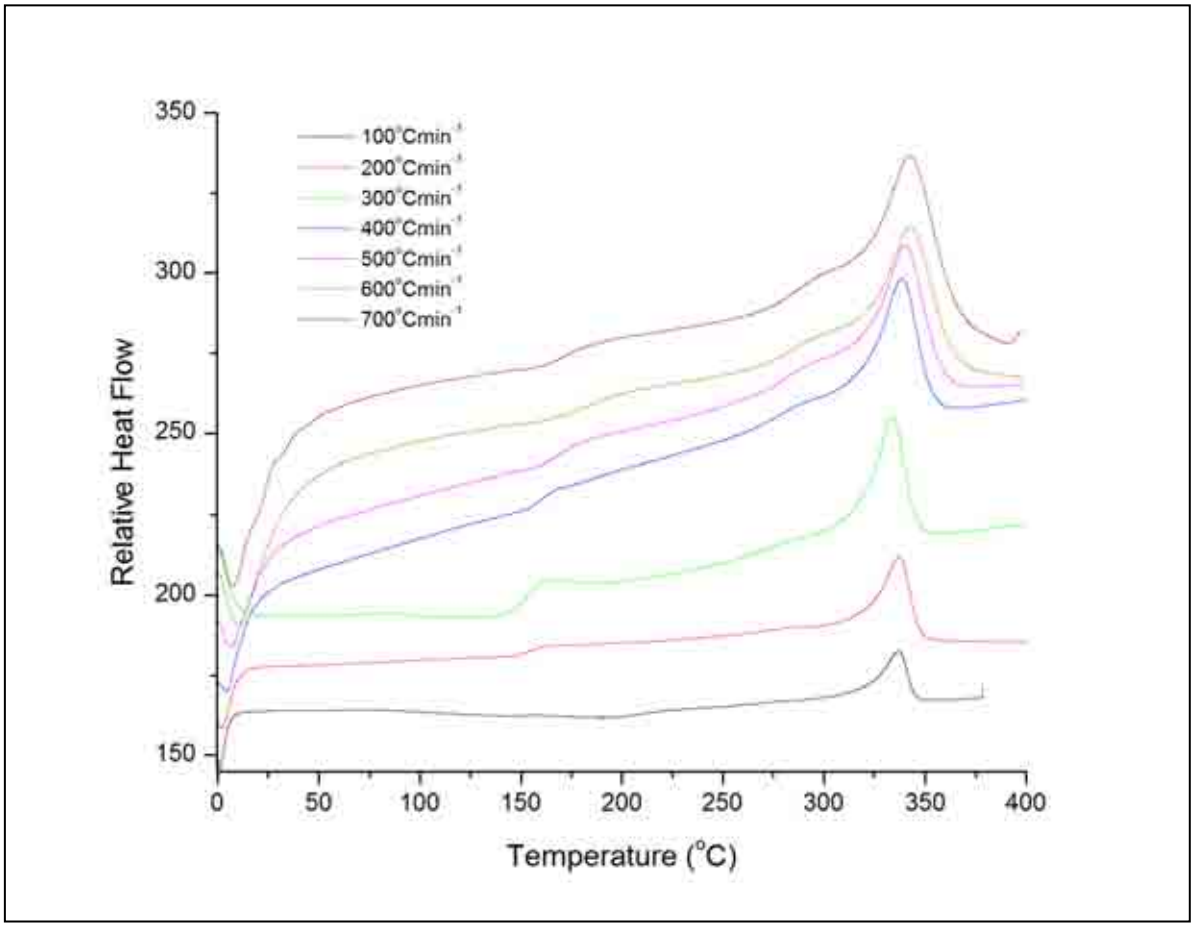

Figure 5.32 Re-heat traces for preconditioned samples of 450PF using Hyper-DSC. (Traces staggered for clarity).

The heating rates offer by Hyper-DSC, in theory, prevent the occurrence of morphological change during the heating run.

Fig. 5.32 shows the thermal response of the pre-conditioned PEEK recorded at a range of heating rates. As heating rate increases the observed T_g of the sample not only shifts towards the melt, but becomes broader (fig 5.33). This change is likely to due to thermal lag. It can also be seen that as heating rate increases, so does the melting temperature of the sample. As the heating rate increases the melting peak of the trace broadens therefore limiting the determination of the onset of melting (fig. 5.32). Therefore a comparison of the peak melting temperature has been made to give insight to the changes occurring with increasing heating rate.

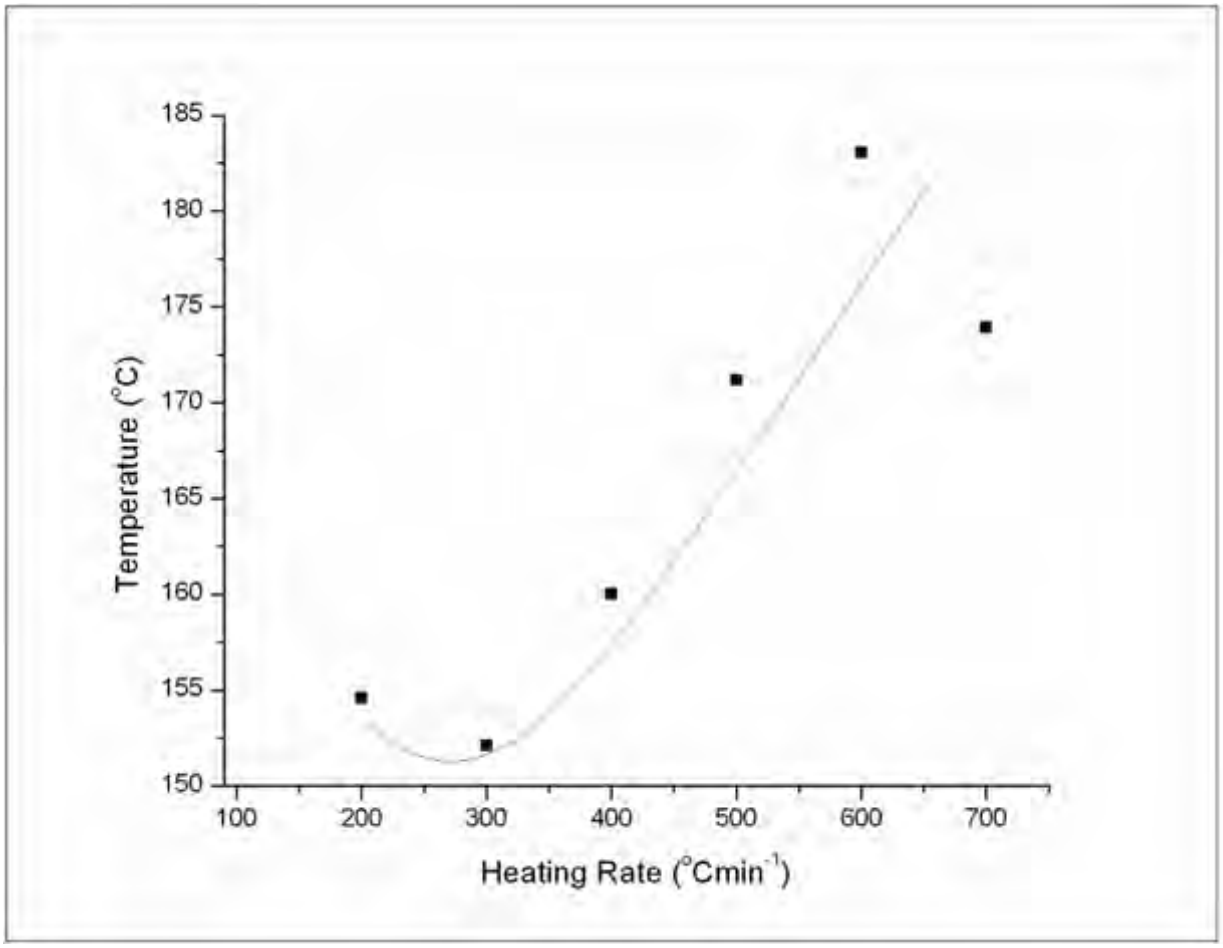

Figure 5.33 Observed T_g against heating rate.

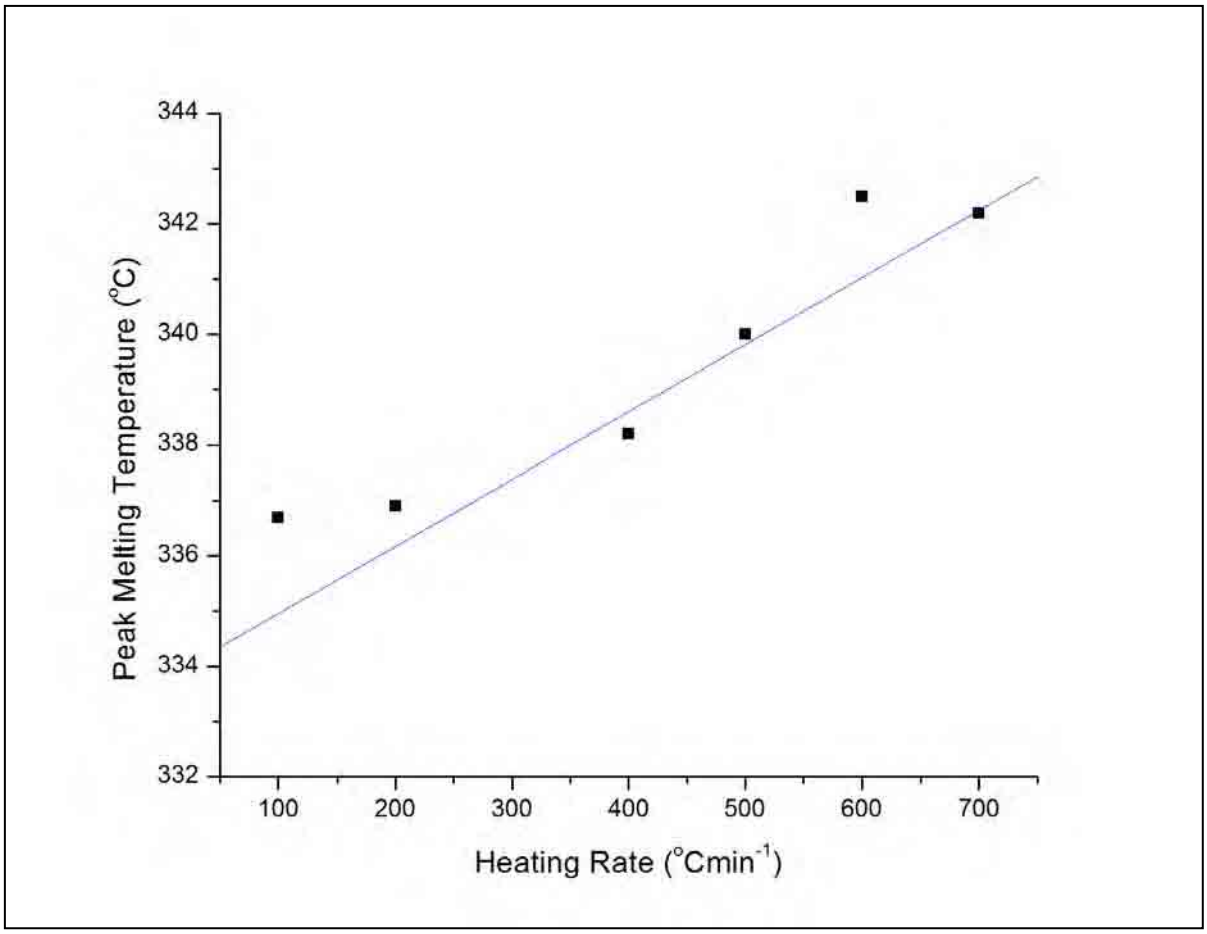

Figure 5.34 Peak melting temperatures of 450PF with increasing heating rate.

From fig. 5.34 it is clear that heating rate increases so does the melting temperature of the sample. This shows that as the sample is heated at such a fast rate of heating, the sample latent time spent at any instantaneous temperature is reduced, therefore allowing the sample to melt at a temperature where sufficient energy allows crystallites to break down. This could be said that higher rates of heating give rise to the actually temperature at which melting occurs. However, this increased melting temperature may also be a product of forced energy upon the system, and further investigation may be needed to determine which rate is optimal for melt determination.

As mentioned previously from fig. 5.35, the increased heating rate subsequently broadens the melting peak of the sample. It also defines the melting peak into two more defined individual peaks. This highlights the different melting temperature of the bulk primary crystallites formed from the primary process, and the smaller and possibly finer structured secondary ones. As you can see from the trace for the sample heated above 400°C, a smaller shoulder is present on the melting peak of the sample. This is typical of crystallites formed during secondary crystallisation, and due to the fast re-heating rate to determine crystallinity, it could be said that these are not crystallites formed during the re-heating process. This therefore increases accuracy of the morphological structure present within the sample when it was first crystallised.

The traces were then used to determine the crystallinity of the sample. The crystallinity of the sample is calculated by determining the heat of fusion, ΔH_f, of the sample. This was determined by calculating the area under the melting peak and was completed in accordance with the standard, ISO 11357-3. This is then used to calculate sample crystallinity using the equation:

$$\frac{\Delta H_f}{\Delta H_{f\infty}} = X_c(\times 100) \quad \text{(Eq. 9)}$$

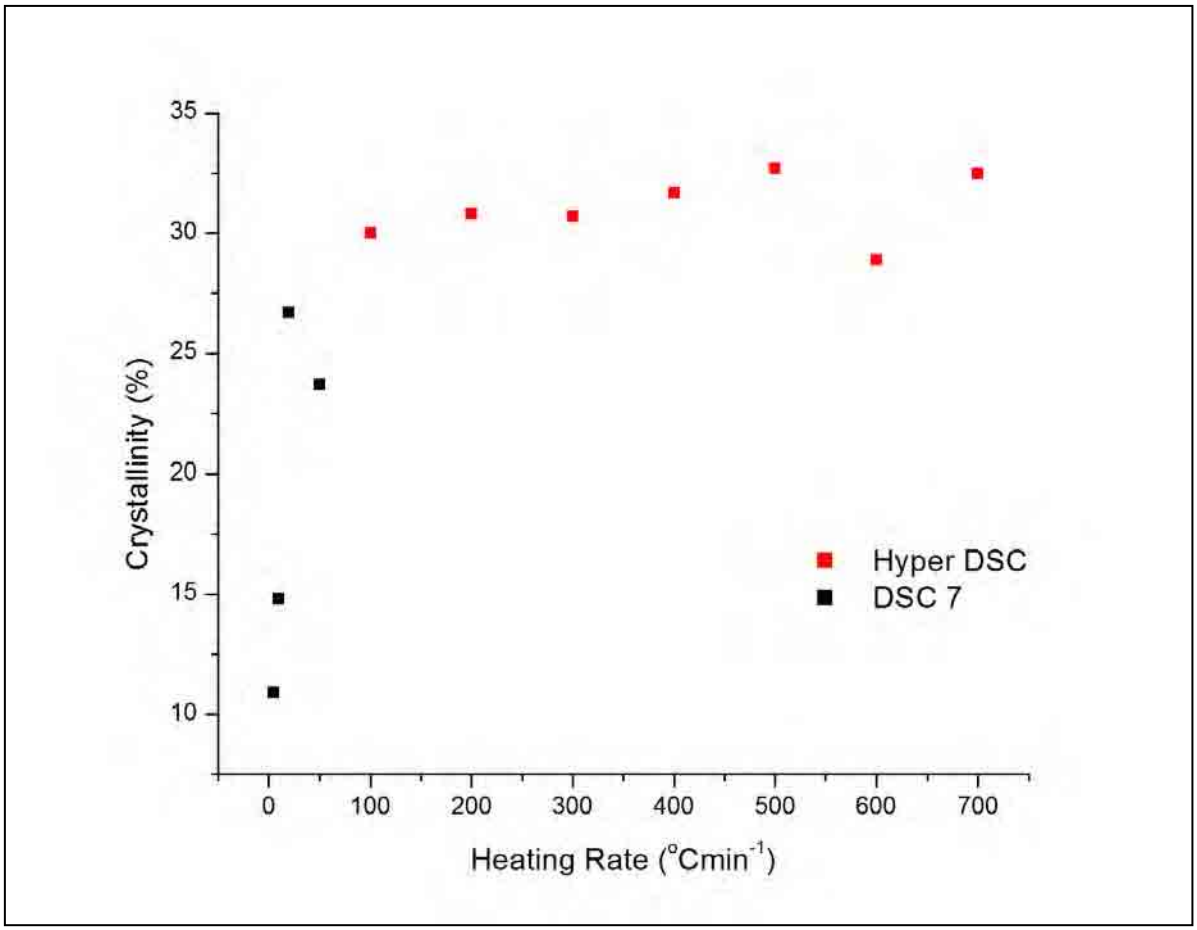

Figure 5.35 Percentage crystallinity against DSC heating rate. All samples were previously cooled at 100°Cmin^{-1}.

From fig 5.35 it can be seen that as samples are heated at varying heating rates, the end crystallinity value is significantly different but stabilises above a heating rate of 100°Cmin^{-1}. Within semi-crystalline PEEK, the morphology of the polymer can change as the polymer is heated through the T_g towards the melt. At heating rates of less than 100°Cmin^{-1} there is the capacity for melting and re-crystallisation before the main melting point. When the heating rate of the polymer is increased to temperatures above 100°Cmin^{-1}, such as 700°Cmin^{-1} when using hyper-DSC, the change in initial and final temperature is so rapid that the molecules of the polymer do not have chance to re-align or change morphological position. This is

significant in that the heating rate used to re-melt a polymer with pre-conditioning history is a crucial factor in defining the degree of crystallinity of the sample.

Fig. 5.35 clearly describes the relationship with heating rate and the accuracy of degree of crystallinity. It can therefore be stated that when calculating the degree of crystallinity within a sample, the higher the rate of heating, the more accurate and stable the value of the crystallinity of the processed part. This result concurs with work by such authors as McGregor[42-44] in that as heating rate increases it reduces the possibility of molecular re-alignment before the sample can reach its target melting temperature. McGregor in 2004, used Hyper-DSC techniques with rates of 250+°Cmin^{-1} to characterise the enthalpy of fusion of particular crystalline forms in pharmaceutical compounds. The crystalline forms that were being studied were sensitive to melting and re-crystallisation during heating, which as a result alters the crystalline forms present within the compound. However, it was found that when heating at rates above 250°Cmin^{-1} re-crystallisation was unable to occur, therefore allowing for an accurate calculation of the enthalpy of fusion of the crystalline forms being observed. This theory can be transferred to semi-crystalline polymers such as PEEK, and the evidence from the current work suggests that using increased heating rates allows for more accurate calculations of the degree of crystallinity. It is therefore imperative that when determining the crystallinity of a sample, a fast heating rate is needed to ensure a more accurate determination and to reduce the possibility of melting and re-crystallisation during the heating process.

6.0 Conclusions

Investigating the crystallisation behaviour of both the 450PF and 450CA30 grades of Victrex® PEEK, gave insight into the effects of short fibre additions to the polymer matrix. At lower isothermal crystallisation temperatures, it could be said that carbon fibre hinders the nucleation process compared to that of neat PEEK. The opposite can then be said at isothermal crystallisation temperatures closer to the melt. Here, carbon fibres act as stress initiators for nucleation and therefore increase the nucleation rate and subsequent growth within the polymer.

Differential Avrami analysis is a more analytical approach to investigating the crystallisation behaviour in semi-crystalline polymers. Using this technique, a more accurate determination of the Avrami exponent, n, could be made and subsequently the $t_{1/2}$ value. This showed evidence, that the Avrami exponent had a higher integer value of near 4 for that of the carbon filled 450CA30 grade of PEEK. This highlights, that there may be a change of mechanism for polymer crystalline growth. This conclusion also concurs with the work undertaken by Jar et al. in 1991. The $t_{1/2}$ value that was produced from the differential approach also shows that as isothermal crystallisation temperature increases, carbon fibre additions to the polymer matrix act as nucleation sites to increase the rate of crystallisation.

FTIR analysis revealed that ATR-FTIR techniques can conclusively characterise the crystallinity presence within semi-crystalline Victrex® 450PF PEEK. From the results, the fingerprint region that signifies the amount of crystalline presence within a material was successfully observed and recorded. When comparing present results to that of Chalmers et al.

1984, a good relationship was seen and a strong linear relationship was seen between degree of crystallinity and cooling rate.

Through Hyper-DSC techniques, differences were found when determining a sample's crystallinity as heating rate was varied. However, as heating rate was increased past 100°Cmin^{-1}, the resulting values become more stable and therefore more reliable. It can therefore be said, that increasing the rate at which a sample is heated to determine the absolute crystallinity value, the more accurate the result will be. This concurs with work by such authors as McGregor[42-44] in that as heating rate increases it reduces the possibility of molecular re-alignment before the sample can reach its target melting temperature. It is therefore imperative that when determining the crystallinity of a sample, a fast heating rate is needed to ensure a more accurate determination. Hyper-DSC could therefore lead to more accuracy and confidence of parts that are being manufactured in that they comply with the desired level of crystallinity.

7.0 Future Work

From the work undertaken within the project there are a few areas which would further reinforce the findings of the present work and give definitive answers to the issues that have been addressed. Firstly, the addition of WAXS x-ray studies could be used to clarify the crystallinity of the polymer samples used the Hyper-DSC investigations. This would then give three different techniques of measuring sample crystallinity. It would reinforce the work undertaken using the Hyper-DSC technique, and would therefore strengthen the validity of the results. These findings could then help to form part of a measuring standard to enable manufacturers to quantifiably measure sample crystallinity using FTIR within parts new out of production, without the need for destructive testing.

Secondly, the use of more samples that have been non-isothermally crystallised, at a range of differing cooling rates would increase the scope and knowledge of the use of Hyper-DSC. With these samples it would be possible to investigate the limitations of the Hyper-DSC technique at quantifying the sample crystallinity.

8.0 References

1. Cogswell, F.N., *Thermoplastic Aromatic Polymer Composites*. First ed. 1992, Oxford: Butterworth-Heinmann Ltd. 277.
2. Cowie, J.M.G., *Polymers: Chemistry & Physics of Modern Materials*. 2nd Edition ed. 1991: Blackie Academic & Professional, an imprint of Chapman & Hall. 436.
3. Daoust, D., et al., *Chemical modification of poly(ether ether ketone) for size exclusion chromatography at room temperature: 2. On the reliability of the derivatization procedure for PEEK molecular-mass determination--application to PEEK-carbon fibre composite.* Polymer, 1994. **35**(25): p. 5498-5503.
4. Baltá Calleja, F.J. and S. Fakirov, *Microhardness of polymers*. 2000: Cambridge University Press.
5. Ebdon, J.R., *Introduction to polymers (second edition) R. J. Young and P. A. Lovell Chapman and Hall, London, 1991. pp. 443, price £16.95. ISBN 0-412-30640-9 (PB); ISBN 0-412-30630-1 (HB).* Polymer International, 1992. **27**(2): p. 207-208.
6. Belbin, G.R. and P.A. Staniland, *Advanced Thermoplastics and Their Composites.* Philosophical Transactions of the Royal Society of London Series a-Mathematical Physical and Engineering Sciences, 1987. **322**(1567): p. 451-464.
7. Platt, D.K., *Engineering and High Performance Plastics*. 2003: Rapra Technology Ltd. 198.
8. Yildiz, E., et al., *Thermal and mechanical properties of poly(arylene ether ketone)s having pendant tertiary butyl groups.* Journal of Polymer Research, 2007. **14**(1): p. 61-66.
9. Dawson, P.C. and D.J. Blundell, *X-ray data for poly(aryl ether ketones).* Polymer, 1980. **21**(5): p. 577-578.
10. Blundell, D.J. and B.N. Osborn, *The morphology of poly(aryl-ether-ether-ketone).* Polymer, 1983. **24**(8): p. 953-958.
11. Blundell, D.J., D.R. Beckett, and P.H. Willcocks, *Routine crystallinity measurements of polymers by d.s.c.* Polymer, 1981. **22**(5): p. 704-707.

12. Blundell, D.J., et al., *Spherulitic Morphology of The Matrix of Thermoplastic PEEK Carbon-fiber Aromatic Polymer Composites.* Journal of Materials Science, 1989. **24**(6): p. 2057-2064.
13. King, M.A., et al., *Modelling Studies of Crystalline PEEK.* Molecular Simulation, 1989. **4**(1): p. 3 - 13.
14. Staniland, P.A., et al., *Synthesis, characterization and study of the thermal properties of new polyarylene ethers.* Polymer, 1992. **33**(9): p. 1976-1981.
15. Johnson, R.N., et al., *Poly(aryl ethers) by Nucleophilic Aromatic Substitution .I. Synthesis and Properties.* Journal of Polymer Science Part a-1-Polymer Chemistry, 1967. **5**(9PA1): p. 2375.
16. Attwood, T.E., et al., *Synthesis and properties of polyaryletherketones.* Polymer, 1981. **22**(8): p. 1096-1103.
17. Rose, J.B., Staniland, P. A., *Thermoplastic aromatic polyetherketones - US Patent 4320224*. 1982: USA.
18. Kricheldorf, H.R. and G. Bier, *New polymer syntheses: II. Preparation of aromatic poly(ether ketone)s from silylated bisphenols.* Polymer, 1984. **25**(8): p. 1151-1156.
19. Avrami, M., *Kinetics of Phase Change. I General Theory.* The Journal of Chemical Physics, 1939. **7**(12): p. 1103-1112.
20. Avrami, M., *Granulation, Phase Change, and Microstructure Kinetics of Phase Change. III.* The Journal of Chemical Physics, 1941. **9**(2): p. 177-184.
21. Avrami, M., *Kinetics of Phase Change. II Transformation-Time Relations for Random Distribution of Nuclei.* The Journal of Chemical Physics, 1940. **8**(2): p. 212-224.
22. Hay, J.N. and M. Sabir, *Crystallization Kinetics of High Polymers . Polyethylene Oxide .2.* Polymer, 1969. **10**(3): p. 203-&.
23. Mehmetalkan, A.A. and J.N. Hay, *The Crystallinity of Poly(ether ether ketone).* Polymer, 1992. **33**(16): p. 3527-3530.
24. Cebe, P. and S.-D. Hong, *Crystallization behaviour of poly(ether-ether-ketone).* Polymer, 1986. **27**(8): p. 1183-1192.
25. Bassett, D.C., R.H. Olley, and I.A.M. Al Raheil, *On crystallization phenomena in PEEK.* Polymer, 1988. **29**(10): p. 1745-1754.

26. Jar, P.Y., W.J. Cantwell, and H.H. Kausch, *Study of the crystal morphology and the deformation behaviour of carbon fibre reinforced PEEK (APC-2).* Composites Science and Technology, 1992. **43**(3): p. 299-306.
27. Mingbi, Q., et al., *Isothermal crystallization behaviour of poly(ether-ether-ketone) (peek) and its carbon fiber composite.* Thermochimica Acta, 1988. **134**: p. 223-229.
28. Sarasua, J.R., P.M. Remiro, and J. Pouyet, *Effects of thermal history on mechanical behavior of PEEK and its short-fiber composites.* Polymer Composites, 1996. **17**(3): p. 468-477.
29. Mishra, A.K. and J.M. Schultz, *Kinetics of Strain-induced Crystallization During Injection-molding of Short Fiber Composites of Poly(ether ether ketone).* Polymer Composites, 1991. **12**(3): p. 169-178.
30. Mehmetalkan, A.A. and J.N. Hay, *The Crystallinity of PEEK Composites.* Polymer, 1993. **34**(16): p. 3529-3531.
31. Victrex Plc., *Victrex Technology Centre, Hillhouse International, Thornton Cleveleys, Lancashire, FY5 4QD.*
32. Chalmers, J.M., N.J. Everall, and S. Ellison, *Specular reflectance: A convenient tool for polymer characterization by FTIR-microscopy?* Micron, 1996. **27**(5): p. 315-328.
33. Chalmers, J.M., W.F. Gaskin, and M.W. Mackenzie, *Crystallinity in Poly(aryl-ether-ketone) Plaques Studied by Multiple Internal-reflection Spectroscopy*. Polymer Bulletin, 1984. **11**(5): p. 433-435.
34. Nguyen, H.X. and H. Ishida, *Molecular analysis of the melting behaviour of poly(aryl-ether-ether-ketone).* Polymer, 1986. **27**(9): p. 1400-1405.
35. Cebe, P., S. Y. Chung, and S.-D. Hong, *Effect of thermal history on mechanical properties of polyetheretherketone below the glass transition temperature.* Journal of Applied Polymer Science, 1987. **33**(2): p. 487-503.
36. Cole, K.C. and I.G. Casella, *Fourier transform infra-red spectroscopic study of thermal degradation in poly(ether ether ketone)-carbon composites.* Polymer, 1993. **34**(4): p. 740-745.
37. Ellis, G., et al., *Fourier transform Raman spectroscopy in the study of technological polymers Part 1: poly(aryl ether ketones), their composites and blends.* Spectrochimica Acta Part A: Molecular and Biomolecular Spectroscopy, 1997. **53**(13): p. 2279-2294.

38. Li, T.Q., et al., *Long-range effects of carbon fiber on crystallization of semicrystalline thermoplastics.* Polymer, 2000. **41**(1): p. 161-168.
39. Van Nimmen, E., et al., *FT-IR spectroscopy of spider and silkworm silks: Part I. Different sampling techniques.* Vibrational Spectroscopy, 2008. **46**(1): p. 63-68.
40. Chalmers, J.M., et al., *Fourier transform infrared microscopy: some advances in techniques for characterisation and structure-property elucidations of industrial material.* Analyst, 1998. **123**(4): p. 579-586.
41. Jonas, A., R. Legras, and J.P. Issi, *Differential Scanning Calorimetry and Infrared Crystallinity Determinations of Poly(aryl ether ether ketone).* Polymer, 1991. **32**(18): p. 3364-3370.
42. McGregor, C., et al., *The use of high-speed differential scanning calorimetry (Hyper-DSC(TM)) to study the thermal properties of carbamazepine polymorphs.* Thermochimica Acta, 2004. **417**(2): p. 231-237.
43. Saunders, M., et al., *The potential of high speed DSC (Hyper-DSC) for the detection and quantification of small amounts of amorphous content in predominantly crystalline samples.* International Journal of Pharmaceutics, 2004. **274**(1-2): p. 35-40.
44. McGregor, C. and E. Bines, *The use of high-speed differential scanning calorimetry (Hyper-DSC(TM)) in the study of pharmaceutical polymorphs.* International Journal of Pharmaceutics, 2008. **350**(1-2): p. 48-52.
45. Lu, X.F. and J.N. Hay, *Isothermal crystallization kinetics and melting behaviour of poly(ethylene terephthalate).* Polymer, 2001. **42**(23): p. 9423-9431.
46. Karakaplan, M., *Fitting Lorentzian peaks with evolutionary genetic algorithm based on stochastic search procedure.* Analytica Chimica Acta, 2007. **587**(2): p. 235-239.
47. Bradley, M., Thermo Fisher Scientific, Madison, WI, USA, *Application Note: 50733 - Curve Fitting in Raman and IR Spectroscopy: Basic Theory of Line Shapes and Applications*. 2007: Thermo Electron Scientific Instruments LLC, Madison, WI, USA. p. 4.
48. Perkin Elmer, P.U., *Personal Communication Regarding Polymer Testing*, D.M. Jenkins, Editor. 2009: Perkin Elmer Plc., Chalfont Road, Seer Green, Beaconsfield, HP9 2FX.

49. ISO-11357-3, *Plastics — Differential scanning calorimetry (DSC) — Part 3: Determination of temperature and enthalpy of melting and crystallization*, I.O.f. Standardization, Editor. 1999: Switzerland.
50. Turnbull, D. and J.C. Fisher, *Rate of Nucleation in Condensed Systems.* The Journal of Chemical Physics, 1949. **17**(1): p. 71-73.
51. John I. Lauritzen, Jr. and D.H. John, *Extension of theory of growth of chain-folded polymer crystals to large undercoolings.* Journal of Applied Physics, 1973. **44**(10): p. 4340-4352.
52. Erukhimovitch, V. and J. Baram, *Nucleation and Growth Transformation Kinetics.* Physical Review B, 1995. **51**(10): p. 6221-6230.
53. Jenkins, M.J., Y. Cao, and S.N. Kukureka, *The effect of molecular weight on the crystallization kinetics and equilibrium melting temperature of poly(tetramethylene ether glycol).* Polymers for Advanced Technologies, 2006. **17**(1): p. 1-5.
54. Blundell, D.J., *On the interpretation of multiple melting peaks in poly(ether ether ketone).* Polymer, 1987. **28**(13): p. 2248-2251.
55. Booth, A. and J.N. Hay, *The use of differential scanning calorimetry to study polymer crystallization kinetics.* Polymer, 1969. **10**: p. 95-104.
56. Cebe, P., *Non-isothermal Crystallization of Poly(etheretherketone) Aromatic Polymer Composite.* Polymer Composites, 1988. **9**(4): p. 271-279.
57. Cho, D., *Isothermal crystallization behaviors and kinetics of an end-crystallizable diblock copolymer.* European Polymer Journal, 1995. **31**(11): p. 1075-1081.
58. Folkes, M.J. and G. Kalay, *The Effect of Heat-treatment on the Properties of PEEK and APC2.* Composites Science and Technology, 1993. **46**(1): p. 77-83.
59. Folkes, M.J., G. Kalay, and A. Ankara, *The effect of heat treatment on the properties of peek and APC2.* Composites Science and Technology, 1993. **46**(1): p. 77-83.
60. Gao, S.-L. and J.-K. Kim, *Cooling rate influences in carbon fibre/PEEK composites. Part 1. Crystallinity and interface adhesion.* Composites Part A: Applied Science and Manufacturing, 2000. **31**(6): p. 517-530.
61. Gao, S.-L. and J.-K. Kim, *Cooling rate influences in carbon fibre/PEEK composites. Part II: interlaminar fracture toughness.* Composites Part A: Applied Science and Manufacturing, 2001. **32**(6): p. 763-774.

62. Gao, S.-L. and J.-K. Kim, *Cooling rate influences in carbon fibre/PEEK composites. Part III: impact damage performance.* Composites Part A: Applied Science and Manufacturing, 2001. **32**(6): p. 775-785.
63. Gornick, F., Hoffman J. D., *Nucleation in polymers.* Nucleation Symposium, 1966. **58**(2).
64. Hay, J.N. and P.J. Mills, *The use of differential scanning calorimetry to study polymer crystallization kinetics.* Polymer, 1982. **23**(9): p. 1380-1384.
65. Hoffman, J.D., *Role of reptation in the rate of crystallization of polyethylene fractions from the melt.* Polymer, 1982. **23**(5): p. 656-670.
66. Hoffman, J.D. and R.L. Miller, *Kinetics of crystallization from the melt and chain folding in polyethylene fractions revisited: Theory and experiment.* Polymer, 1997. **38**(13): p. 3151-3212.
67. Hoffman, J.D. and J.J. Weeks, *Rate of Spherulitic Crystallization with Chain Folds in Polychlorotrifluoroethylene.* The Journal of Chemical Physics, 1962. **37**(8): p. 1723-1741.
68. Hosier, I.L. and D.C. Bassett, *A study of the morphologies and growth kinetics of three monodisperse n-alkanes: C122H246, C162H326 and C246H494.* Polymer, 2000. **41**(25): p. 8801-8812.
69. Jenkins, M.J. and K.L. Harrison, *The effect of molecular weight on the crystallization kinetics of polycaprolactone.* Polymers for Advanced Technologies, 2006. **17**(6): p. 474-478.
70. Jenkins, M.J., J.N. Hay, and N.J. Terrill, *Structure evolution in melt crystallised PEEK.* Polymer, 2003. **44**(22): p. 6781-6787.
71. Liu, C. and M. Muthukumar, *Langevin dynamics simulations of early-stage polymer nucleation and crystallization.* Journal of Chemical Physics, 1998. **109**(6): p. 2536-2542.
72. Ming, C. and C. Chia-Ting, *Crystallinity of isothermally and nonisothermally crystallized poly(ether ether ketone) composites.* Polymer Composites, 1998. **19**(6): p. 689-697.
73. Olley, R.H., D.C. Bassett, and D.J. Blundell, *Permanganic Etching of PEEK.* Polymer, 1986. **27**(3): p. 344-348.

74. Ozawa, T., *Kinetics of Non-isothermal Crystallization.* Polymer, 1971. **12**(3): p. 150-&.

75. Pasti, L., et al., *Application of Fourier transform to multivariate calibration of near-infrared data.* Analytica Chimica Acta, 1998. **364**(1-3): p. 253-263.

76. Richard, P. and E.M. Jan-Anders, *Prediction and analysis of nonisothermal crystallization of polymers.* Journal of Polymer Science Part B: Polymer Physics, 1997. **35**(6): p. 875-888.

77. Staniland, P.A., Allen, G., Bevington, J. C., *Poly(ether ketone)s in Comprehensive Polymer Science*. Vol. 5. 1989, New York: Pergamon Press.

78. Tan, S., et al., *Crystallization kinetics of poly(ether ether ketone) (PEEK) from its metastable melt.* Polymer, 1999. **40**(5): p. 1223-1231.

79. Tierney, J.J. and J.W. Gillespie Jr, *Crystallization kinetics behavior of PEEK based composites exposed to high heating and cooling rates.* Composites Part A: Applied Science and Manufacturing, 2004. **35**(5): p. 547-558.

80. Velisaris, C.N. and J.C. Seferis, *Crystallization kinetics of polyetheretherketone (peek) matrices.* Polymer Engineering & Science, 1986. **26**(22): p. 1574-1581.

81. Verdonck, E., K. Schaap, and L.C. Thomas, *A discussion of the principles and applications of Modulated Temperature DSC (MTDSC).* International Journal of Pharmaceutics, 1999. **192**(1): p. 3-20.

82. Zhaobin, Q., et al., *Nonisothermal melt and cold crystallization kinetics of poly(aryl ether ketone ether ketone ketone).* Journal of Applied Polymer Science, 2000. **77**(13): p. 2865-2871.

9.0 Appendices

9.1 Appendix I

Table 9.0 Deconvolution data for 450PF

Sample	Peak #	Peak Type	Centre X (cm^{-1})	Height	FWHH	Area	
Amorphous	1	Lorentzian	1163.9	0.52	66.1151	53.6815	
	2	Lorentzian	1220.96	0.8058	24.4035	30.8192	
	3	Lorentzian	1277.28	0.1907	19.2558	5.759	***Ratio***
	4	Lorentzian	1305.83	0.1884	11.9235	3.5249	0.61

Sample	Peak #	Peak Type	Centre X (cm^{-1})	Height	FWHH	Area	
Cooled at 10°Cmin^{-1}	1	Lorentzian	1153.413	0.3687	166.8326	96.0092	
	2	Lorentzian	1220.466	0.2717	23.1497	9.8714	
	3	Lorentzian	1280.317	0.0929	13.0089	1.8968	***Ratio***
	4	Lorentzian	1307.79	0.1348	13.5219	2.8622	1.51

Sample	Peak #	Peak Type	Centre X (cm^{-1})	Height	FWHH	Area	
Cooled at 20°Cmin^{-1}	1	Lorentzian	1154.584	0.2914	68.4439	31.1355	
	2	Lorentzian	1219.718	0.341	34.7157	18.538	
	3	Lorentzian	1280.633	0.1084	13.7348	2.3359	***Ratio***
	4	Lorentzian	1308.158	0.1568	12.8852	3.1698	1.36

Sample	Peak #	Peak Type	Centre X (cm^{-1})	Height	FWHH	Area	
Cooled at 30°Cmin^{-1}	1	Lorentzian	1156.525	0.2637	65.6665	27.0335	
	2	Lorentzian	1220.612	0.326	38.3555	19.5718	
	3	Lorentzian	1280.324	0.1131	15.2932	2.7138	***Ratio***
	4	Lorentzian	1308.078	0.1591	13.9233	3.4745	1.28

Sample	Peak #	Peak Type	Centre X (cm^{-1})	Height	FWHH	Area	
Cooled at 40°Cmin^{-1}	1	Lorentzian	1156.677	0.2731	62.047	26.4579	
	2	Lorentzian	1220.806	0.3587	38.4185	21.5686	
	3	Lorentzian	1280.361	0.1194	15.1084	2.8301	***Ratio***
	4	Lorentzian	1308.119	0.1681	13.5081	3.5618	1.25

Sample	Peak #	Peak Type	Centre X (cm^{-1})	Height	FWHH	Area	
Cooled at 50°Cmin^{-1}	1	Lorentzian	1157.529	0.3797	58.6443	34.7713	
	2	Lorentzian	1221.122	0.5061	35.8464	28.3933	
	3	Lorentzian	1280.302	0.1444	15.212	3.4449	***Ratio***
	4	Lorentzian	1308.151	0.1977	12.7256	3.9476	1.15

Sample	Peak #	Peak Type	Centre X (cm^{-1})	Height	FWHH	Area	
Cooled at 60°Cmin^{-1}	1	Lorentzian	1184.906	0.1929	6.9902	2.1171	
	2	Lorentzian	1221.366	0.393	30.8736	19.0327	
	3	Lorentzian	1280.007	0.1493	18.8442	4.4144	***Ratio***
	4	Lorentzian	1308.431	0.2008	15.9581	5.0285	1.13

Sample	Peak #	Peak Type	Centre X (cm^{-1})	Height	FWHH	Area	
Cooled at 70°Cmin^{-1}	1	Lorentzian	1185.052	0.2353	7.3165	2.7024	
	2	Lorentzian	1221.155	0.4704	30.8078	22.7285	
	3	Lorentzian	1279.926	0.1626	19.6081	5.0046	***Ratio***
	4	Lorentzian	1308.317	0.214	14.8469	4.9862	1.01

Sample	Peak #	Peak Type	Centre X (cm^{-1})	Height	FWHH	Area	
Cooled at 80°Cmin^{-1}	1	Lorentzian	1184.954	0.2599	7.0798	2.8894	
	2	Lorentzian	1220.688	0.51	28.328	22.6596	
	3	Lorentzian	1279.792	0.1632	19.1827	4.9122	***Ratio***
	4	Lorentzian	1308.207	0.2152	14.9445	5.0476	1.02

Sample	Peak #	Peak Type	Centre X (cm^{-1})	Height	FWHH	Area	
Cooled at 90°Cmin^{-1}	1	Lorentzian	1185.259	0.2864	7.1503	3.215	
	2	Lorentzian	1221.348	0.5516	29.3135	25.357	
	3	Lorentzian	1279.589	0.1684	21.2678	5.6179	***Ratio***
	4	Lorentzian	1308.181	0.2147	14.7949	4.9856	0.88

Sample	Peak #	Peak Type	Centre X (cm^{-1})	Height	FWHH	Area	
Cooled at 100°Cmin^{-1}	1	Lorentzian	1184.031	0.3317	12.7815	6.6528	
	2	Lorentzian	1219.813	0.529	40.5134	33.5586	
	3	Lorentzian	1279.247	0.1648	24.9815	6.4551	***Ratio***
	4	Lorentzian	1308.69	0.2041	18.8784	6.043	0.94